國 立 交 通 大 學

電 子 工 程 學 系 電 子 研 究 所

碩 士 論 文

低溫製程之奈米碳管場發射背光模組和利用三極結構增進均勻性之研究

Study on the Carbon Nanotube Field Emission Backlight Units with Low Temperature Processes and Enhancement of Uniformity by Utilizing a Triode Structure

研 究 生：李 建 穎

指導教授：鄭 晃 忠 博士

中華民國 九十七 年 七 月

低溫製程之奈米碳管場發射背光模組和利用三極結構增進均勻性之研究

Study on the Carbon Nanotube Field Emission Backlight Units with Low Temperature Processes and Enhancement of Uniformity by Utilizing a Triode Structure

研 究 生：李 建 穎　　Student: Lee Chein-Ying

指導教授：鄭 晃 忠　博士　　Advisor: Dr. Huang-Chuang Cheng

國立交通大學

電子工程學系　電子研究所碩士班

碩士論文

A Thesis

Submitted to Department of Electronics Engineering & Institute of Electronics

College of Electrical and Computer Engineering

National Chiao Tung University

In Partial Fulfillment of the Requirements for the Degree of Master

in

Electronics Engineering

2008

Hsinchu, Taiwan, Republic of China

中華民國 九十七年 七月

低溫製程之奈米碳管場發射背光模組和利用三極結構增進均勻性之研究

研究生：李建穎　　指導教授：鄭晃忠 博士

國立交通大學電子工程學系　　電子研究所碩士班

摘　要

此篇論文主題之一為研究多層催化金屬在低溫下合成柱狀結構之奈米碳管場發射陣列來進行場發射，同時探討其應用於背光源之可靠度和均勻性。依據之前本實驗室之研究，利用多層式的催化金屬可以有效的降低製程所需的溫度，利用共鍍合金催化金屬的方式可以提升碳管的可靠度。所以本實驗將結合兩者的優點，嘗試多層共鍍催化金屬在低溫下合成柱狀結構之奈米碳管的研究。經過量測發現以鈷鈦共鍍在鋁上(鈷-鈦/鋁)可以在550℃得到最佳柱狀結構的碳管，其碳管的場發射起始電場為3.6 V/μm，在6 V/μm的電場之下其電流密度為1272 μA/cm^2，另外可以在6.7 V/μm高電場之下維持2小時擁有變動值小於7%的優異可靠度，其在1平方公分的總面積之下擁有發光均勻性的改善。然而在探討成長時間對於其特性的影響

之後，近一步發現在成長時間是 90 分鐘時，其碳管高度大約是 8 μm 時，可以得到最佳之場發射特性，起始電壓為 3.5 V/μm，而在 6.7 V/μm 固定電場下 2 小時的電流衰減度低於 0.1%，由材料分析可以獲知若成長時間超過 90 分鐘會造成非結晶相增加，而使場發射特性變差。此外，由於利用微影方式，可以控制柱體密度和調變柱體間的間距，來降低電場遮蔽效應，所以當碳管直徑為 6 μm 且高度為 8 μm 時，獲得在間距 9 μm 附近為最佳的場發射特性。

為了符合場發射低電壓操作的目的，所以製造利用閘極控制的奈米碳管之場發射三極元件，碳管方面利用在低溫合成催化金的技巧，且利用三極結構的電子束發散來增進背光元件的均勻性，經由多次的模擬所得到最佳結構的參數:閘極到發射源距離為 2 μm，閘極和發射源的高度皆為 1 μm。透過實驗獲知操作電壓可降至 43 V，且經由發光測試確認均勻性之改善。未來在大面積場發射平面背光源的運用上，藉由此低溫成長之最佳發光均勻性的結構，具有製程簡單以及成本便宜的優勢下，因此本研究所提結構與技術將具有相當大之應用潛力。

Study on the Carbon Nanotube Field Emission Backlight Units with Low Temperature Processes and Enhancement of Uniformity by Utilizing a Triode Structure

Student: Lee Chein-Ying Advisor: Dr. Huang-Chung Cheng

Department of Electronics Engineering &

Institute of Electronics

National Chiao Tung University

Abstract

In this research, we studied on the pillar-like CNT field emission arrays synthesis with co-deposited multilayer catalyst at low temperatures and try to improve their uniformity and reliability by testing as field emission backlight units (FE-BLUs). According to our group's previous researches, we could effectively decrease the growth temperature of CNTs by utilizing multilayer catalyst and remarkably improve the reliability of CNTs by utilizing co-deposited catalysts. Firstly, we combined these two techniques to preparing co-deposited multilayer catalyst for synthesis of pillar-like CNTs at low temperatures. As a result, CNTs grown with catalysts of co-deposited Co and Ti on Al (Co-Ti/Al) showed the best morphology and field emission properties, which revealed a low turn-on field (~3.6 V/μm), a high current density of 1272 μA/cm^2 under 6V/μm electric field, and superior short-term stability with

current variation below 7% under the electric field of 6.7 V/μm in 2 hours. In addition, the photo luminescent image of 1cmx1cm pillar patterns illuminated uniformly. Secondly, we obtained an optimum growth time was determined to be 90 min for synthesis of the pillar-like CNTs at 550℃. Height of CNTs was about 8 μm, which revealed a low turn-on field of 3.5 V/μm, and excellent reliability was shown by the degradation of current below 0.1% under the electric field 6.7 V/μm in 2 hours. Based on the material analysis, the amorphous carbon would increase with increasing the growth time, and then the field emission characteristics became worse. Thirdly, we utilized photolithography to pattern different spacings between the pillar-like CNTs for finding out the optimum field emission characteristics by the compromising between screening-effect and emission area. Accordingly, the optimum electrical characteristics for the pillar-like CNTs with the pillar diameter of 6 μm and the pillar height of 8 μm would happen at the inter-pillar spacing of about 9 μm, which exhibited good electrical characteristics.

Finally, we utilized triode-typed CNT field emission array to reduce the operation voltage, and the beam spreading to improve the emission uniformity. The optimum parameters of the triode field emission device were obtained according to the simulations, the gate-to-emitter length was 2 μm, and the vertical distance between gate and CNTs was 1 μm. And experimental results and the resultant driving voltage was as low as 43 V. In future, this structure is promising for the applications in a planar backlight because of the large-area uniformity and simple fabrication process with low cost.

誌 謝

在這邊我要感謝交通大學無論材料系還是電子所教導過我的老師，特別是指導教授—鄭晃忠老師，非常感謝他在這兩年之中耐心且細心的指導，使我獲益良多以及能夠順利的完成碩士學位。

其次要感謝在研究上為我指點迷津的賴瑞霖學長和林高照學長，謝謝他們在實驗上的啟發以及幫助，並且常常給予適當的引導和關心。還有謝謝已經畢業的陳俠威學長、張珮琪學長和林君翰學長，他們在實驗上的經驗傳承和機台訓練。

接下來還要感謝交通大學奈米中心（NFC）和國家毫微米實驗室（NDL）提供完善的實驗設備，尤其是要感謝奈米中心的技術人員-林聖欽先生、倪月珍小姐、范秀蘭小姐、陳明麗小姐、陳悅婷小姐、鄭淑娟小姐…等，在實驗設備及維護上給予最大的支持與協助，使我的研究得以順利完成。也感謝何惟梅小姐、顏似妙小姐和簡秀芳小姐在行政方面的協助。

再來要謝謝所有 309B 實驗室的學長、同學以及學弟妹，謝謝同組的小組長張加聰學長、交大材料系系花許育瑛、機台一直考不過的魏英彰和用功不翹課的蔡萬霖。還有要特別感謝長期幫我拍攝電子顯微鏡照片的劉政欽，以及撞針王林偉凱、最色的水餃店老闆涂仕煒和很有 fu 的李序恆。感謝實驗室的逸哲學長、柏宇學長、全平學長給我不吝嗇的指教，還有感謝晚上都不回家的大腸學長，讓夜晚寂寞的實驗室增添不少陽氣。此外還要感謝 TFT 組學弟妹們的協助，你們超厲害，上課都超認真而且從來不翹課，感謝清大材料的學長幫忙拍攝穿透式電子顯微鏡照片。

最後還要感謝我所有的家人和所有關心以及給我鼓勵的朋友，讓我深深體驗到陳之藩先生在謝天一文中所提到的“*即是無論什麼事，得之於人者太多，出之於己者太少。因為需要感謝的人太多了，就感謝天罷*”。

Contents

Table Lists

Chapter 1

Chapter 2

Chapter 3

Figure Captions

Chapter 1:

Chapter 2:

Chapter 3:

Chapter 1

Introduction

1.1 Overview of Vacuum Microelectronics

1.1.1 History of Vacuum Microelectronics

In 1948, vacuum tubes have been gradually replaced by solid state devices, which tiny volume, low cost, better reliability, and more power efficient transistors were invented by John Bardeen, Walter Bratain, and William Shockley [1.1].

But nowadays, there has been a growing interest in vacuum microelectronics. Some reasons for the increasing interest have to do with the superior theoretical electrical characteristics of the vacuum microelectronic devices over semiconductor devices. The so called vacuum microelectronic devices using the professional micro fabrication technology have been successfully fabricated and gave a new life to vacuum electronics due to great improvements on semiconductor manufacturing technology for the past decades.

"Vacuum state" devices have many superior advantages with respect to the present "solid state" devices, including radiation hardness, temperature insensitivity, and fast drift velocity. For example, there is negligible radiation effect in vacuum devices due to medium being damaged as the electrons fly in the vacuum [1.2].

Moreover, there is no medium for electrons fly in the vacuum, so there is no lattice scattering or bulk carrier generation/recombination. Therefore, the vacuum microelectronic devices can suffer to 500 ℃ or above as long as the structures of the vacuum devices do not destroyed and greatly reduced (nearly eliminated) temperature sensitivity problem which usually comes along with semiconductor devices. Additionally, the saturation drift velocity is limited to less than 3×10^7 cm/s in all semiconductor due to scattering mechanism whereas the

saturation drift velocity in vacuum is limited theoretically to 3×10^{10} cm/s and practically to about $6\text{-}9\times10^{8}$ cm/s [1.3].

Table 1-1

Comparison between vacuum microelectronics and solid-state electronics.

Items	Solid State Microelectronics	Vacuum Microelectronics
Current Density	$10^4 - 10^5$ (A/cm^2)	similar
Turn-on Voltage	0.1 – 0.7 V	5 – 300 V
Structure	solid/solid interface	solid/vacuum interface
Electron Transport	in solid	in vacuum
Electron Velocity	3×10^7 (cm/sec)	3×10^{10} (cm/sec)
Flicker Noise	due to interface	due to emission
Thermal & Short Noise	comparable	comparable
Electron Energy	< 0.3 eV	a few to 1000 eV
Cut-off Frequency	< 20 GHz (Si) & 100 GHz (GaAs)	< 100 – 1000 GHz
Power	small – medium	medium – large
Radiation Hardness	poor	excellent
Temperature Effect	-30 – 50 °C	< 500 °C
Fabrication & Materials	well established (Si) & fairly well (GaAs)	not well established

Table 1-1 shows the comparison between vacuum microelectronic and semiconductor devices.Vacuum electronics can be broadly separated into two categories: Thermionic emission or Field emission. The theory of field emission started in 1928, when R. H. Fowler and L. W. Nordheim published the first theory of electron field emission (Fowler- Nordheim theory) from metals using quantum mechanics [1.4]. The difference concerns the way electrons are emitted from the cathode. Thermionic emission relies on a heated electron emitter, or cathode. The cathode is heated up enough such that the electrons receive enough

kinetic energy to leave the surface of the cathode. Field emission, unlike thermionic emission, is possible with a cold cathode. Field emission is a form of quantum tunneling in which electrons pass through a barrier in the presence of a high electric field. This phenomenon is highly dependent on both the properties of the material and the shape of the particular cathode, so that higher aspect ratios produce higher field emission currents. According to the Fowler-Nordheim theory, an applied electric field of approximately 10^3 V/m is needed for electrons to tunnel through the sufficiently narrow barrier [1.2]. To reach this high field at reasonable applied voltage, it is customary to machine the field emitters into protruding objects to take advantage of field enhancement.

It was not until 1968 when C. A. Spindt camp up with a fabrication method to create very small dimension metal cones that vacuum microelectronic triodes became possible [1.2]. Fig.1-1 is a schematic diagram of the triode fabricated by Spindt [1.5]. From the late 1960s to the year 1990, Ivor Brodie, Henry F. Gray, and C. A. Spindt made many contributions to this field. Also, most of research was focused on the devices similar to the Spindt cathode during the past three decades.

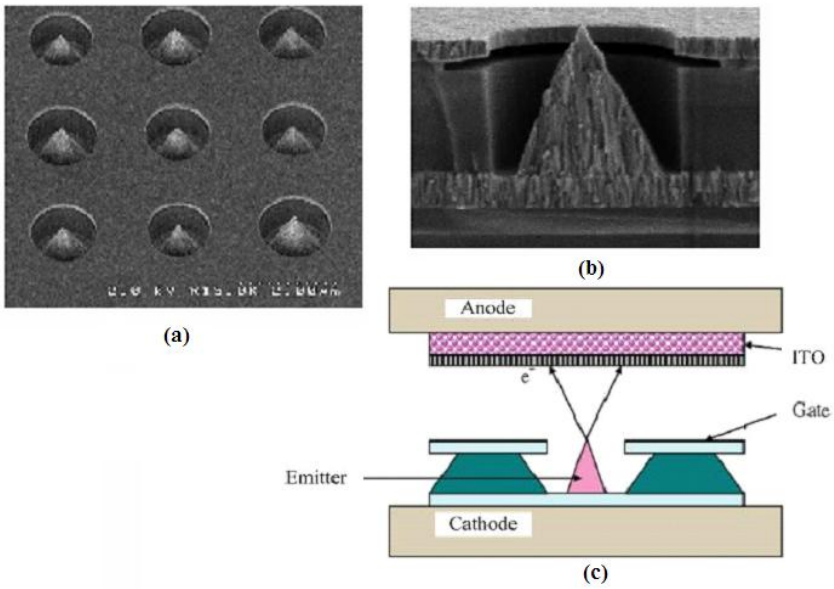

Figure 1-1 The SEM micrograph of (a) Spindt type triodes array, (b) Spindt type field emission triode, (c) Emitting way of spindt type triode. [1.5]

In 1991, a group of research of the French company LETI CHEN reported a microtip display at the fourth International Vacuum Microelectronics Conference [1.6]. Their display was the first announcement of a practical vacuum microelectronic device. From then on, a great amount of researchers all over the world devoted themselves to this interesting, challenging, and inventive field. Part of the work focused on fabricating very small radius silicon tip by utilizing modern VLSI technology [1.7-1.8]. Some of them increased the emission current by coating different metals, such as W, Mo, Ta, Pt etc., even diamond on field emission arrays [1.9-1.10]. Different device schemes also have been proposed to enhance the emission current density, stability, and reliability.

1.1.2 Theory Background

In quantum mechanical, electron field emission is a tunneling phenomenon of electrons extracted from the conductive solid surface, such as a metal or a semiconductor, where the surface electric field is extremely high.

If a sufficient electric field is applied on the emitter surface, electrons will be emitting through the surface potential barrier into vacuum, even under a very low temperature. On the other hand, thermionic emission is the hot electron emission under high temperature and low electric field. Fig. 1-2(a) demonstrates the band diagram of a metal-vacuum system.

Here W_0 is the energy difference between an electron at rest outside the metal and an electron at rest inside, whereas W_f is the energy difference between the Fermi level and the bottom of the conduction band. The work function ϕ is defined as $\phi = W_0 - W_f$. If an external bias is applied, vacuum energy level is reduced and the potential barrier at the surface becomes thinner as shown in Fig. 1-2(b).

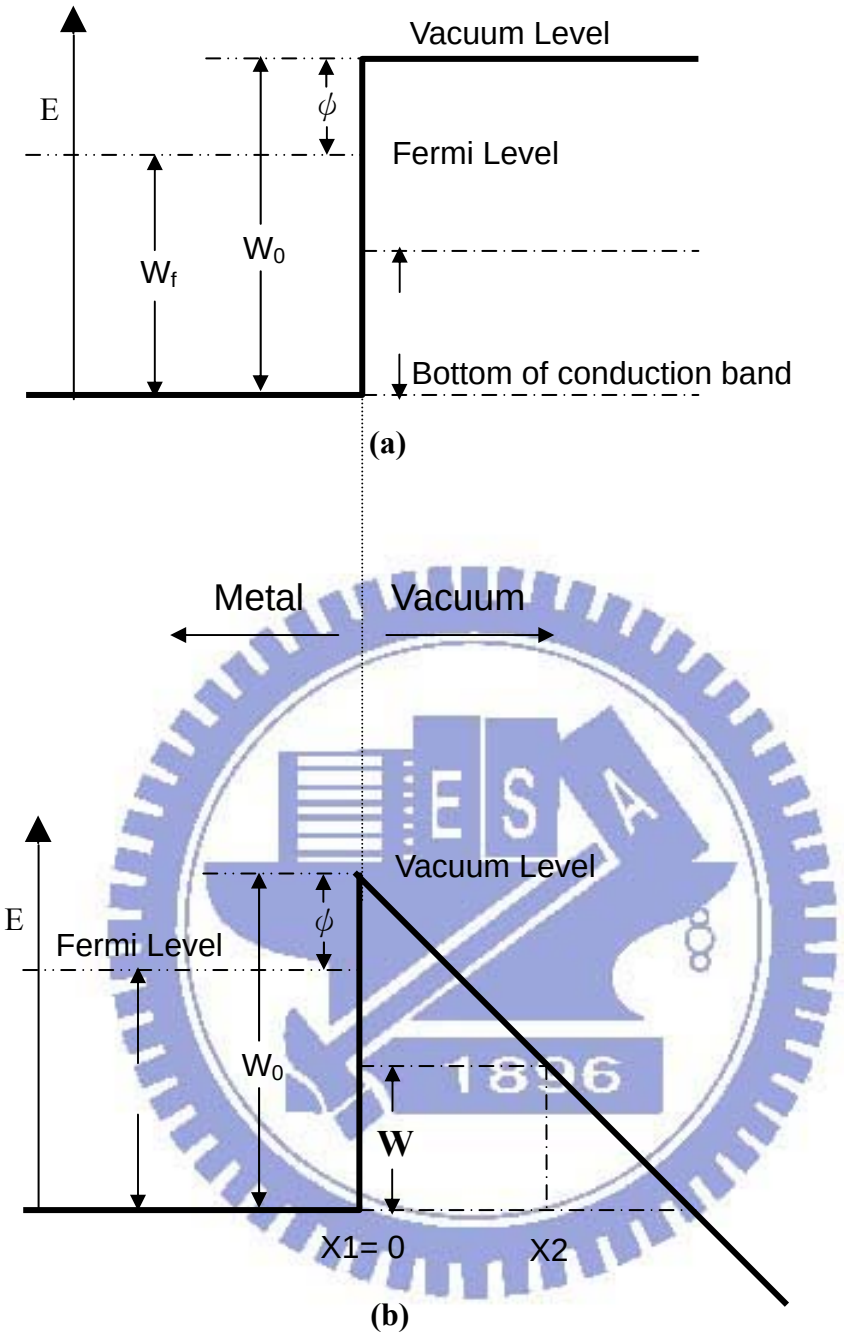

Figure 1-2 Energy diagrams of vacuum-metal boundary: (a) without external electric field; and (b) with an external electric field.

Then, an electron having energy "W" has a finite probability of tunneling through the surface barrier. Fowler and Nordheim derive the famous F-N equation (1.1) as follow [1.2]:

$$J = \frac{aE^2}{\phi t^2(y)} \exp[-b\phi^{\frac{3}{2}} v(y)/E], \tag{1-1}$$

where J is the current density (A/cm^2). E is the applied electric field (V/cm), ϕ is the work function (in eV), a = 1.56×10^{-6}, b = -6.831×10^{-7}, y = 3.79x10^{-4}×10^{-4}E$^{1/2}$/ϕ, t^2(y)~1.1 and v(y) can be approximated as [1.10]

$$v(y) = \cos(0.5\pi y), \tag{1-2}$$

or

$$v(y) = 0.95 - y^2. \tag{1-3}$$

Typically, the field emission current I is measured as a function of the applied voltage V. Substituting relationships of J = I/α and E = βV into Eq.(1-1), where α is the emitting area and β is the local field enhancement factor of the emitting surface, the following equation can be obtained

$$I = \frac{A\alpha\beta^2 V^2}{\phi t^2(y)} \exp[-bv(y)\frac{\phi^{\frac{3}{2}}}{\beta V}]. \tag{1-4}$$

Then taking the log. form of Eq. (1-4) and v(y) ~ 1

$$\log(\frac{I}{V^2}) = \log[1.54\times10^{-6}\frac{\alpha\beta^2}{\phi t^2(y)}] - 2.97\times10^7(\frac{\phi^{3/2}v(y)}{\beta V}), \tag{1-5}$$

from Eq. (1-5), the slope of a Fowler-Nordheim (F-N) plot is given by

$$S \equiv slope_{FN} = 2.97\times10^7(\frac{\phi^{\frac{3}{2}}}{\beta}), \tag{1-6}$$

The parameter β can be evaluated from the slope S of the measured F-N plot if the work function ϕ was known

$$\beta = -2.97\times10^{7}(\frac{\phi^{\frac{3}{2}}}{S}) \quad (\text{cm}^{-1}), \tag{1-7}$$

The emission area α can be subsequently extracted from a rearrangement of Eq.(1-5)

$$\alpha = (\frac{I}{V^{2}})\frac{\phi}{1.4\times10^{-6}\beta^{2}}\exp(\frac{-9.89}{\sqrt{\phi}})\exp(\frac{6.53\times10^{7}\phi^{\frac{3}{2}}}{\beta V}) \quad (\text{cm}^{2}). \tag{1-8}$$

For example, the electric field at the surface of a spherical emitter of radius r concentric with a spherical anode (or gate) of radius r+d can be represented analytically by

$$E = \frac{V}{r}(\frac{r+d}{d}), \tag{1-9}$$

Though a realistic electric field in the emitter tip is more complicated than above equation, we can multiply Eq.(1-9) by a geometric factor β` to approximate the real condition.

$$E_{tip} \equiv \text{function of (r,d)} = \beta`\frac{V}{r}(\frac{r+d}{d}), \tag{1-10}$$

where r is the tip radius of emitter tip, d is the emitter-anode(gate) distance and β` is a geometric correction factor [1.11].

For a very sharp conical tip emitter, where d >> r, E_{tip} approaches to β`(V/r). And for r>>d, $E_{tip}$ approaches to $\beta$`(V/d) which is the solution for a parallel-plate capacitor and for a diode operation in a small anode-to-cathode spacing.

As the gated FEA with very sharp tip radius, Eq. (1-10) can be approximated as:

$$E_{tip} = \beta`(\text{V/r}). \tag{1-11}$$

Combining E = βV and Eq. (1-11), we can obtain the relationship:

$$E_{tip} = \beta V = \beta`(V/r), \text{ and } \beta` = \beta r. \quad (1\text{-}12)$$

The tip radius r is usually in the range from a few nm to 50 nm, corresponding to the parameter $\beta`$ ranging from 10^{-1} to 10^{-2}.

Besides, transconductance g_m of a field emission device is defined as the change in anode current due to the change in gate voltage [1.1].

$$g_m = \frac{\partial I_C}{\partial V_g}|_{Vc}, \quad (1\text{-}13)$$

Transconductance of a FED is a figure of merit that gives as an indication of the amount of current charge that can be accomplished by a given change in grid voltage. The transconductance can be increased by using multiple tips or by decreasing the gate-to-cathode spacing for a given anode-to-cathode spacing.

The following approaches may therefore be taken to reduce the operating voltage of the field emission devices according to the equations above mentioned:

a. Narrow the cone angle for increasing β

b. Reproducibly sharpen the tips to the atomic level for increasing β

c. Choose the tip material which has the lower work function (ϕ)

d. Reduce the gate-opening diameter for increasing β.

1.2 Applications of Vacuum Microelectronic Devices

Due to the superior properties of vacuum microelectronic devices, potential applications include high brightness flat-panel display [1.12-1.16], high efficiency microwave amplifier and generator [1.17-1.19], ultra-fast computer, intense electron/ion sources [1.20-1.21], scanning electron microscopy, electron beam lithography, micro-sensor [1.22-1.23], temperature insensitive electronics, and radiation hardness analog and digital circuits

1.2.1 Vacuum Microelectronic Devices for Electronic Circuits

Either vacuum or solid-state devices can generate power at frequency in the GHz range. Solid-state devices, such as impact avalanche transit time (IMPATT) diodes, Si bipolar transistors, and GaAs FETs [1.24], are typically used in the lower power (up to 10 W) and frequency (up to 10 GHz) range. Vacuum devices still remain the only technology available for high power and high frequency applications. These devices include traditional multi-terminal vacuum tubes, like triodes, pentodes, and beam power tubes, and distributed-interaction devices, such as traveling wave tubes (TWTs), klystrons, backward-wave oscillators (BWOs).

The performance of FEAs in conventionally modulated power tubes, like TWT, is determined primarily by their emission current and current density capability. On the other hand, application of FEAs in the microwave tubes in which modulation of the beam is accomplished via modulation of the emission current at source, such as capacitance and transconductance. Successful operation of a gated FEA in a 10 GHz TWT amplifier with conventional modulation of electron beam has been demonstrated by NEC Corporation of Japan [1.25]. The amplifier employed a modified Spindt-type Mo cathode with circular emission area of 840 μm in diameter. The modified cathode structure incorporated a resistive poly-Si layer as a current limiting element. The emission current from the cathode was 58.6

mA. The prototype TWT could operate at 10.5 GHz with the output power of 27.5 W and the gain of 19.5 dB. The bandwidth of the tube was greater than 3 GHz. The prototype was operated for 250 h.

1.2.2 Field Emission Displays

Among wide range applications of the vacuum microelectronics, the first commercial product could be the field emission flat-panel display. The field emission fluorescent display is basically a thin cathode ray tube (CRT), which was first proposed by SRI International and later demonstrated by LETI [1.6].

Various kinds of flat-panel displays, such as liquid crystal display (LCD), electroluminescent display (EL), vacuum fluorescent display (VFD), plasma display panel (PDP), and light emitting display (LED), are developed for the better characteristics of small volume, light weight, and low power consumption. LCDs have become the most popular flat panel displays, however, LCDs have some drawbacks, such as poor viewing angle, temperature sensitivity and low brightness. As a result, some opportunities still exist and waiting for the solutions from other flat panel displays such as FED.

FED features all the pros of the CRTs in image quality and is flat and small volume. The schematic comparisons are revealed in Fig. 1-3 [1.24]. The operation of CRTs involves deflection of the beam in such a way that the electron spot scans the screen line-by-line. In FEDs, multiple electron beams are generated from the field emission cathode and no scanning of beams is required. The cathode is a part of the panel substrate consists of an X-Y electrically addressable matrix of field emission arrays (FEAs). Each FEA is located at the intersection of a row and a column conductor, with the row conductor serving as the gate electrode and the column conductor as the emitter base. The locations where the rows and columns intersect define a pixel. The pixel area and number of tips are determined by the desired resolution and luminance of the display. Typically, each pixel contains an FEA of

4-5000 tips. The emission current required for a pixel varies from 0.1 to 10 μA, depending on the factors such as the luminance of the display, phosphor efficiency and the anode voltage.

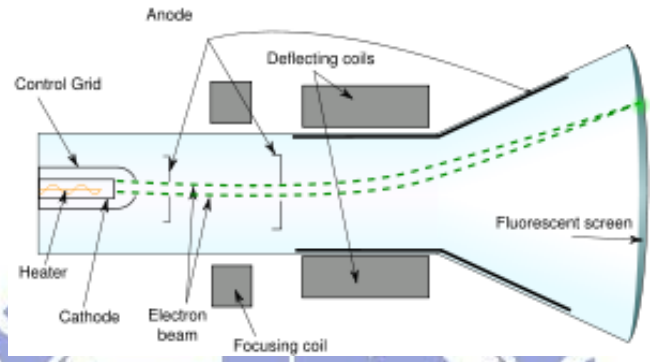

(a)

(b)

Figure 1-3 The schematic diagram of (a) conventional CRT and (b) comparison between CRT and FED. [1.24].

Compared to the active matrix LCDs and PDPs, FEDs are energy efficient and could provide a flat panel technology that features less power consumption. They can also be cheaper to make, as they have fewer total components. Moreover, FEDs could generate three times the brightness with wilder viewing angle at the same power level. Full color FEDs have been developed by various research groups from different aspects such as Motorola, PixTech, Futaba, Sony/Candescent, Samsung, and Canon-Toshiba are presently engaged in commercially exploiting FEDs. the products of above mentioned companies are shown in Fig. 1-4.

(a)

(b)

(c)

(d)

(e)

(f)

Figure 1-4 The full color FED products: (a) Motorola 5.6” color FED based on Spindt-type , (b) Pixtech 5.6” color FED based on Spindt-type, (c) Futaba 7” color FED based on Spindt-type, (d) Sony/Candescent 13.2” color FED based on Spindt-type, (e) Samsung 32“ under-gate CNT-FED, and (f) Canon-Toshiba 36” SED-TV.

1.2.3 Cathode Structure and Materials for Field Emission Displays

Field emission display is one of the most promising emissive type flat-panel displays, which can overcome the drawbacks of TFT-LCD, such as poor viewing angle, temperature sensitivity, low contrast and low brightness. This section introduces some novel cathode structures and synthesizes these novel emitter materials for FED operations

1.2.3.1 Spindt-type Field Emitters

The "Spindt" cathode was first proposed by C. A. Spindt in 1968 [1.25]. The scanning electron microscope (SEM) image of a spindt type field emission triode has been shown in Fig. 1-1 agian. It was first invented by Spindt of SRI and improved for the electron source of high-speed switching devices or microwave devices [1.2]. In 1970s, Meyer of LETI applied Spindt-typed emitters for a display and introduce a resistive layer as the feedback resistance to stabilizing the field emission from Spindt-type emitters [1.26].

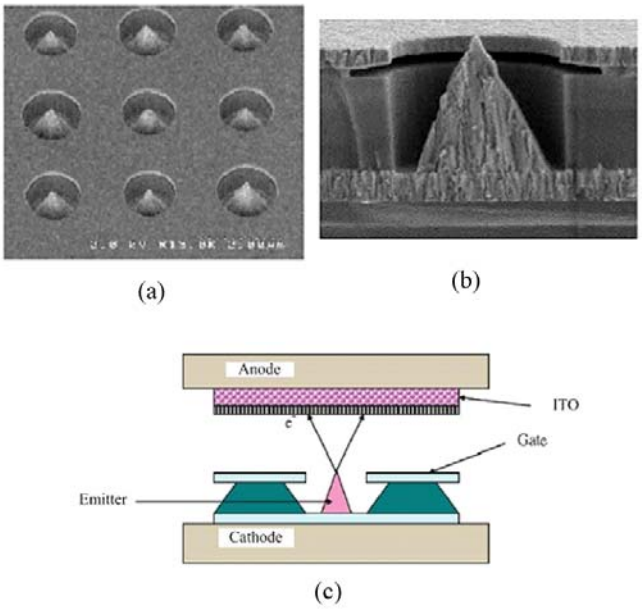

Figure 1-1 The SEM micrograph of (a) Spindt type triodes array, (b) Spindt type field emission triode, and (c) Emitting way of spindt type triode. [1.5]

The structure of Spindt-type FED includes a substrate, a cathode electrode of an electron emission unit formed thereon having a substantially conical shape, and a gate electrode of a lead-out electrode stacked on a substrate around the cathode electrode having an insulating layer. In the Spindt type FED a voltage is applied between the cathode electrode and the gate electrode in a vacuum to thereby produce a high electric field. As a result, electrons are emitted from a tip end of the cathode electrode through the electron emission mechanism in an electric field. In addition, the Spindt-type FED has a conical electron emission portion formed on a cathode electrode. It higher electron drawing efficiency since the electron emission portion is arranged in the vicinity of the center of the gate electrode where the electric field is most concentrated, and the directivity of electron emission is regular.

The merits of the Spindt-type field emitters are summarized as following: (1) High emission current efficiency, more than 98 % anode current to cathode current can be achieved for the symmetric structure of Spindt tip and the gate hole, the lateral electric field to the metal tip can be cancelled out. (2) The fabrication is self-aligned, easy process; uniform field emission arrays can be fabricated easily. Some research groups have successfully fabricated commercial FED products based on Spindt-type field emitters such as motorola, Pixtech, Futaba and Sony/Candesent.[1.27], the products of above mentioned companies are shown in Fig. 1-4.

However, there are some drawbacks of Spindt-type field emitters when fabricating Spindt-type FED such as (1) High gate driving voltage required; for a Spindt-type field emission triode with 4 μm gate aperture, the driving voltage is typically more than 60 V, which results in the high cost of the driving circuits. To reduce the gate driving voltage, frontier lithography technologies such as E beam lithography must be applied to reduce the gate aperture to the sub-micron level. (2) The emission property degrades for the chemically instable of the metal tips. (3) Huge, expensive high vacuum deposition system required during fabricating large area Spindt-type FED.

1.2.3.2 Silicon Tip Field Emitters

An alternative approach to fabricate tip type field emitters is to fabricate the Si tip field emitters based on the semiconductor fabricating process. Figure 1-5 depicts the SEM micrographs of Si tips array, Si tip field emission triodes array formed by chemical mechanical polishing (CMP) [1.28] and double gate of Si field emitter arrays [1.29]. Symmetric device structure and similar advantages with Spindt-type field emitters can be obtained. However, high temperature oxidation sharpening process prohibits Si tip from large area fabrication

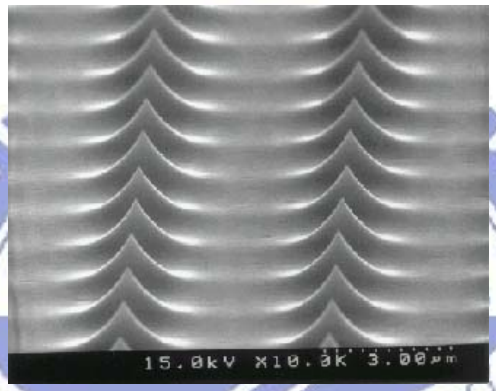

(a)

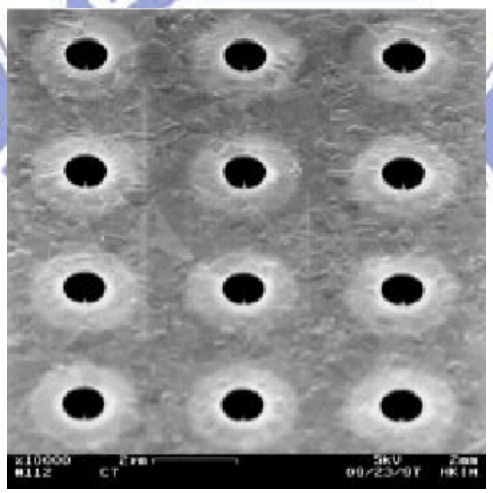

(b)

Figure 1-5 (a) Si tip formed by isotropic etching and (b) Si tip field emission triodes array formed by CMP [1.28] [1.29]

1.2.3.3 Surface Conduction Electron Emitters

A surface conduction electron emitter (SCE) display is a flat panel display technology that uses surface conduction electron emitters for every individual display pixel. The surface conduction emitter emits electrons that excite a phosphor coating on the display panel, the same basic concept found in traditional CRT televisions. The key technology to the electron emitters begins with the creation of an extremely narrow slits (~ several nanometers) between two electric poles in thin film of PdO (Palladium Oxide). Electrons are emitted from one side of the slit when approximately 10 V of electricity are applied. Some of these electrons are scattered at the other side of the silt and accelerated by the voltage (approximately 10 kV) applied between the glass substrates; causing light to be emitted when they collide with the phosphor-coated glass plate. The PdO film is coated by inject printing or screen-printing technology and this is a low cost process. This means that SEDs use small cathode ray tubes behind every single pixel (instead of one tube for the whole display) and can combine the slim form factor of LCDs and plasma displays with the superior viewing angles, contrast, black levels, color definition and pixel response time of CRTs. The major problem of SED is that the efficiency is still low and the power consumption will be very high. Fig. 1-6 shows the SEM image of SCE cathode array, structure and a 36-inch display of SED [1.30][1.31].

The research of SED was began by Canon in 1986, and in 2004, Toshiba and Canon announced a joint development agreement originally targeting commercial production of SEDs. In October 2006, Toshiba's president announced the company plans to begin full production of 55" SED TVs in 2007. In December 2006, Toshiba President and Chief Executive Atsutoshi Nishida said Toshiba is on track to mass-produce SED TV sets in cooperation with Canon by 2008.

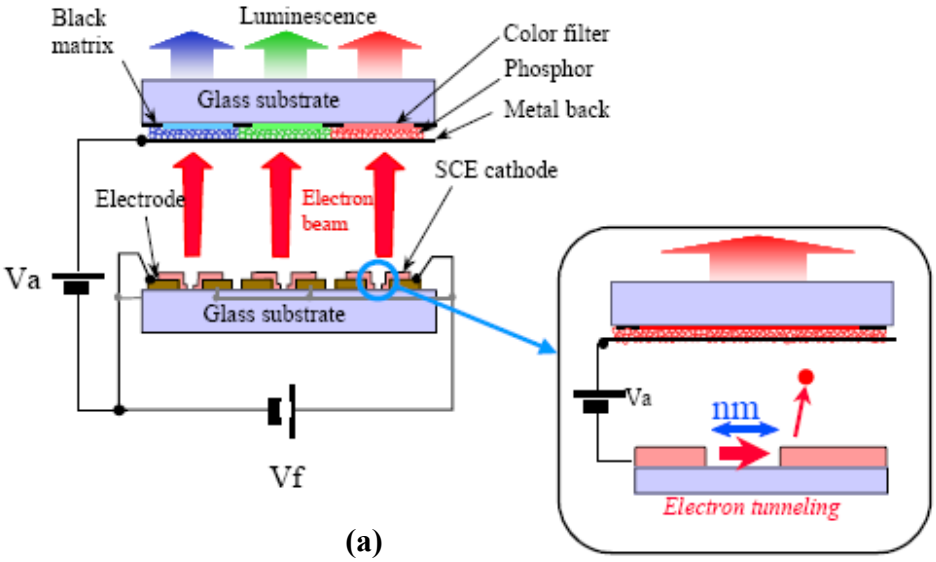

(a)

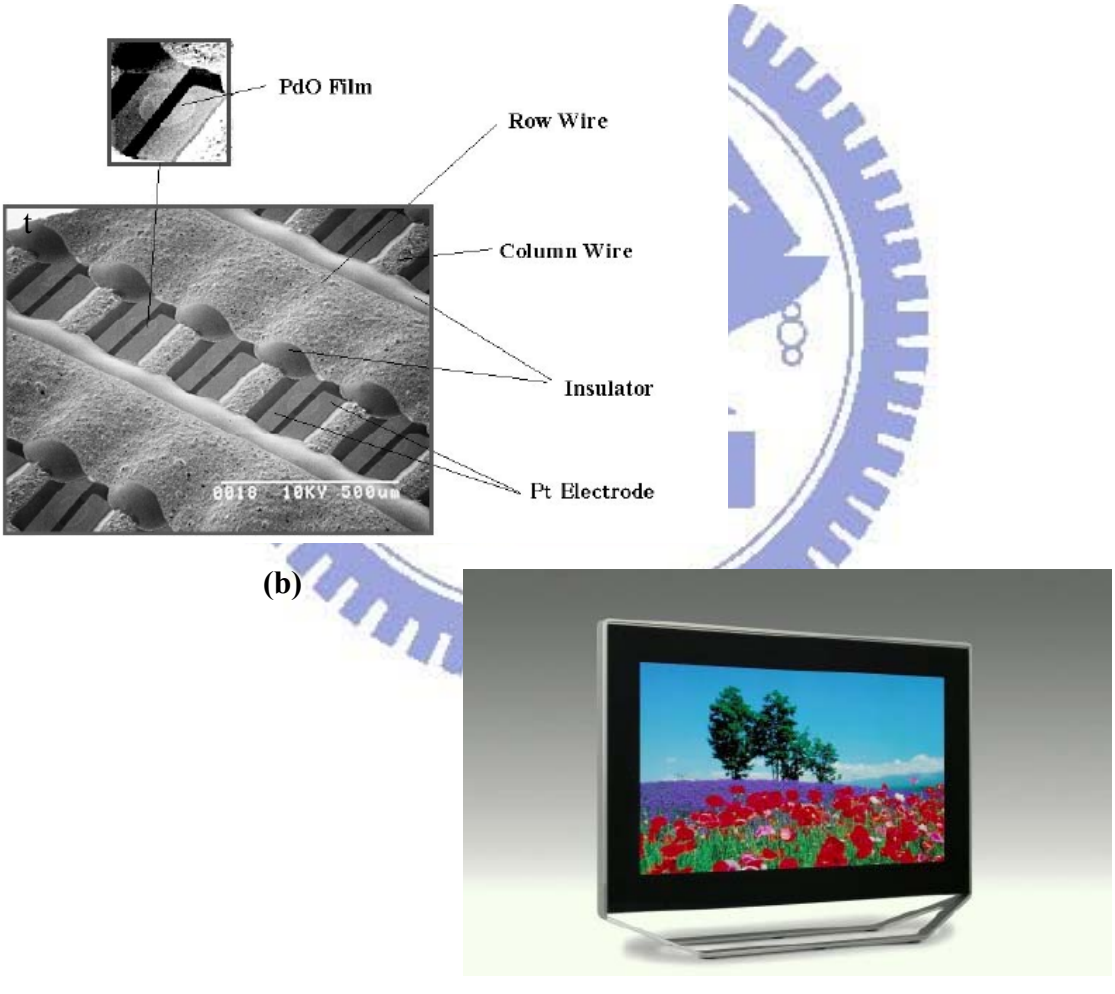

(b)

(c)

Figure 1-6 (a) The structure of SED, (b) SEM image of SCE cathode array, and (c) A 36-inch prototype of surface conduction electron emitter display. [1.30] [1.31]

1.2.3.4 Carbon and Nano-sized Emitters

So-called carbon nanotubes (CNTs) is the nano-sized and carbon emitters, is known to be useful for providing electron emission in field emission devices, such as cold cathodes that are used in a field emission display. Although Spindt-type emitters are generally used for FEDs, they still have a problem in that the life span of micro-tips is shortened due to atmospheric gases or a non-uniform field during a field emission operation. Moreover, the work function of the conventional metal emitters is too high to decrease a driving voltage for field emission. To overcome the problem, CNTs which have a substantially high aspect ratio, excellent durability due to their structure and excellent electron conductivity have been instead of Spindt-type emitters for field emission. CNTs are are anticipated to be an ideal electron emission source since they feature a low work function, the resultant electron emission source can be driven by applying low voltages, and the method of fabricating the same is not complicated. They will thereby offer advantages to realize a large size panel display in terms of view angle, definition, power consumption, and temperature stability.

1.3 Field Emission Properties of Carbon Nanotubes

Since the discovery of carbon nanotubes (CNTs) by Iijima in 1991, [1.32] CNTs have attracted considerable interests because of their unique physical properties and many potential applications [1.33]. CNTs have numerous potential applications in nanoelectronics, nanometer-scale structural materials, hydrogen storage, field-emission devices, and so on. Among these applications, CNTs seem to be very promising as electron emitters for field-emission displays (FEDs).

1.3.1 The Synthesis Methods of Carbon Nanotubes

Carbon nanotubes (CNTs) have been extensively investigated for the synthesis using arc discharge, laser vaporization, pyrolysis, solar energy, and plasma-enhanced chemical vapor deposition (CVD), for its unique physical and chemical properties and for applications to nanoscale devices. However, common methods of CNT synthesis include: (1) arc-discharge [1.34], (2) laser ablation [1.35], (3) thermal CVD [1.36-1.38], and (4) plasma enhanced CVD [1.39][1.40].

The laser ablation can synthesize pure carbon nanotubes in high fabrication temperature, but large scale display panel can not be fabricated in the high fabrication temperature above the melting point of glass substrate. The arc discharge can synthesize carbon nanotubes in shorter fabrication times, but it has some issues, such as (1) poor purity, (2) hard to control growth orientations of carbon nanotubes, and (3) poor emission uniformity.

Compared to laser ablation and arc discharge, using CVD for carbon nanotube growth has some features, such as (1) high purity carbon nanotubes, (2) selective growth only for catalyst metal, (3) controlling growth direction, and (4) much suitable to semiconductor fabrication procedure. However, with the display technology trend, it is the time for large

panel display. We need to synthesize carbon nanotubes using CVDs on large panel substrates. For this reason, carbon nanotube growth at low temperatures is unavoidable, but the purity of carbon nanotubes at low temperatures is poor. So, we still try some methods to increase growth rates at low temperatures, such as (1) multilayer catalysts, (2) plasma CVDs, (3) post-treatment, and so on.

1.3.2 Structure and Properties of Carbon Nanotubes

CNTs can be divided into two categories. The first is called multiwalled carbon nanotubes (MWNTs). MWNTs are close to hollow graphite fibers [1.41], except that they have a much higher degree of structural perfection. They are made of sheets of carbon atoms with a cylindrical shape and generally consist of co-axially arranged 2 to 20 cylinders「Fig. 1-7(b)」. The interlayer spacing in MWNT ($d_{(002)}$ = 0.34 nm) is slightly larger than that in single crystal graphite ($d_{(002)}$ = 0.335 nm) [1.42]. This is attributed to a combination of tubule curvature and van der Waals force interactions between successive garphene layers. The second type of the nanotube is made up of just a single layer of carbon atoms. These nanotubes are called the single-walled nanotubes (SWNTs) and possess good uniformity in diameter about 1.2 nm「Fig. 1-7(a)」. They are close to fullerenes in size and have a single-layer cylinder extending from end to end [1.43][1.44].

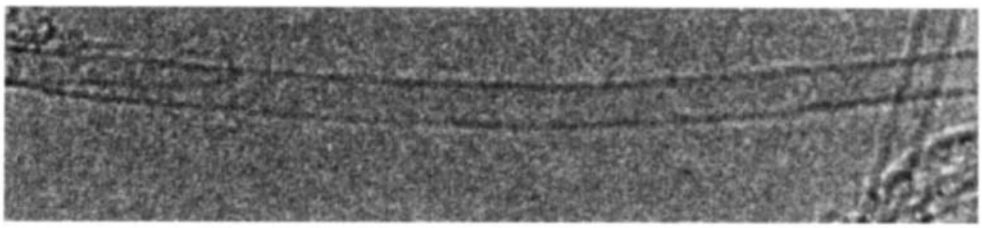

(a)

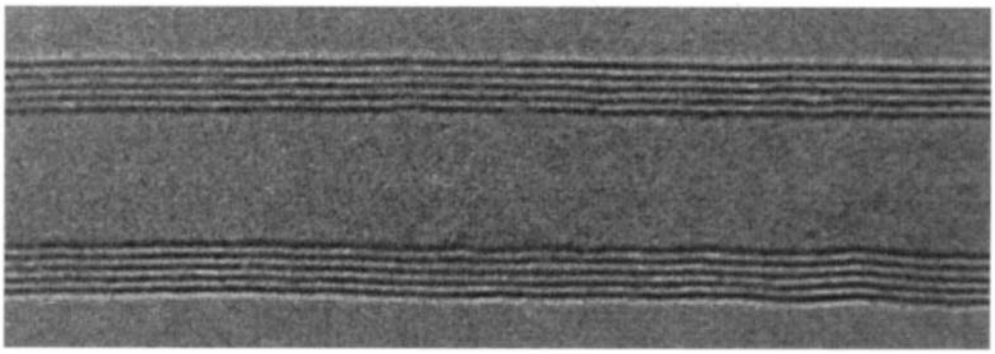

(b)

Figure 1-7 High-resolution transmission electron microscopy images of (a) SWNTs, and (b) MWNTs. Every layer in the image (fringe) corresponds to the edges of each cylinder in the nanotube assembly [1.42].

Most experimentally observed CNTs are multi-walled structures with outer most shell diameters exceeding 10 nm. Since current conduction in a MWNT is known to be mostly confined to the outermost single-walled nanotube and since band gap of a SWCNT varies inversely with its diameter, MWNTs are metallic in nature. SWNTs can be either metallic or semiconducting depending on the way the roll-up of the graphene sheet occurs - an aspect termed as Chirality, and if all the roll-up types are realized with equal probability, 1/3 of the SWNTs end up being metallic and 2/3 semiconducting. The structure of a SWNT can be conceptualized by wrapping a one-atom-thick layer of graphite called graphene into a

seamless cylinder. The way of the graphene sheet is wrapped is represented by a pair of indices (*n*,*m*) called the chiral vector. The integers *n* and *m* denote the number of unit vectors along two directions in the honeycomb crystal lattice of graphene. If *m*=0, the nanotubes are called "zigzag". If *n*=*m*, the nanotubes are called "armchair". Otherwise, they are called "chiral". Fig. 1-8 depicts these structures of a SWNT [1.45] [1.46].

CNTs have been attracting much attention for their unique physical and chemical properties such as high mechanical strength, chemical stability, high aspect ratio, super-therml conductivity, and electron emission properties [1.47] [1.48]. CNTs could be one of the strongest and stiffest materials known, in terms of tensile strength and elastic modulus respectively. This strength results from the covalent sp^2 bonds formed between the individual carbon atoms. The highest tensile strength an individual multi-walled carbon nanotube has been tested to be is 63 GPa [1.49]. Under excessive tensile strain, the tubes will undergo plastic deformation, which means the deformation is permanent. This deformation begins at strains of approximately 5% and can increase the maximum strain the tube undergoes before fracture by releasing strain energy. For the thermal conductivity of CNTs , it is predicted that carbon nanotubes will be able to transmit up to 6000 watts per meter per kelvin at room temperature; compare this to copper, a metal well-known for its good thermal conductivity, which only transmits 385 W/m/K. The temperature stability of carbon nanotubes is estimated to be up to 2800 degrees Celsius in vacuum and about 750 degrees Celsius in air [1.50].

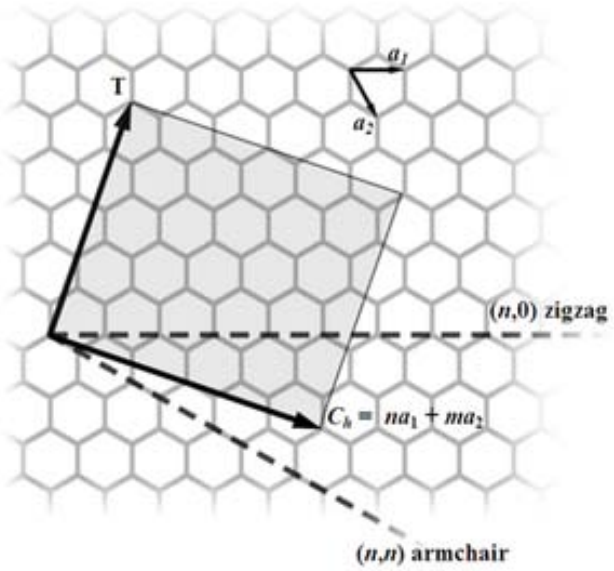

(a)

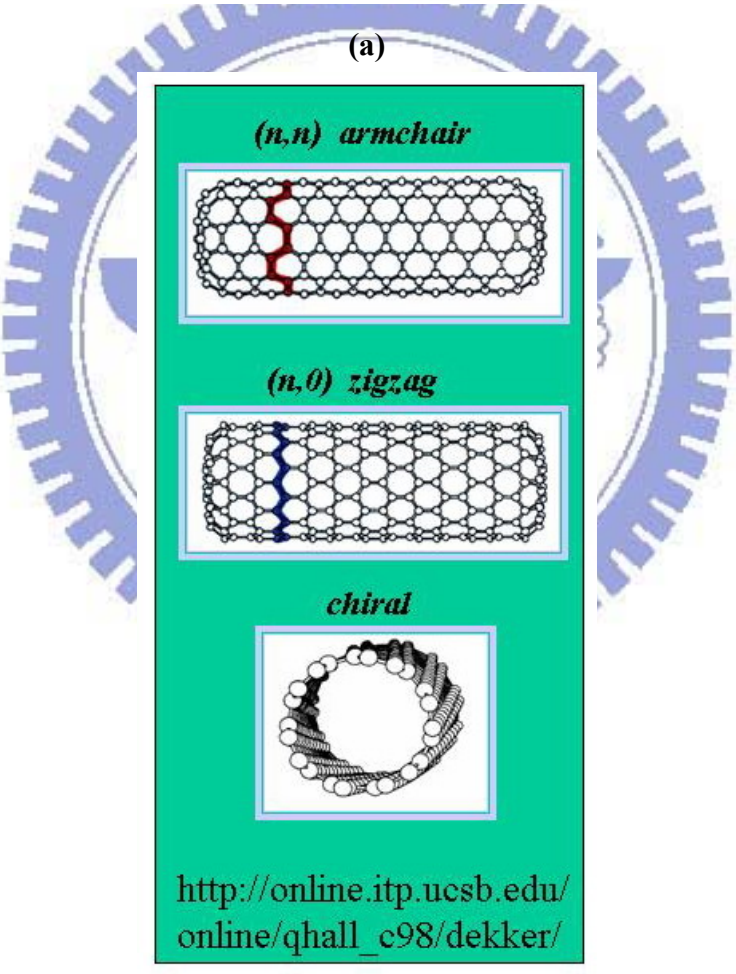

(b)

Figure 1-8 Molecular models of SWNTs with (a) chiral vector (b) the categories of the configuration [1.45] [1.46].

1.3.3 Potential Applications of Carbon Nanotubes

Since the discovery of CNTs in 1991, CNTs had attracted much attention for their unique physical and chemical properties. Their extensively potential applications lead them to become a super star of nano technology, which cover: (1) Chemical sensor [1.51], (2) IR detector, (3) Nano-conducting Wire, (4) Vehicles for Hydrogen Storage [1.52], (5) Field Effect Transistor [1.53], (6) Field Emission Display (FED), (7) Probe of AFM and etc.

In the wide-ranging applications of CNTs, FED arouses researchers' interest particularly. In virtue of the superior field emission characteristics, CNTs are applied to the emitting source of cold cathode. The advantages of FED are its low response time, wide view angle, high brightness, high working temperature range and well combination with mature phosphor technology. However, a major problem needs to be solved in this field. It is not allowed to effectively analyze CNTs on a flat panel at relatively lower temperature (<500˚C) and this barrier restriction obstructs the development of CNT-FED so far. The products of CNTs FED is shown in Fig. 1-9.

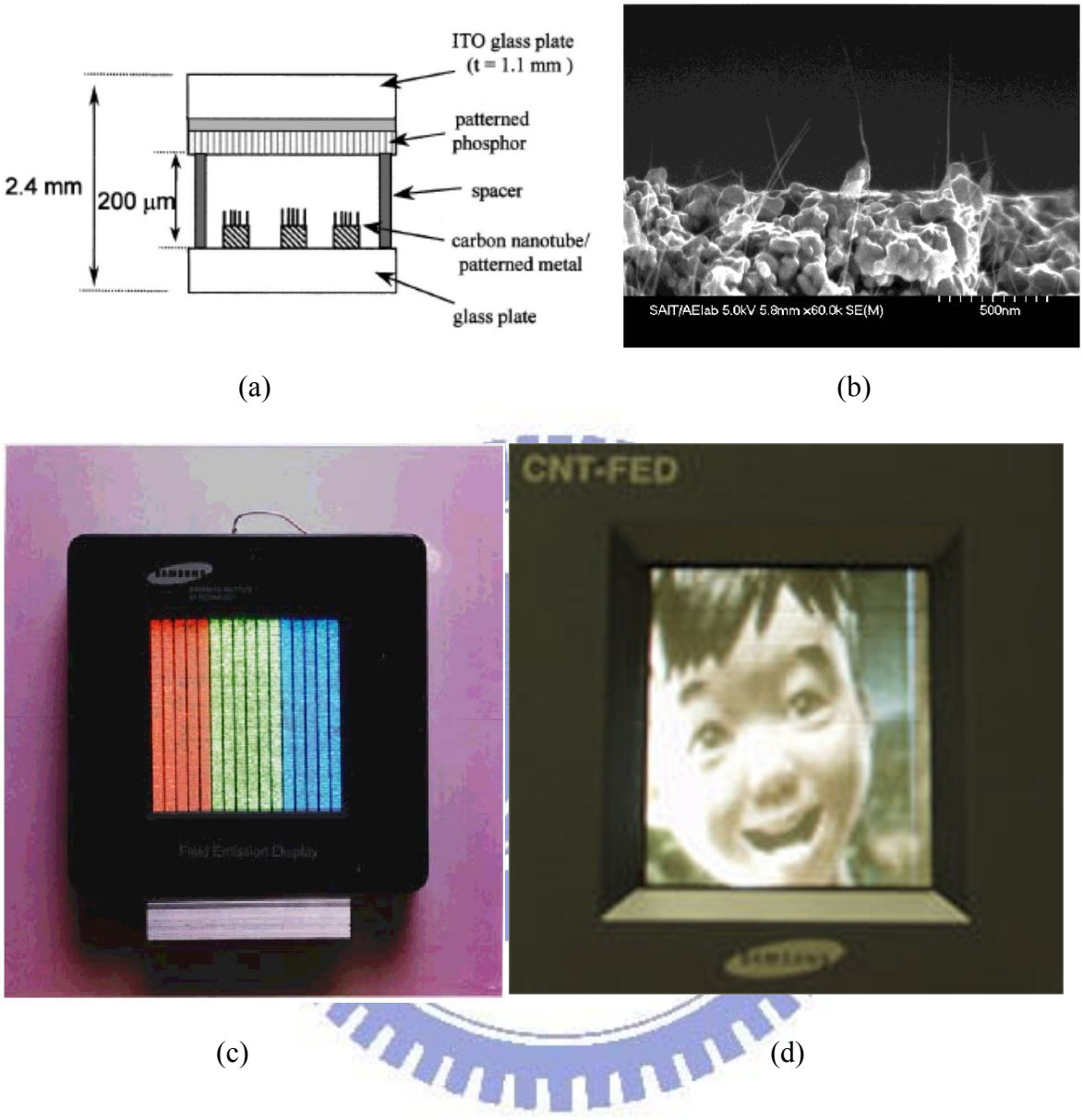

Figure 1-9 (a) Schematic structure of the fully sealed 128 lines matrix-addressable CNT-FED. (b) Cross section SEM image of CNT cathode from Samsung's FED.(c) A 4.5-inch FED from Samsung, the emitting image of fully sealed SWNT-FED at color mode with red, green, and blue phosphor columns. (d) A prototype of 5" CNT flat panel display by Samsung. [1.54]

1.4 Motivation

For technological commercialization of products today, the cost is the most important issue. The main concern for manufactures is cost down. It is worth noted that lower cost will provide more advantages for a product. In our research of CNT field-emission backlight unit (FE-BLU), we ensure that if the cost of field-emission backlight unit (FE-BLU) continuously decreases, it can even replace the traditional light bulbs or light-emitting diode (LED) in the future. So the following motivation will focus on decreasing the cost and increasing the quality of CNT FE-BLU.

Nowadays, the backlight unit of liquid crystal display (LCD) is CCFL, but CCFL backlight system contains several components for providing planar and uniformity illumination. The following are designs of LED-BLU:

1. Reflection sheet is used to reflect the light beam of wrong direction from the lamp.
2. Light guide panel is used to transform spot or linear light source to planar light source.
3. The prism sheet and diffusion sheet are playing the crucial roles in spreading the brightness.

Fig. 1-10 shows the complex system of LED backlight unit on LCD below [1.55] [1.56]. The uniformity become better due to the uniformity-assisted layer of backlight system, but thickness and cost increase obviously. For a LCD, the cost of backlight system on the total cost is about 14% for 17inch TFT-LCD, and 21% for 32inch TFT-LCD, which are shown in Fig. 1-11 [1.57]. As this result, we could easily to make a prediction that we will require more cost on backlight system for a larger size TFT-LCD.

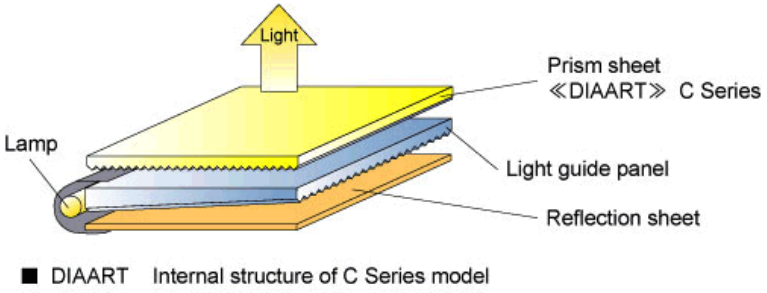

■ DIAART Internal structure of C Series model

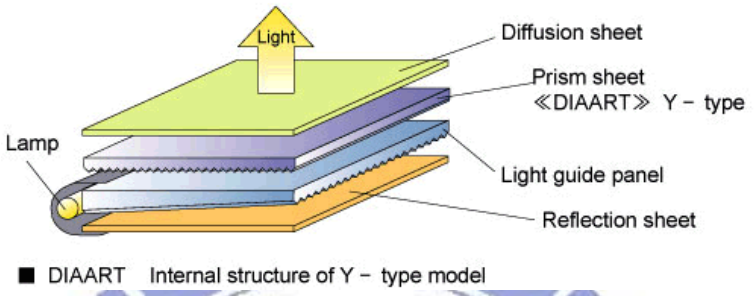

■ DIAART Internal structure of Y－ type model

(a)

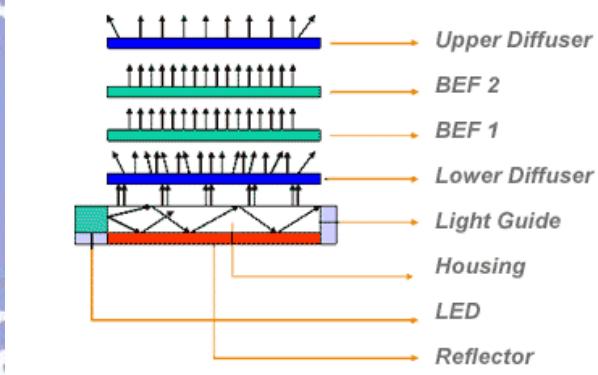

(b)

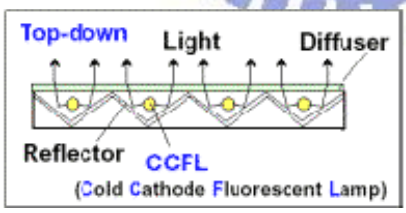

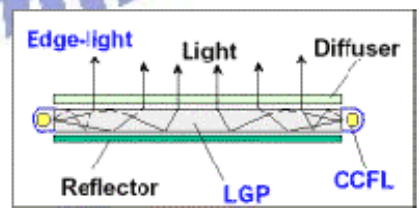

(c) (d)

Figure 1-10 The profile of LED backlight system (a) shows names of every sheet. [1.55] (b) direction of light beams in backlight system. (c) bottom lighting type of backlight system. (d) edge lighting type of backlight system. [1.56]

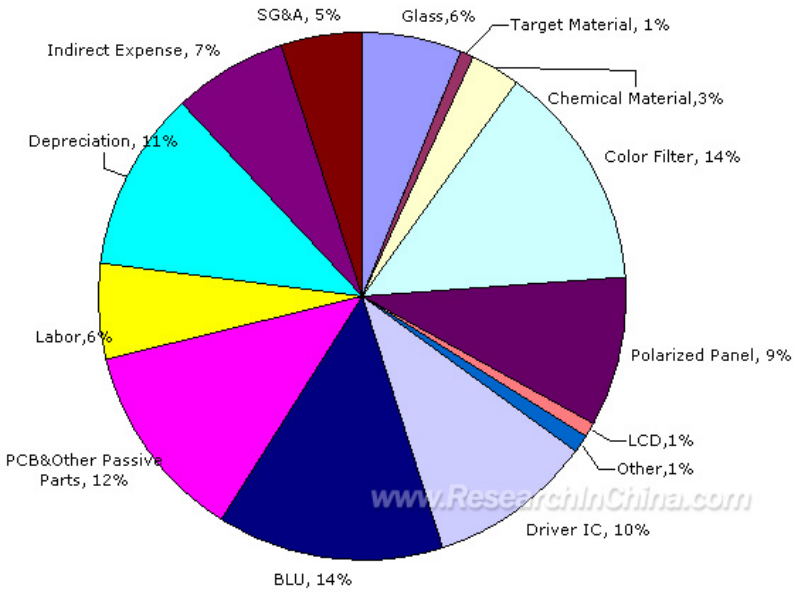

(a)

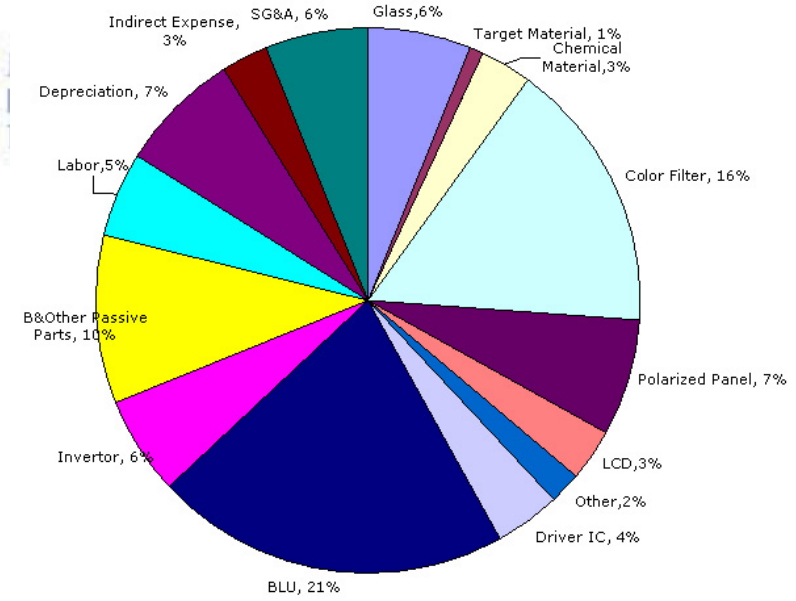

(b)

Figure 1-11 The cost of the overall (a) 17inch (b) 32inch TFT-LCD [1.57].

Instead of LED-BLU, FE-BLU is another aspect for illumination. Comparing between LED and FE backlight system, we could observe easily few advantages of FE-BLU shown below:

1. The efficiency of FE-BLU is not affected by thermal-effect. Since it is a proto-type of vacuum microelectronic. But thermal-effect give rise to degradation of the brightness or efficiency of LED decrease obviously.
2. FE-BLU is a planar light source showing a better feasibility for larger scale as compare with LED spot light source.
3. For TFT-LCD, using FE-BLU will reduce cost of backlight system and decrease the thickness of display as well.

In our research, we have chose the carbon nanotubes as the emitters of FE-BLU because of some superior properties of CNTs for field-emission. One of the superior properties is low work function (~5eV), high conductivity, small tip of radius curvature, low turn-on electric-field, and high emission current density. Another properties are high chemical stability and high mechanical strength, so CNTs emitter is still stable under high electric-field and current density.

Although CNTs have superior field emission characteristics, there are still some drawbacks needed to be overcome, i.e. uniformity and reliability. The degradation of field emission current and brightness due to week adhesion between CNTs and substrates will result in poor reliability. Problem of uniformity is caused by screening-effect, which is determined by dense of emission emitters. The screening-effect is shown in the Fig. 1-12, indicating that the effective field is affected by the height and density of emitter.[1.58]

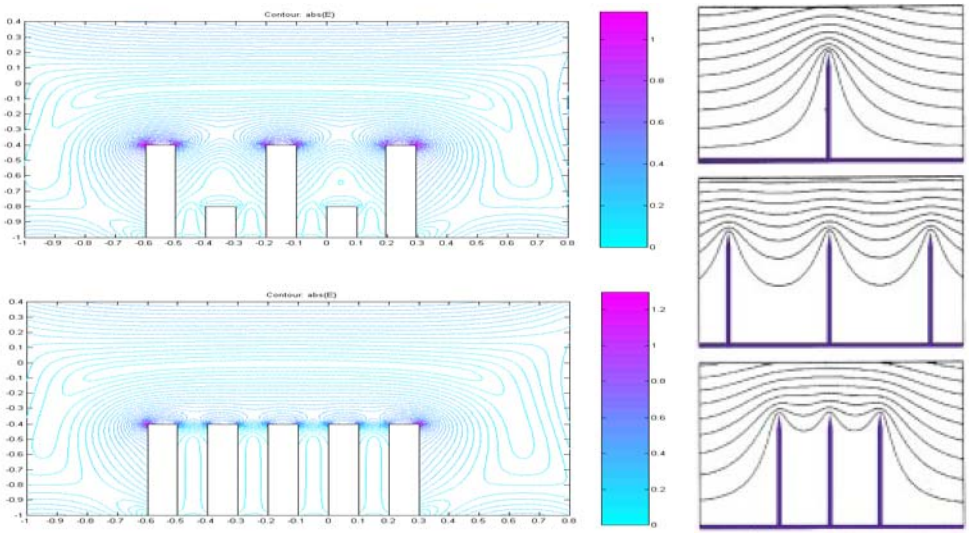

(a) (b)

Figure 1-12 The screening-effect occurred (a) because of height (b) because of distance between emitter sites [1.58].

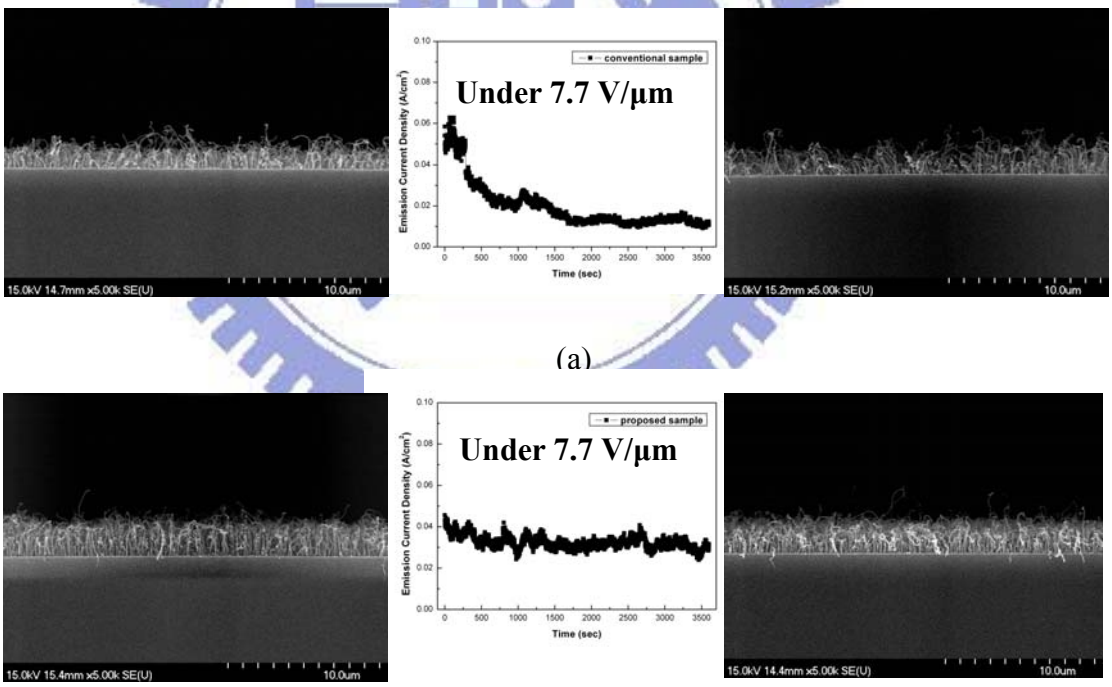

Figure 1-13 Improvement of Luminescent Uniformity via Synthesizing the Carbon Nanotubes on an Fe–Ti Co-deposited Catalytic Layer (a) conventional catalyst (b) co-deposited catalyst [1.62].

There are many ways to solve problem of reliability. One is mechanical coating on grown CNTs, such like spin-on-glass (SOG) coating and polymethyl methacrylate (PMMA) coating [1.59][1.60]. Another is CNT printing with Zinc powder mixture [1-61]. Although two method improve the adhesion of CNTs on substrate, it is also increase the cost due to a complex step in the procedure. The way provides with both increasing reliability and keeping low cost is co-deposition of catalyst and buffer layer. Co-deposition means that we produce a solid-solution of catalyst and one buffer metal. In our group, we already got a result of co-deposited catalyst and it really improved the reliability shown in Fig. 1-13 [1-62].

Uniformity is also a very important issue of CNT FE-BLU. There were a lot of ways to enhance uniformity, such as (a) growing CNTs on AAO[1.63], (b) plasma post-treatment[1.64], (c) elastomer or biasing printing[1.65][1.66]… and so on. Here we use the patterned pillar-like CNTs improving the uniformity of emitters. CNT pillar arrays have well-control density and morphology of CNTs, and, moreover, it has been reported that the screening-effect of CNTs can be effectively reduced by the density control of the pillars. Therefore, not only the field emission characteristics can be enhanced from the compromise of screening-effect and emitter sites, but also the uniformity will slightly be enhanced from the decreasing of screening-effect. By using pillar-like CNTs as a light source for BLU, high brightness and excellent uniformity could be achieved by easy and cheap process.

In the growth reaction of CNTs, the diffusion of carbon in the catalyst metal has been believed to be the rate-determining step. The growth rate of CNTs can be described by an Arrhenius equation that the activation energy is the diffusion energy of carbon in the metal [1.67]. Plasma-enhance chemical vapor deposition (PECVD) is more suitable method for CNT synthesis because PECVD has the much lower activation energy compared to thermal CVD [1.68]. However, PECVD has some drawbacks, such like poor plasma uniformity, and hard to fabricate large panel display or large-size BLU.

For the reasons of cost down and fabrication of large-size BLU, we have utilized the

thermal CVD (TCVD) in our study. It has been investigated that the nano-size catalyst could enhance CNTs growth at low temperature because nano-size catalyst particles are more active compared to bulk catalyst and the melting point of particles decrease as their sizes decrease [1.69][1.70]. The following Fig. 1-14 shows surface diffusion or surface pre-melting of nano-size particles takes place when the temperature is raised above 500˚C whose temperature is close to $0.4T_m$ [1.70].

A multilayer catalyst, Co/Ti/Al, was successfully employed to synthesize CNTs at 550℃ and 500℃ by thermal CVD previously. Following this result, we could fabricate CNTs on the glass coated with electrode or indium tin oxide (ITO), for large area application.

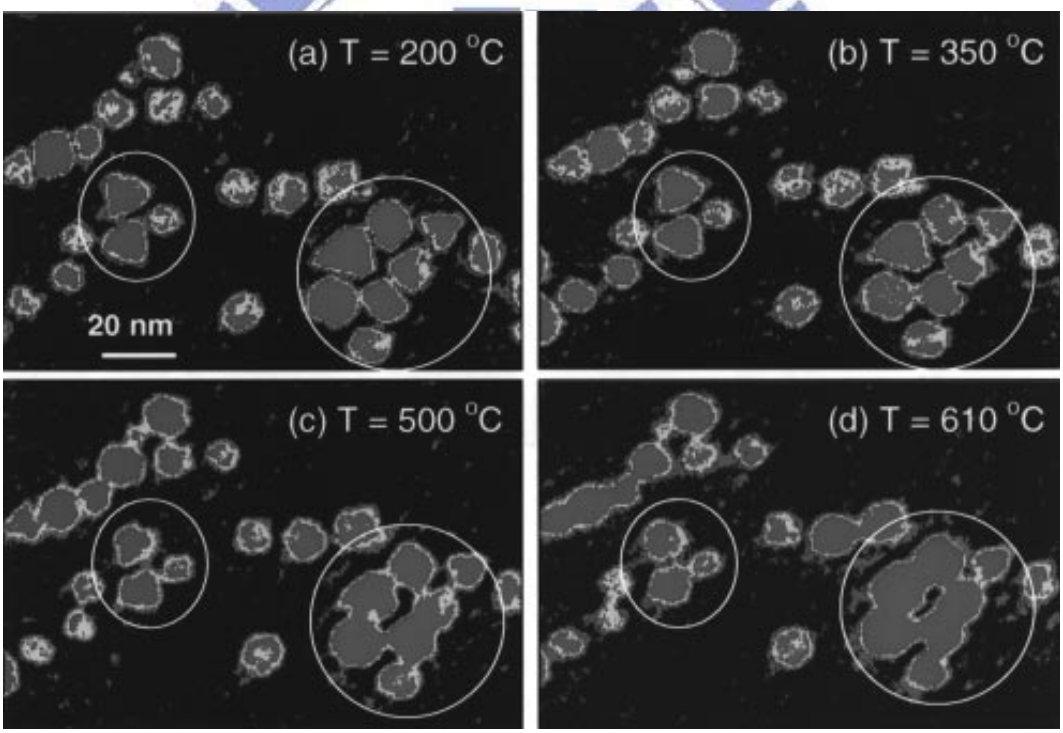

Figure 1-14 In-situ TEM images recorded from a region of capped Pt nano-crystals at various specimen temperatures. Surface diffusion or surface pre-melting of nano-size particles takes place when temperature is raised about $0.4T_m$.

The normal triode gate structure is shown in Fig. 1-15[1.71][1.72].The phosphors provide high efficiency into light by bombardments of electrons at enough high voltages of the anode plate. For field emission display (FED), there is a problem of triode gate structure, i.e. cross-talk noise, which is due to the electron beam spreading caused by gate electrode. Cross-talk noise is a drawback for FED, but it has merits for FE-BLU since the electron spreading would result in large area of beam overlapping, which could improve the uniformity of photo-luminescent images on anode plates. Therefore, uniformity could be enhanced just because of enlargement of cross-talk noise.

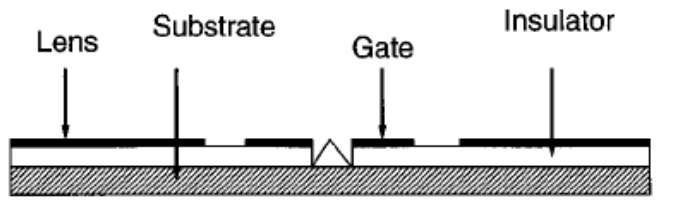

(a)

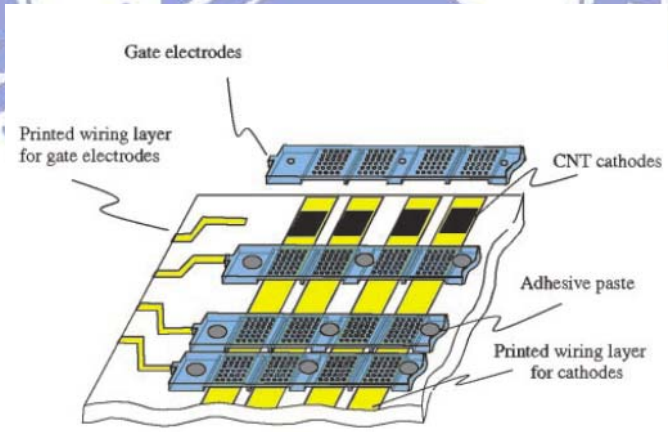

(b)

Figure 1-15 Examples of triode gate structure

(a) planar gate [1.71] (b) mesh gate. [1.72].

1.5 Thesis Organization

In Chapter 1, the overview of vacuum microelectronics, basic principles of field emission theory, and research motivations are described.

In Chapter 2, we utilize the Co-Ti/Al (5nm/10nm) co-deposited catalyst compared to other kind of multilayer catalyst from our prior study. The improvements of reliability and uniformity in CNT FE-BLU, and increasing growth rate at low temperature are included to realize the properties and mechanism of Co-Ti/Al co-deposited catalyst thin film.

A simply lateral triode field emission device is fabricated in Chapter 3, we have utilized the cross-talk noise, which is one of the triode FE structure drawback, enhancing the uniformity of backlight unit.

Finally, the summary and conclusion are provided in chapter 4.

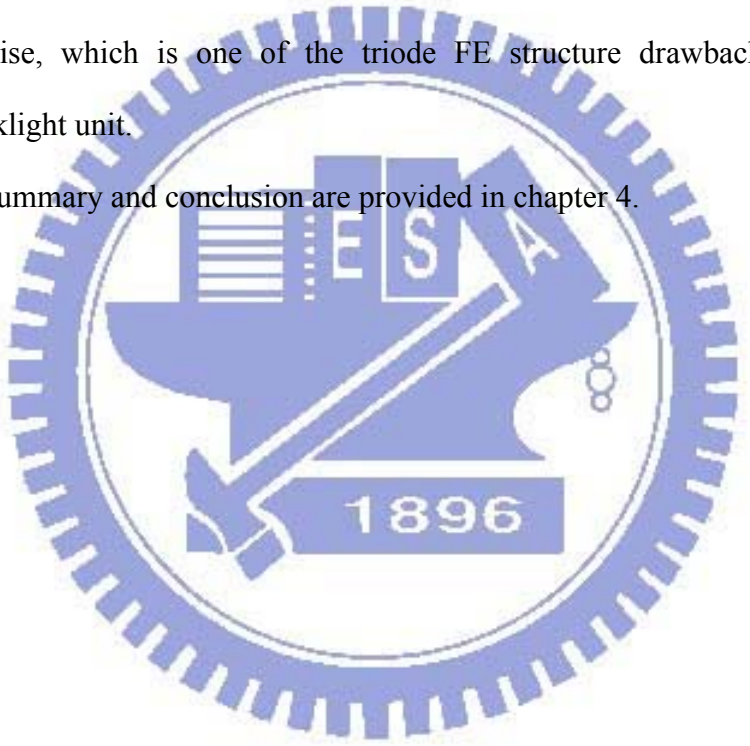

Chapter 2

Fabrication of Pillar-like CNT Field Emitters with Low Temperature Processes

2.1 Introduction

CNTs own some attractive physical and chemical characteristics, like high aspect ratio, adequate work function (~5eV), small tip radius of curvature, good chemical stability, strong mechanical strength, high conductivity, and electron emission properties [2.1-2.2].

However CNT-BLUs exist two crucial problems: one is inadequate lifetime which caused by poor reliability, and the other is bad uniformity which caused by screening-effect.

For reliability, two kinds of issues were observed: (1) abrupt decreases in emission current with increasing electric field and (2) a gradual degradation in emission current with high emission current density for a long period. Several reports indicated the weak adhesion on the interface of CNTs and substrate could cause an abrupt decrease in emission current resulting from a mechanical damage at high electric field [2.3]. Furthermore, high contact resistance between CNTs and substrate could result in a gradual degradation in emission current because of the Joule heat generated in a high resistive contact region [2.4]. Some methods have been reported for improving the adhesion or lowering contact resistance on the interface by post-treatment such as spin-on-glass (SOG) or polymethyl methacrylate (PMMA) coating, and zinc powder mixture [2.5-2.6]. Nevertheless, some of them might increase the complexity of processes and the cost of fabrication.

For uniformity issue, the screening-effect and non-uniform height of CNTs play the two most important roles. The simulation of the equipotential lines of the electrostatic field is shown in Fig.2-1 [1.58]. In order to avoid screening-effect, on some reported researches, such

as plasma post-treatment [2.7] and growing on AAO substrate [2.8], however these methods also increase the complexity and cost of processes.

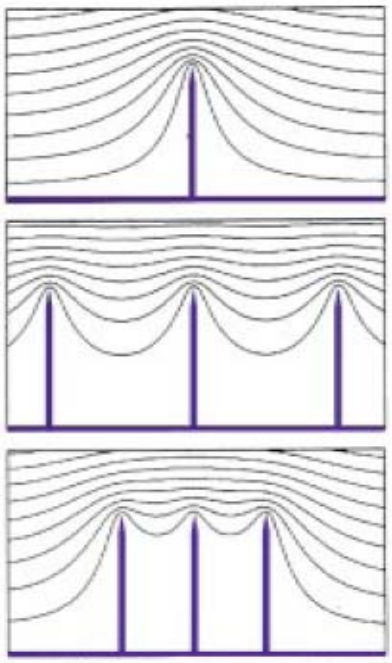

Figure 2-1 Simulation of the equipotential lines of the electrostatic field for tubes of different distances between tubes. [1.58]

By thermal-CVD, the growth rate of CNTs at low temperature is slow. It has been known the size of catalyst nano-particles after pretreatment is critical importance of the CNTs growth, including the each CNT's diameter, length, and density. Therefore controlling of the surface morphology of nano-sized catalyst particles is an essential prior to the CNTs growth. According to Lindemann criterion, the melting point decreases as the catalyst particles sizes reduces as the Fig. 2-2 [2.9].

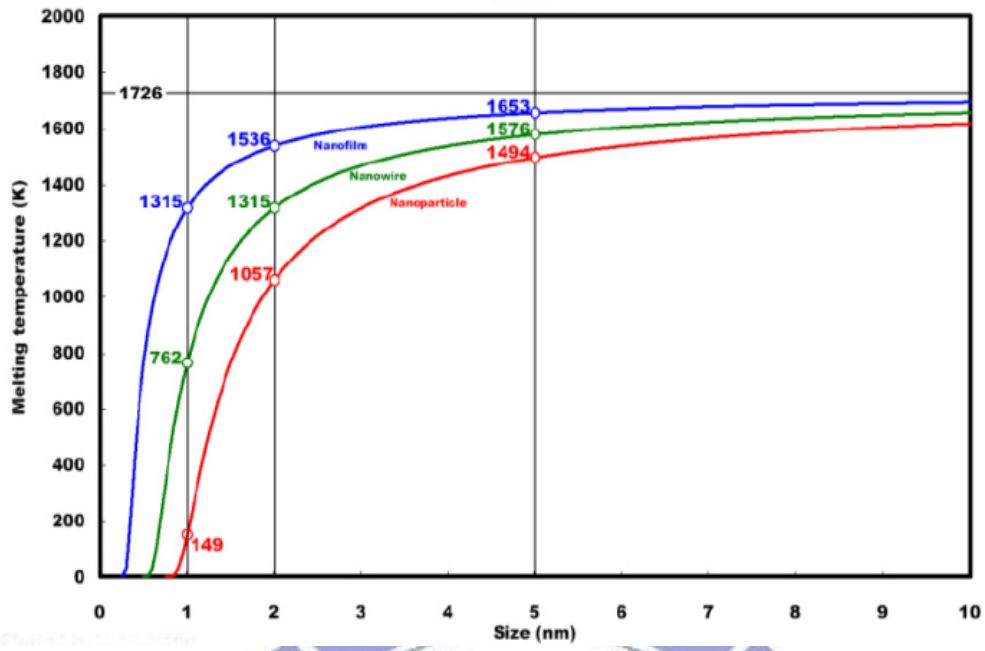

Figure 2-2 Lindemann criterion. [2.9]

And the nano-sized catalyst particles are more active compared with bulk catalyst metals due to surface effect [2.10]. The melting temperature of nano-particles is based on size-dependent cohesive energy by considering the surface effects. The melting temperature of nano-particles (T_{mp}) is linear to the reciprocal of the crystal size, i.e., $T_{mp}= T_{mb}(1-C/D)$, where T_{mb} is the melting temperature of the corresponding bulk materials, D is the crystal size, and C is a material constant. Apparently, the proper determination of D is key issue. The smaller catalyst nano-particles with the lower melting temperature could be utilized to the CNTs growth at low temperature in thermal CVD to increase growth rates. From the AFM image as Fig.2-3 [2.11], the nano-particles of the co-deposited catalyst sample are more uniform and smaller than those of the conventional one. Accordingly, we applied the novel method to CNTs growth at low temperature for understanding the properties and mechanism of co-deposited catalyst.

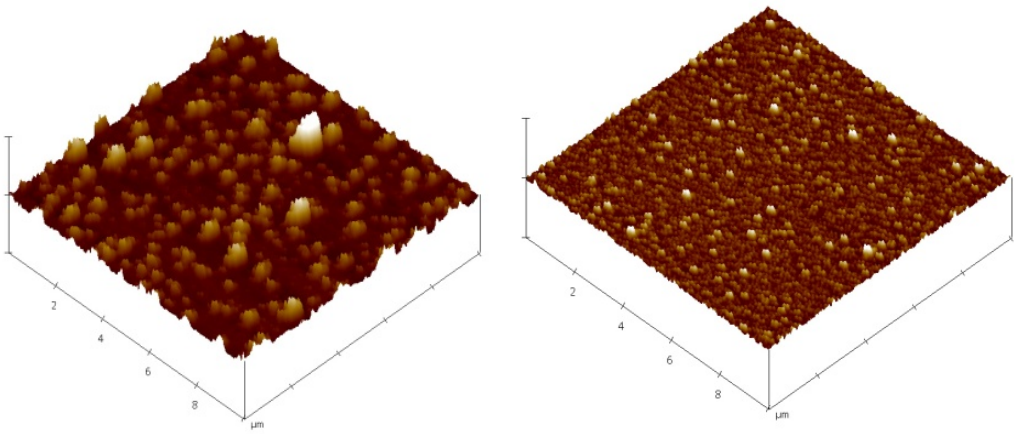

Figure 2-3 AFM of the nano-particles after pretreatment

(a) the pure Fe catalyst layer, and (b) the Ti-Fe co-deposited catalyst layer. [2.11]

The schematic of a typical BLU is shown in Fig.2-4 [2.12] including light source, reflector, light guide, diffuser, and brightness enhancement film (BEF). The light source can be an incandescent light bulb, light emitting diodes(LED), cold cathode fluorescent lamp (CCFL), hot cathode fluorescent lamp (HCFL). All the backlights employ a diffuser and a BEF. The diffuser posited between the light source and the display panel is used to scatter the light for display uniformity. The BEF is used to enhance display brightness. The cost structure of materials for TFT-LCDs is described as Fig. 1-10 [1.57].

If we success to solve the reliability and uniformity problems, CNT-BLU will replace the traditional backlight system of LCD, it will be ensure to decrease amount of cost.

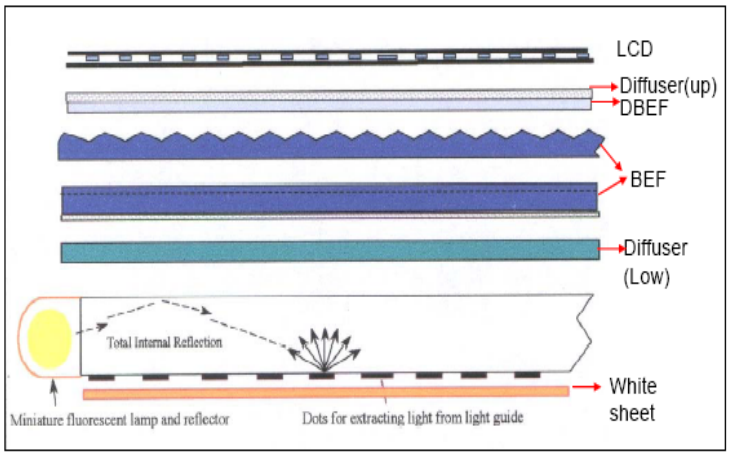

Figure 2-4 schematic of a typical backlight unit. [2.12]

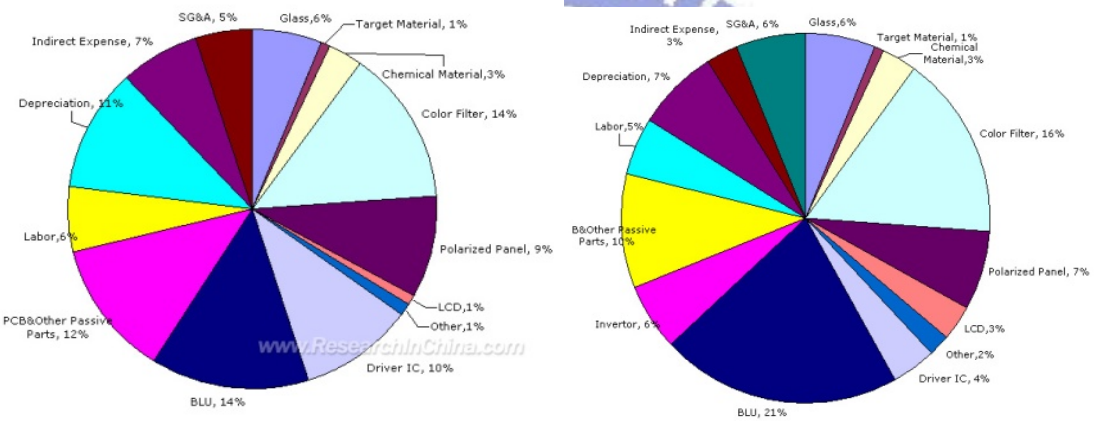

Figure 1-10 cost structure of materials for TFT-LCDs of

(a) 17inch LCD (b)32inch LCD. [1.57]

First of all, we used titanium as interlayer of the multilayer catalysts for CNT synthesis because it was found the most fitting one for CNT growth at low temperature. Then we fabricated pillar-like CNTs pattered structure on silicon substrate to improve the morphologies. Our group has done some research on multilayer and co-deposited catalysts, but the catalyst are not the optimization for growing CNTs at low temperature. Finally, we accomplished some analysis for the above mentioned. The whole experimental procedures is shown below.

2.2 Experimental Procedures

2.2.1 Forward Arrangement

We have chosen 4 inch n-type silicon (100) wafer as our experimental substrate. After RCA clean and lithography processes, we defined several kinds of pillar-like circle patterns for CNT flied emission arrays which diameter is 6μm. The pillar-spacing is (1) 25 μm in experiment A, (2) 25 μm in experiment B, and (3) 3 to 30 μm in experiment C.

In our research, 1000Å Chromium layer was deposited by dual E-gun evaporation (JAPAN ULVAC EBX-10C) as the cathode between the substrate and catalyst. The catalyst in experiment A, we have chosen four kinds of different catalysts:

1. (Fe-Ti) 20Å iron and 30Å titanium co-deposited catalyst,
2. (Co-Ti) 20Å cobalt and 30Å titanium co-deposited catalyst,
3. (Co-Ti/Al) 20Å cobalt and 30Å titanium co-deposited on 100Å aluminum catalyst,
4. (Co/Ti/Al) multilayer catalyst formed of 20Å cobalt, 30Å and 100Å aluminum.

These catalysts were sequentially deposited on substrates by magnetron sputtering (Ion Tech Microvac 450CB) at the pressure of 7.6×10^{-2} Torr at room temperature. This sputtering system consisted of three sputtering source for different material targets and two power source for co-deposition, so our multilayer catalysts could be sequentially deposited without breaking the vacuum environment and co-deposited uniformly.

2.2.2 CNTs Synthesis

In our researches, an atmospheric pressure thermal chemical vapor deposition (T-CVD) system is used for CNTs synthesis, shown in Fig.2-5. It consists of a 2-inch-diameter horizontal quartz tube, an electric heating system, reaction gas supply, and related mass flow controllers.

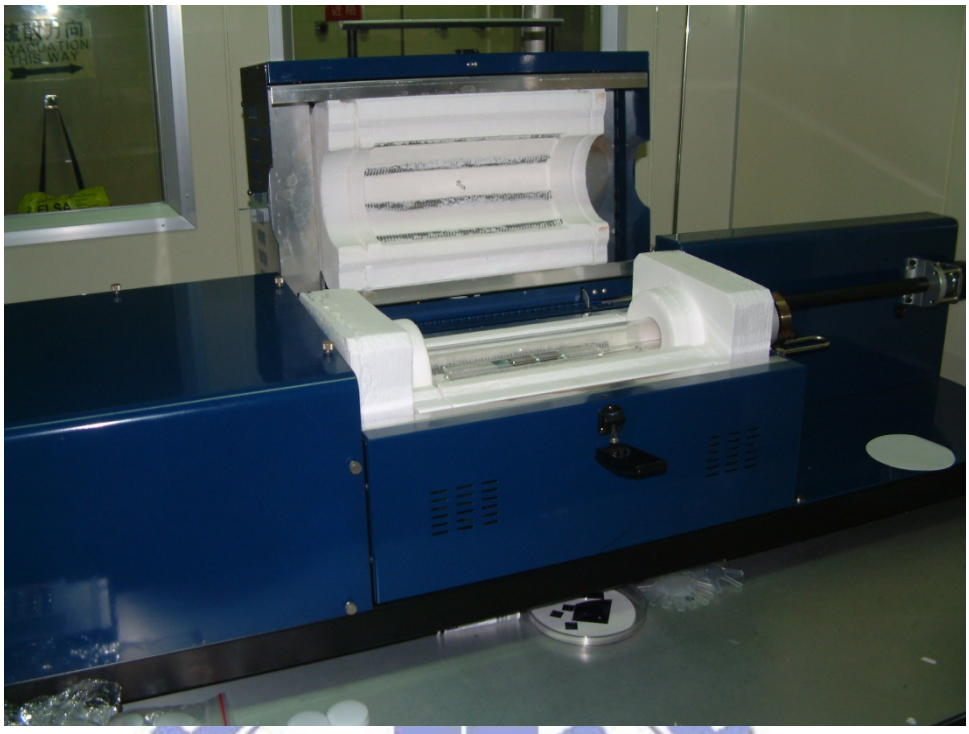

(a)

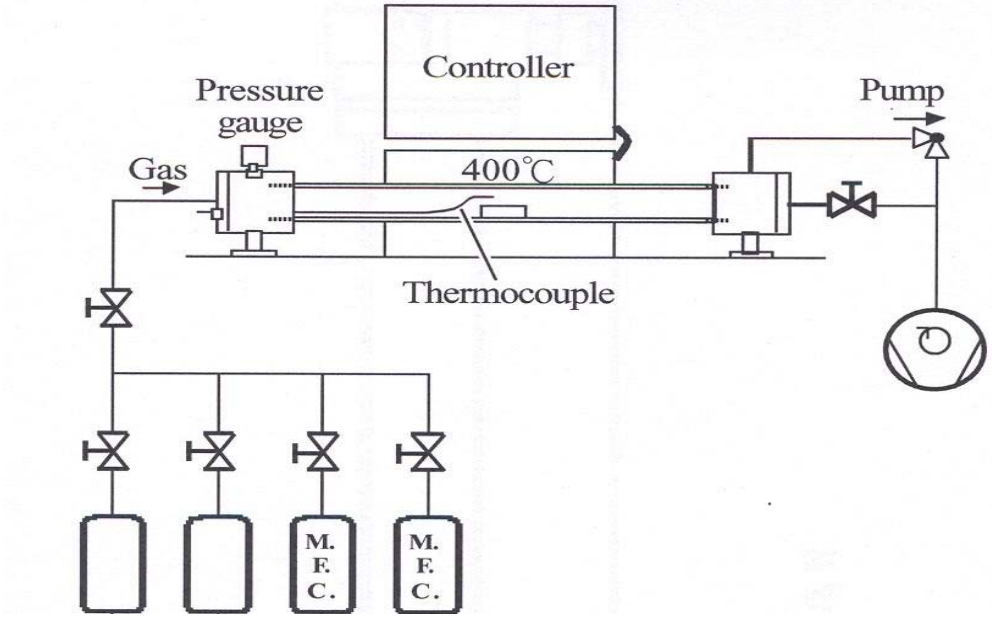

(b)

Figure 2-5 (a) Photograph and (b) schematic picture of thermal CVD.

Firstly, Samples loaded into the quartz tube were heated to the predetermined temperatures (500℃ to700℃) in nitrogen flow (1000 sccm) to avoid catalyst be reacted during steps of heating. Secondary, before CNTs growing, hydrogen flow (50 sccm) was into

quartz tube about 5 minutes to reduce the catalyst metal to the metallic phase, then transforming into nano-particles. Thirdly, CNTs were grown at designated temperatures according to the optimal results of our group past researches, we had decided the flow rate of hydrogen is 10 sccm, 1000 sccm for nitrogen and 125 sccm for ethylene[2.13]. Last of all, samples were furnace-cooled to room temperature in nitrogen flow (3000 sccm). The schematic of process is shown below in Fig.2-6.

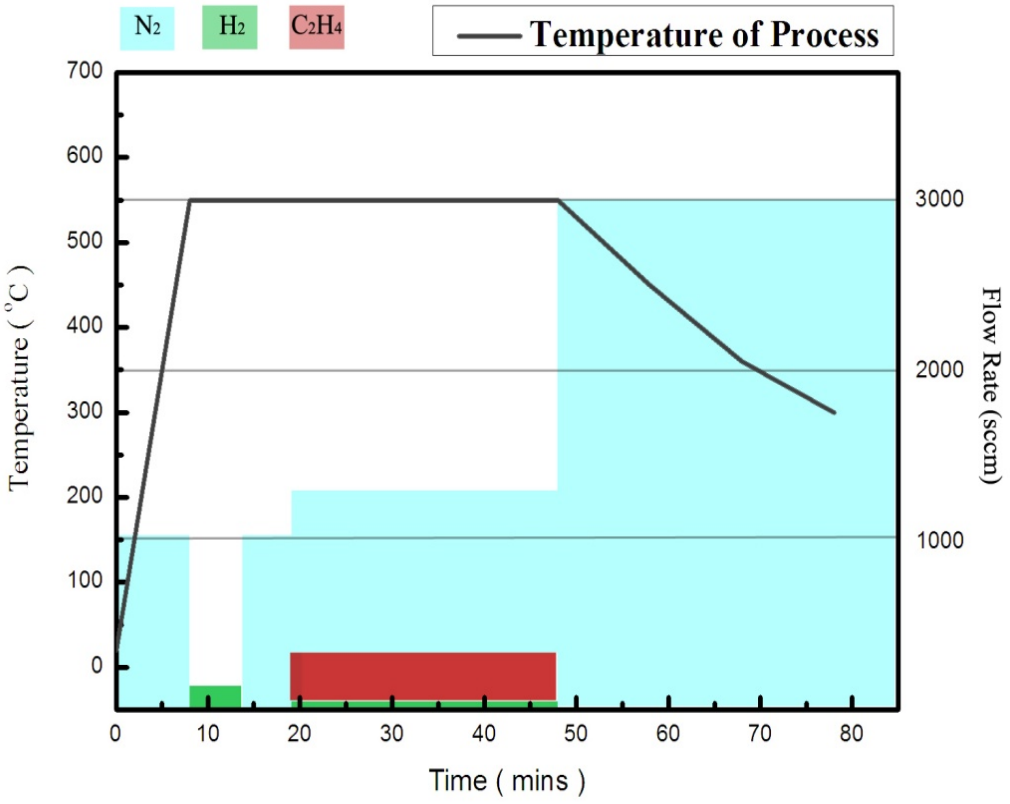

Figure 2-6 Process of CNTs synthesis (an example of CNTs growing 45 min at 550℃.

2.2.3 Analysis

The morphologies of pre-treatment catalyst were observed by atomic force microscopy (AFM), and the morphologies of CNTs' samples were characterized by scanning electron microscopy (SEM), and we have used Hitachi S-4700I SEM in our researches. The finer internal structures of interface of CNTs and nano-sized catalytic materials were examined by high-resolution transmission electron microscopy (HRTEM), JEOL JEM-2000EX and X-ray energy dispersive spectroscopy (EDS) respectively.

Electric characteristics of CNTs field emission were measured with a parallel diode-type configuration in a high-vacuum chamber with the pressure of 5×10^{-6} Torr. A glass substrate coated with indium tin oxide (ITO) and P22 phosphor (ZnS: Cu, Al) was used as the anode plate, and the distance between the cathode and the anode plate was set to be 150 μm. The emitting area was variable, which was determined by pillar-spacing and pattern-area.

Anode voltages is sweep-type from 0 V to 1000 V which were applied at intervals of 10 V by a source measure unit (Keithley 237), as Fig. 2-7 for the verification of field emission characteristics while the cathode was biased at 0 V.

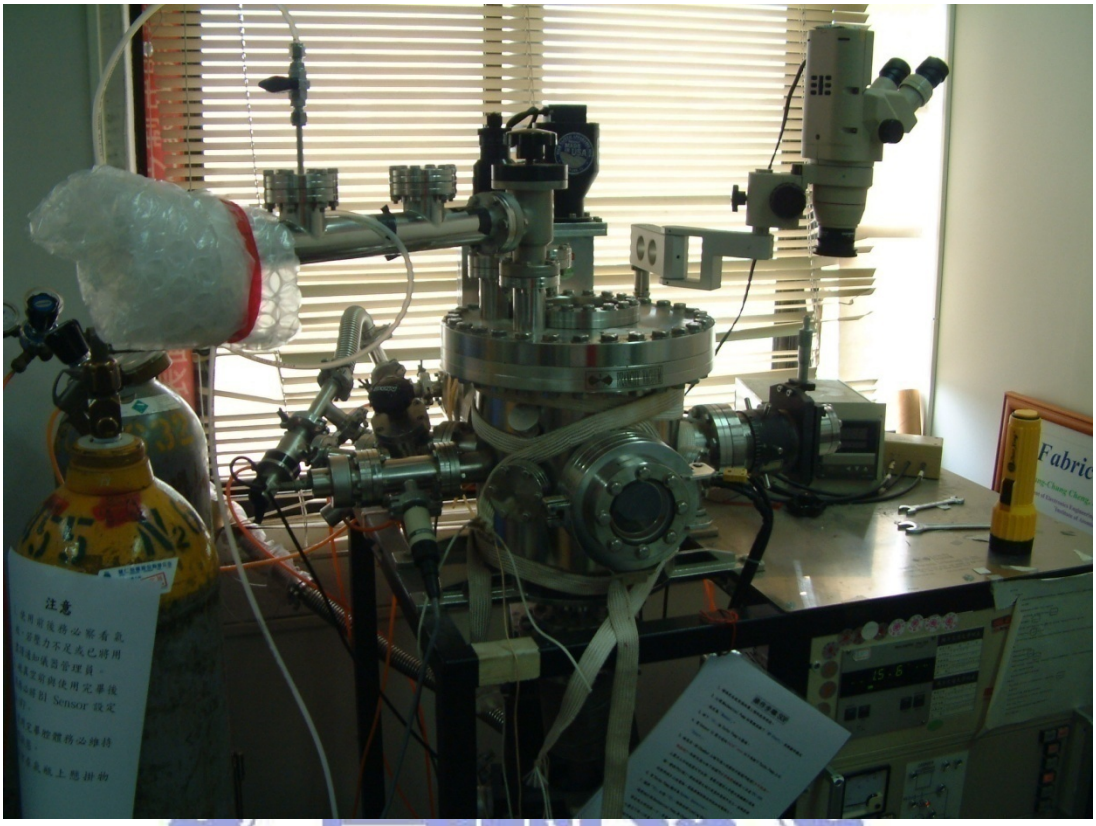

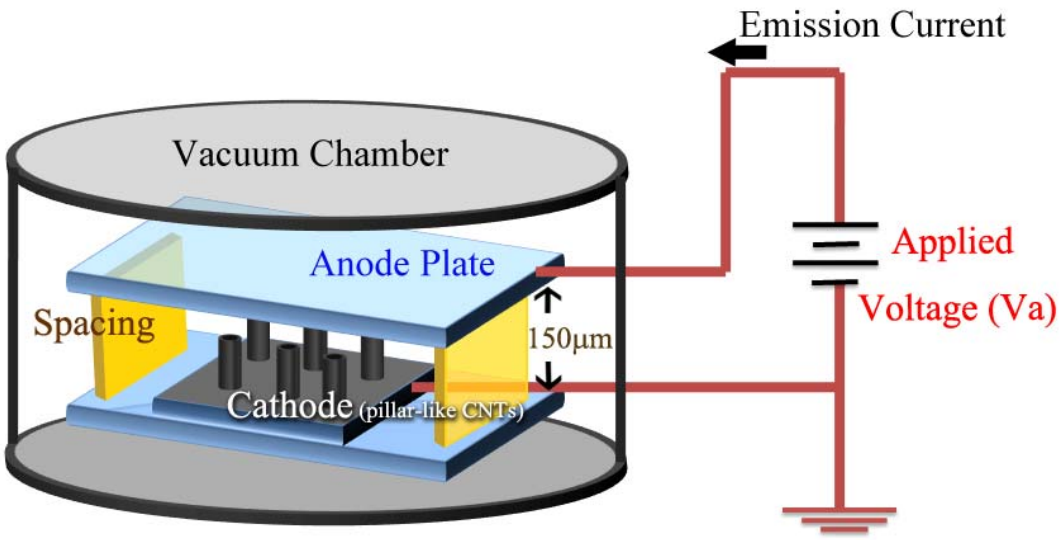

Figure 2-7 High vacuum measurement system.

2.3 Experimental Design

The scheme of the whole experimental procedures was shown below as Fig. 2-8.

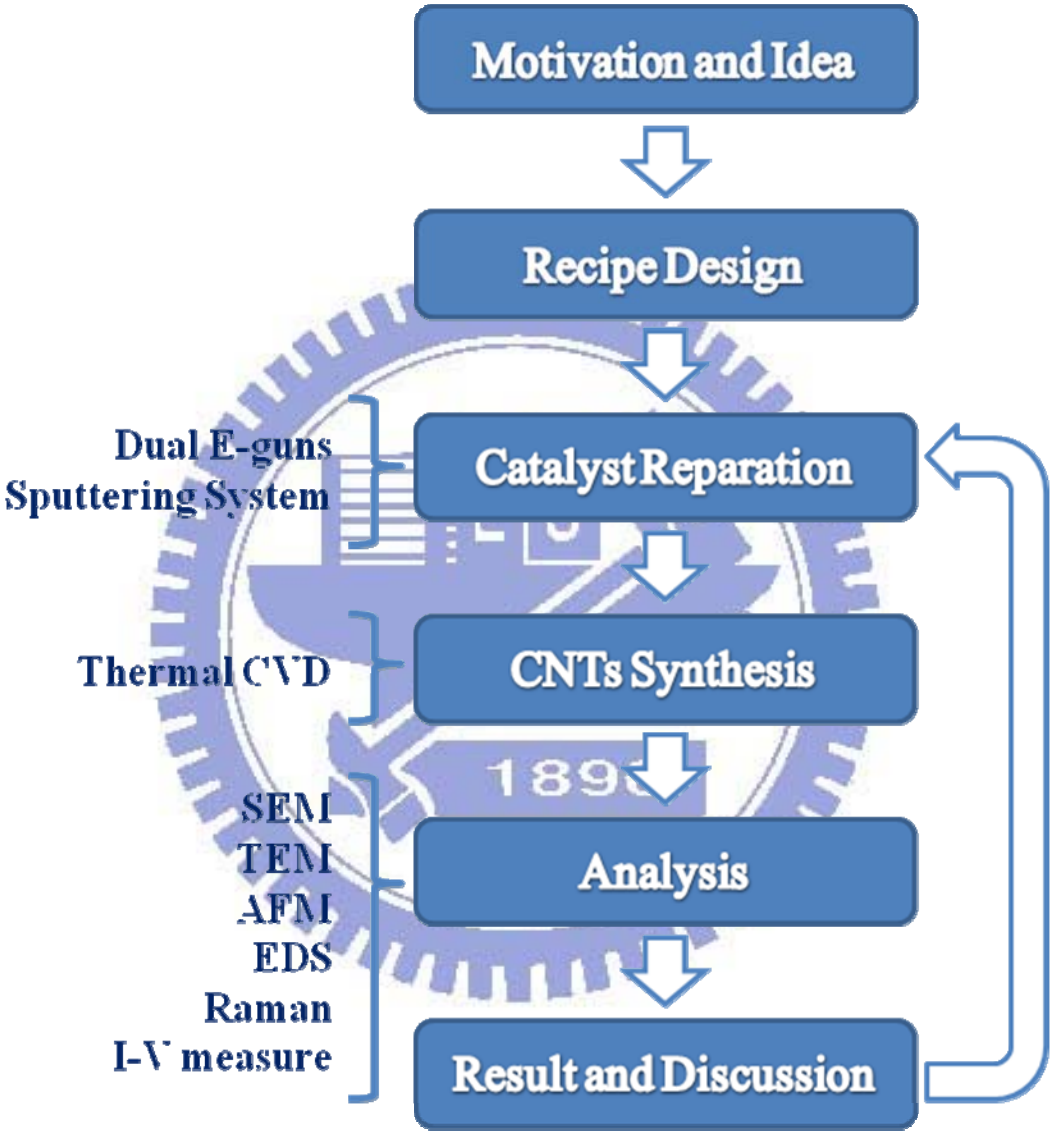

Figure 2-8 The scheme of the whole experimental procedures.

2.3.1 Experiment A: Comparing Different Catalyst for CNT Growth

Constituent of catalyst is important to provide catalysis for CNTs' growing, different materials and constituents give different reactivities. Here, four kinds of different catalysts, (Fe-Ti) 20Å iron and 30Å titanium co-deposited catalyst, (Co-Ti) 20Å cobalt and 30Å titanium co-deposited catalyst, (Co-Ti/Al) 20Å cobalt and 30Å titanium co-deposited on 100Å aluminum catalyst, (Co/Ti/Al) multilayer catalysts formed of 20Å cobalt, 30Å and 100Å aluminum were sequentially deposited on substrate by magnetron sputtering system. The total experimental process of profile was shown schematically in Fig. 2-9 on next page.

The procedures of pretreatment and CNTs growth was shown in Fig.2-6 before. The growing time is 60 minutes for each temperature, which vary from 500℃ to 700℃ with interval of 50℃. Finally, this method should be successful to find out the most appropriate constituent of catalyst for our predictive growing temperature.

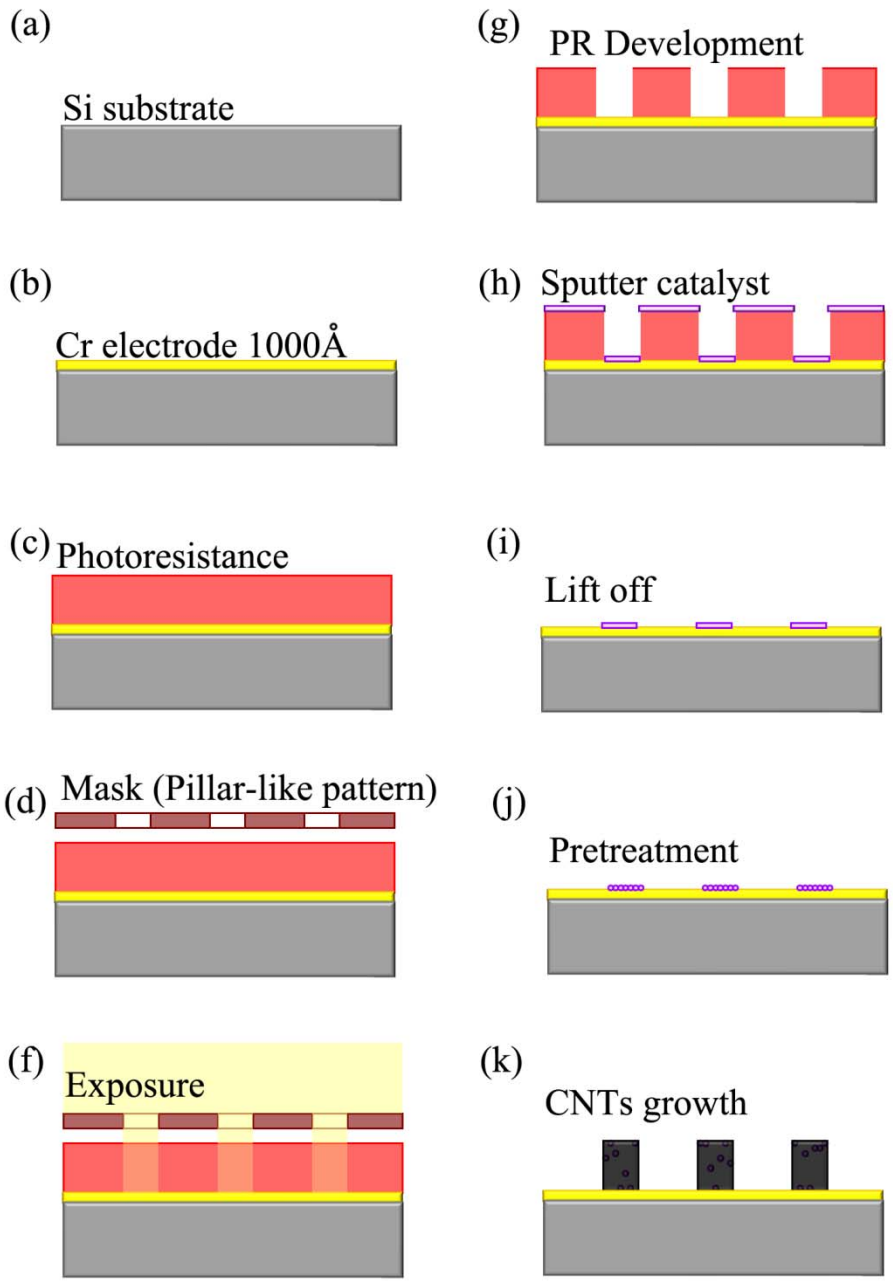

Figure 2-9 Fabrication flow diagrams (a) ~ (k). (b) 100 nm Cr electrode deposited by E-gun, (f) four constituents kinds of catalyst by sputtering system, (j) pretreatment with H_2 (50 sccm), and (k) CNTs growing under C_2H_4 atmosphere.

2.3.2 Experiment B: Effect of Growth Time

The growing time is a great part of cost for CNT-BLUs fabrication, because we need to keep high temperature during the CNTs growing duration. So the optimal growing time will obviously obtain both better field emission properties and lower cost we need.

In experiment B, the schematic of process is same as Fig. 2-6 except the growing time, and we designed five different durations at 550℃, that was 10 minutes, 30 minutes, 60 minutes, 90 minutes, and 120 minutes. The height of CNTs was predicted to increase as increasing of growing time. Following the F-N theory, we could easily know that higher pillar-like CNTs provide better field emission characters. However that character maybe not still be existed, because of too longer time of growth.

Lastly, we predicted we could optimize the growing time economically at high temperature in experiment B for low cost.

2.3.3 Experiment C: Optimization of Pillar Spacing

One of the critical drawbacks of CNT field emission backlight unit is non-uniform light region. So we were trying to overcome this drawback by using pillar-like pattern in order to avoid screening-effect.

In our researches, we chose several spacings between two pillar patterns, such as 3μm, 6μm, 9μm, 12μm, 15μm, 20μm, 25μm, and 30μm. The schematic of process is using the optimal growing time and predetermined temperature. Recipes were shown in 2.3.1 already and fixing these recipes except the spacing between pillars.

Finally, we predicted we could overcome the screening-effect and attain the most uniform lighting region, and find out the just spacing in experiment C.

2.4 Results and Discussion

2.4.1 Optimum Catalyst for CNTs Grown at Low Temperature (Experiment A)

Prior to CNTs growing, the catalyst is the first recipe we should focus on. According to our group's researches, there were many advantages of CNT field emission characters by using novel co-deposition of catalyst, as Fig. 1-13.

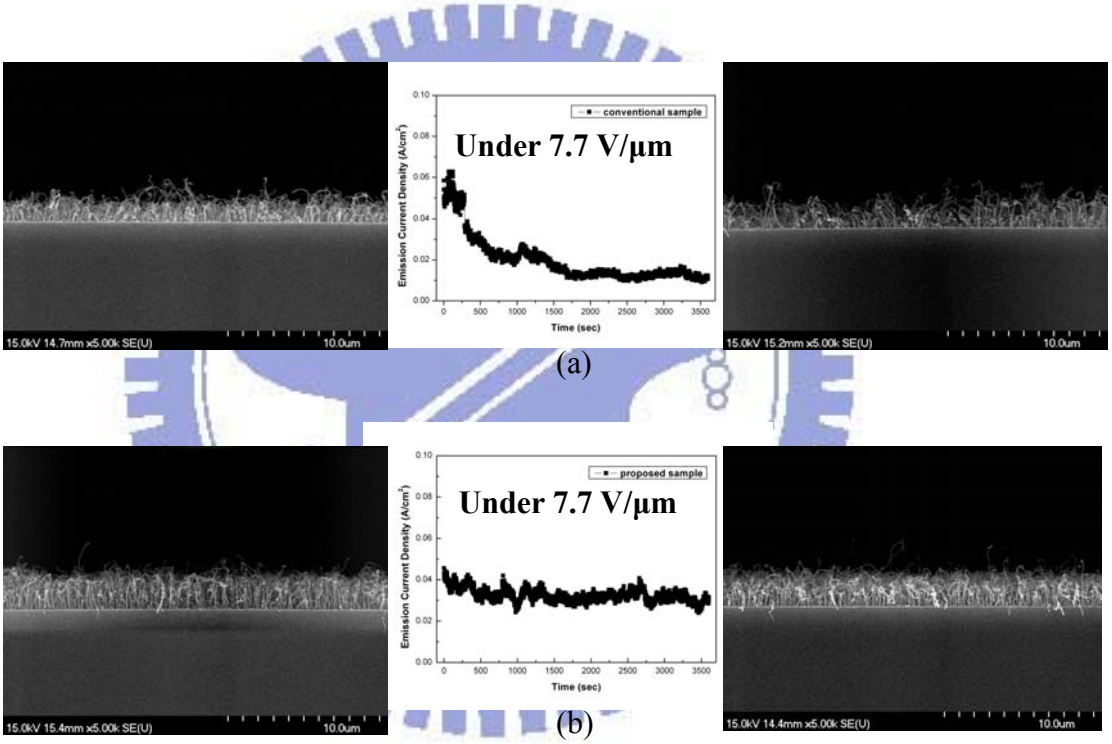

Figure 1-13 Improvement of Luminescent Uniformity via Synthesizing the Carbon Nanotubes on an Fe–Ti Co-deposited Catalytic Layer. [1.62]

The most obvious character was the reliability increased quite substantially. We have guessed this phenomenon is caused by decreasing the diameter of nano-sized particles, so finer particle provide higher activity and lower melting temperature. As a result, we chose

cautiously several kinds of catalyst compounds in order to obtain the just catalyst at predetermined temperature.

Fig. 2-10 shows the schematic profiles of thin film catalyst change into nano-sized particle during pretreatment, Fig. 2-10(a) illustrated two separations of two films and Fig. 2-10(b) illustrated co-deposited catalyst.

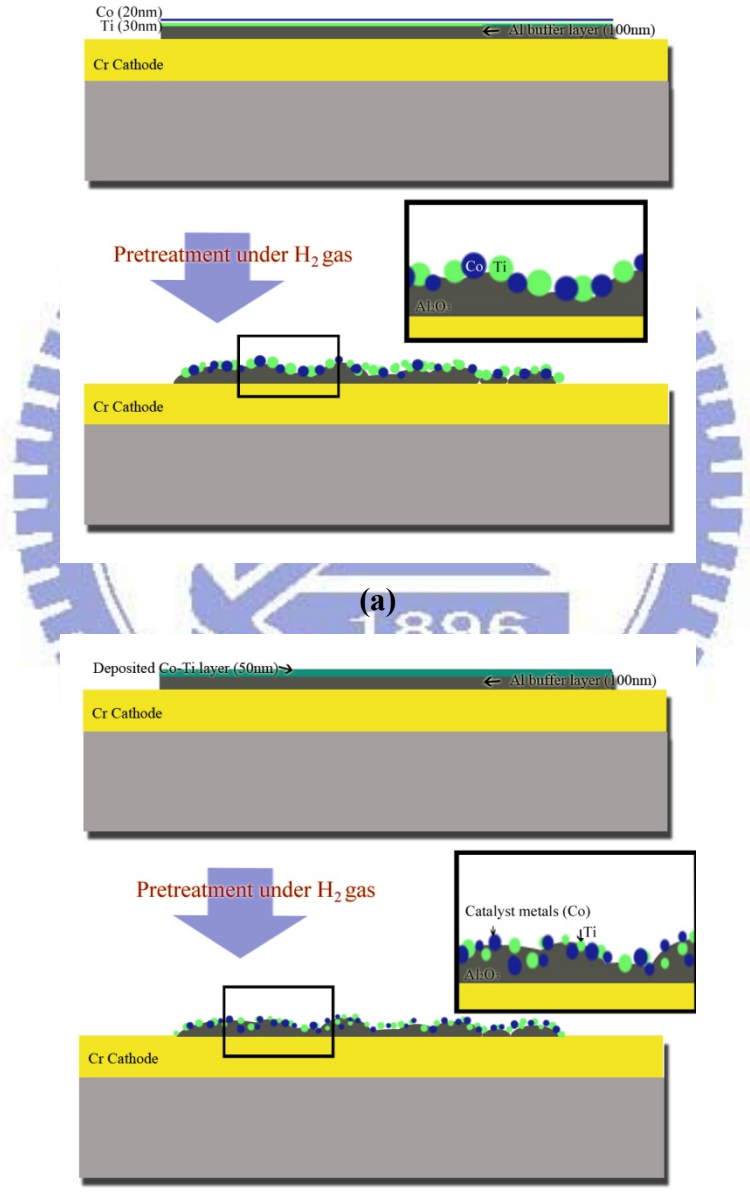

Figure 2-10 The schematic profiles of thin film catalyst change into nano-sized particle

during pretreatment (a) multilayer (b) Co-Ti co-deposited layer.

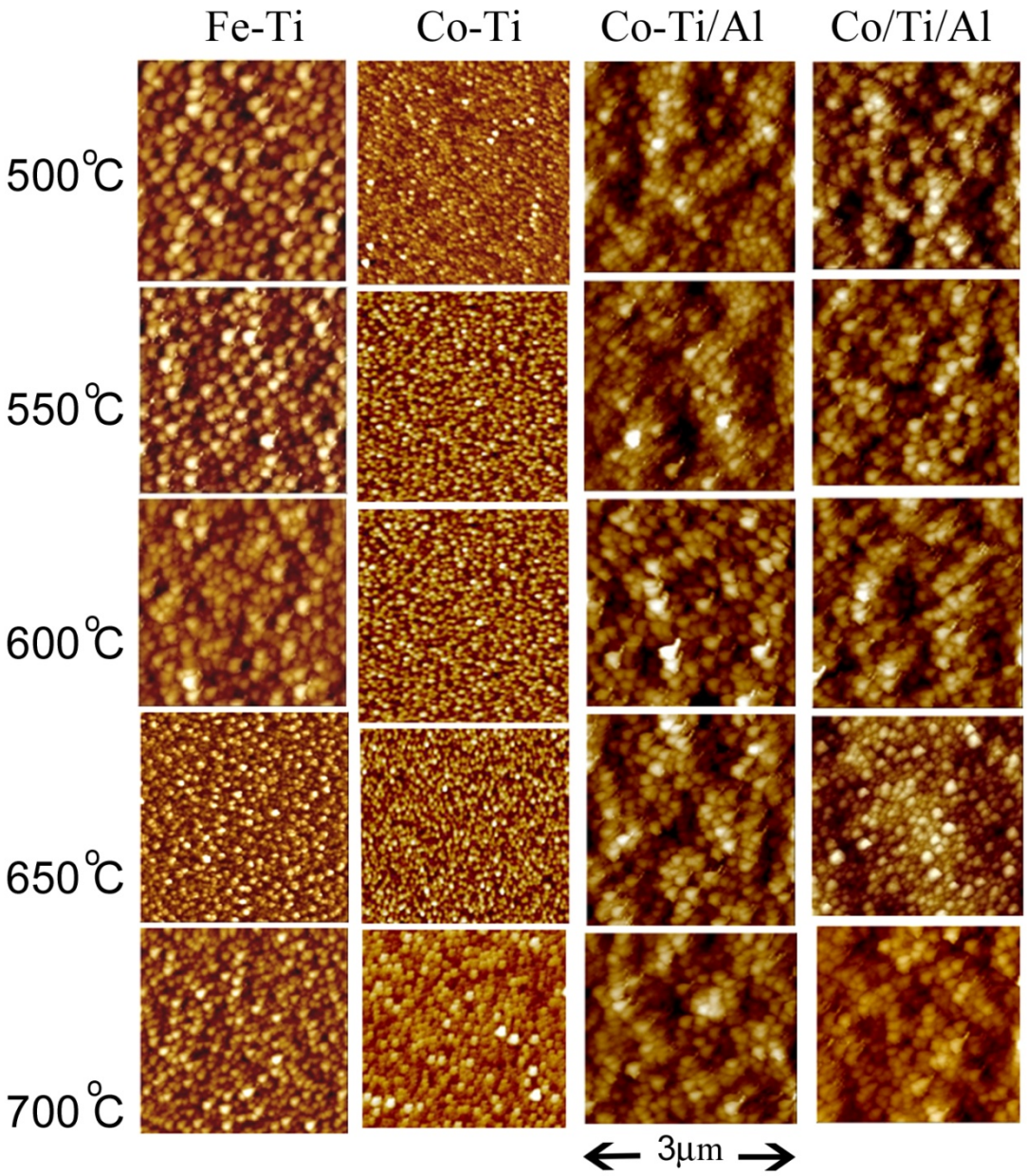

Figure 2-11 AFM images of different catalysts growing at different temperatures.

First, experiments with several catalysts of different constituents were only processing the pretreatment steps with hydrogen at 500, 550, 600, 650, and 700℃ separately for observing the reactive properties, roughness, and particle size. The AFM top view is the easiest method for making a comparison and it will clearly show the particle size and roughness. Following Fig. 2-11 is the whole AFM images in experiment A, the white pixel is standing for highest pick and the dark pixel is standing for the valley.

Next, we compared catalysts of tri-components with catalysts of bi-components, with or without aluminum between electrode and other catalyst layers. Subsequently, we could easily find out the differences. The fluctuation of catalyst surface showed simple and repeated nano-sized particle when pretreatment of bi-components catalyst without 10 nm Al buffer film, on the other hand, the fluctuation of catalyst surface was complex and additional curvature under those nano-sized particles when using the tri-components catalyst with 10 nm Al layer. As this result, we knew that Al plays a role of providing an additional curvature for surface of catalyst and quite increasing roughness mean square (RMS). The advantage of increasing RMS is raising the density of catalyst particle on the same top view area, as Fig 2-12, and then we could obtain better density of CNTs of one pillar after the growing step.

As well as some drawbacks of CNT growth at low temperature are poor density of CNTs and weak adhesion between CNTs and substrate. We estimated that increasing CNTs density will not only improve the density of emission sites, but also solve problem of weak adhesion by increasing Van Der Waal force between CNTs.

(a) **(b)**

Figure 2-12 The catalyst after pretreatment (a) without Al buffer layer (b) with Al buffer layer.

Secondly, focusing on the Co-Ti/Al and Co/Ti/Al, the differences between them were methods of deposition, multilayer and co-deposited layer. Following the AFM [Fig.2-13(a)-(b)] and SEM [Fig.2-14(c)-(d)] images at 500℃, the phenomenon due to co-deposition different from multilayer was more obvious in SEM image, as shown below:

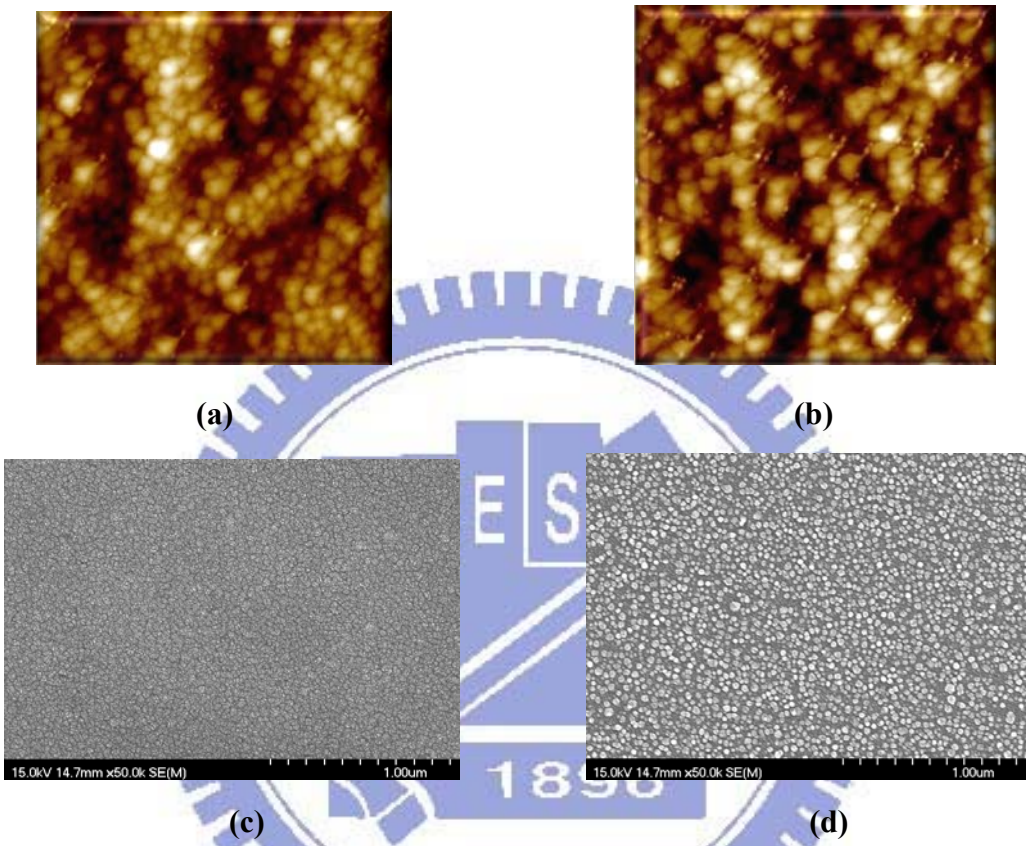

Figure 2-13 The top view at 500℃ (a) AFM of Co-Ti/Al, (b) AFM of Co/Ti/Al, (c) SEM of Co-Ti/Al, and (d) SEM of Co/Ti/Al.

Here, we assumed two mechanisms for phenomena of each method of deposition. For multilayer catalyst film, we explained that by surface energy of interface, the most effective factor is the melting point and difference of surface energy. But for co-deposited catalyst film, we took it as an alloy or a solid solution, it meant the constituent is uniform as same as other alloys. It precipitated when we pretreated at higher temperature, consequently explaining that by not only surface energy mechanisms but also nucleation and growth mechanisms.

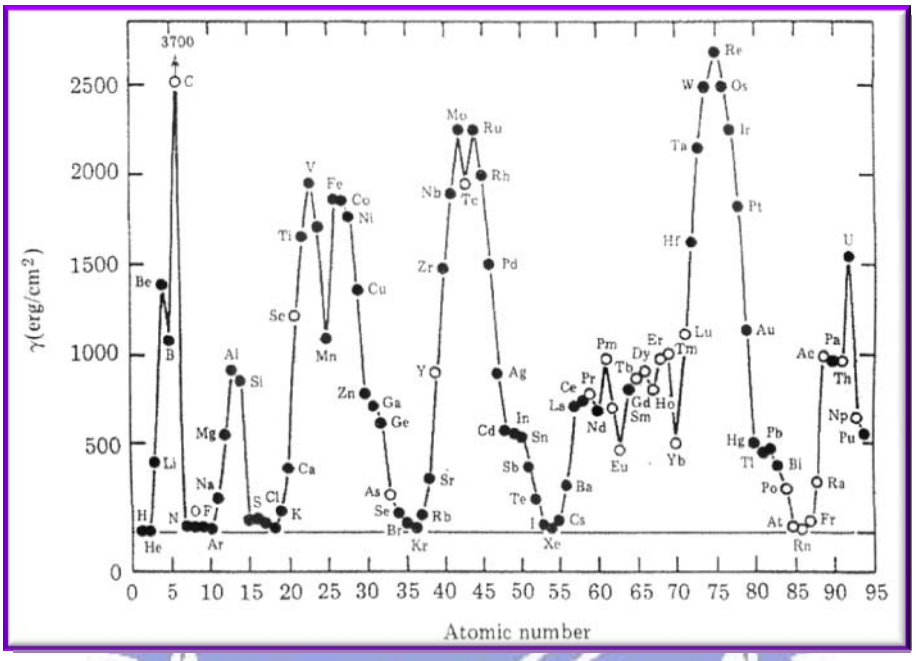

(a)

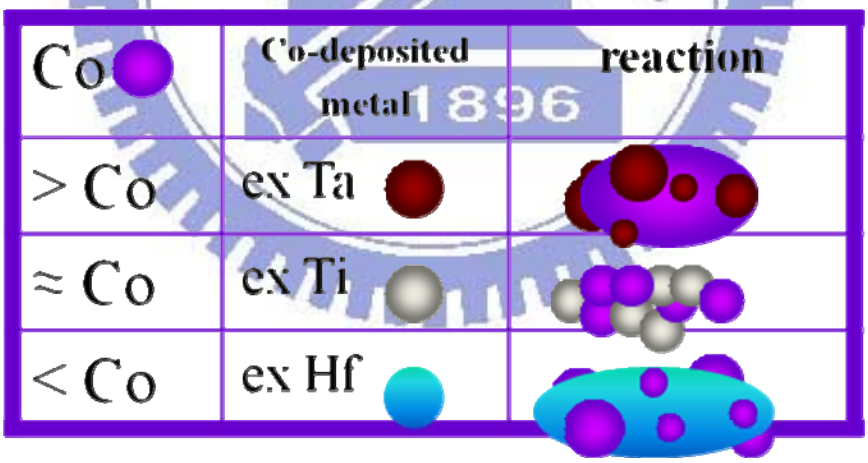

(b)

Figure 2-14 The surface energy effected on interface reaction.

Surface energy of different atomic numbers are shown in Fig. 2-14(a) [2.14]. Focusing on three kinds of atoms “Fe, Co, and Ti” was utilized, we could easily get a unique character that those surface energy are nearly the same, about 1700~1800 erg/cm^2. We expected to achieve the finest nano-particles of Co or Fe catalyst particles, and depending on the theory of surface energy, the most important rule is that everything of a system prefer to keep or diffuse to the lowest energy state after a long time diffusion. Following are three situations effected by difference of surface energy [as Fig. 2-14(b)]:

First, if the surface energy of buffer-component Ta we used is lower than Co (Co and Ta as an example), the lowest energy state will be larger Co particle and finer Ta, and almost Ta particles are inside of Co particle just for decreasing the total Ta surface area, so we may obtain larger and rougher catalyst particles with buffer-component of larger surface energy.

Second, if we choose a buffer-component with smaller surface energy, for example Co and Hf, the condition will be similar to the first situation. We could obtain the finer nano-sized catalyst particles by utilizing Hf buffer-component, but lots of Co catalyst particles were in the inside of larger Hf particles and could not react with carbon atom when CNTs growth.

Third, if the two elements with nearly same surface energy, as Co and Ti, the particles of each element will dispread uniformly to the similar sized nano-particles after hydrogen pretreatment. Depending on the past researches in our group, we were experimentally success demonstrating the Ti is the best buffer-component when we utilized Co or Fe as the catalyst element, the result was demonstrated our assumption, so we just used Ti as buffer-component in this study.

Another mechanism is nucleation and growth, which is the main factor of liquid phase transform to solid phase or solid solution phase precipitate particle when annealing as Fig. 2-15.

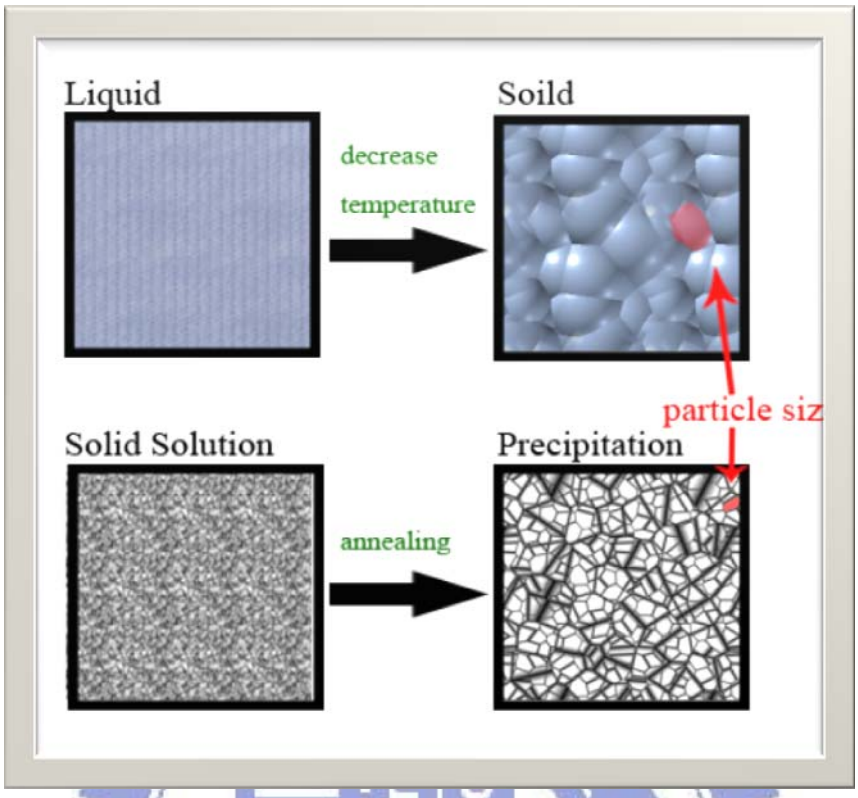

Figure 2-15 Liquid phase transform to solid phase or solid solution phase precipitate particle when annealing.

The co-deposited catalyst, as a solid solution was partial determined by nucleation and growth rate except the surface energy in our assumption. Based on this theory, there are two major factors affecting the nucleation rate:

(1) One is the instability of solid solution state as an over-saturated solution. So the more instability provides the higher driving force and faster rate of nucleation.

(2) Another is the diffusion rate of atoms into clusters, that means faster particle creation bring with the higher diffusion rate.

These two factors interact with each other, the scheme of the nucleation rate is Fig.2-16(a).

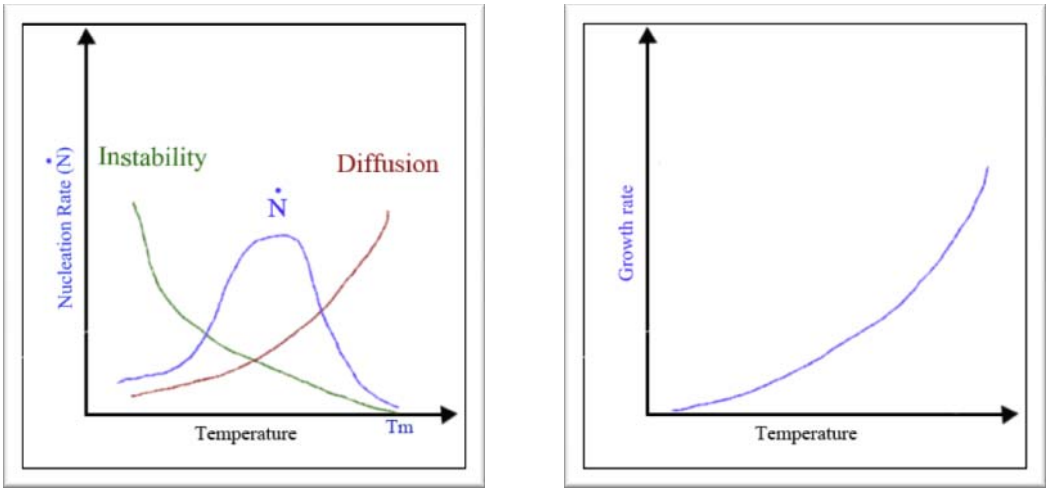

(a) **(b)**

Figure 2-16 The scheme of (a) the nucleation rate, and (b) the growth rate.

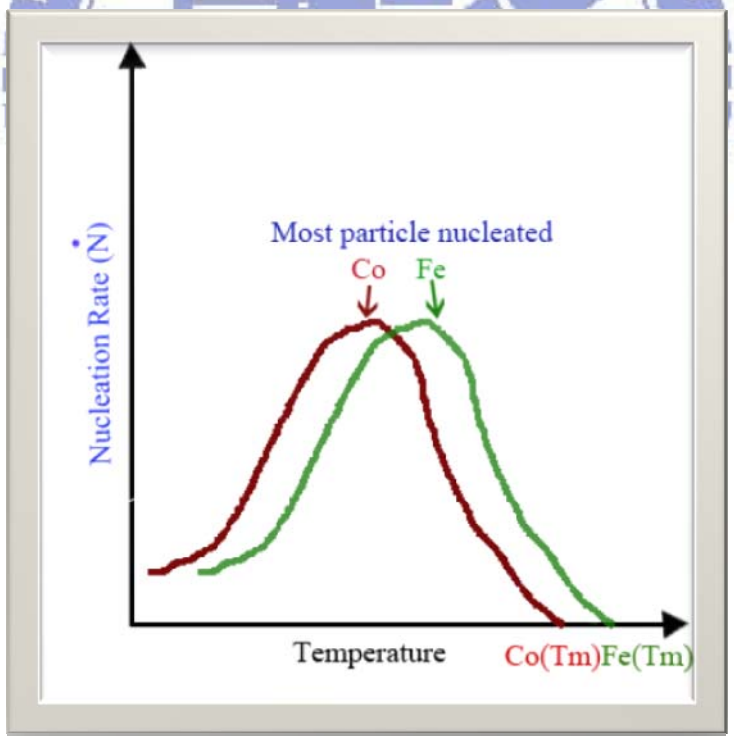

Figure 2-17 The nucleation rate of Co and Fe.

As Fig.2-16(a), the vertical axis was nucleation rate, the horizontal axis was temperature,

and T_m represented the melting temperature. The first curve represented increasing of nucleation rate as increasing of instability, the second curve represented increasing of nucleation rate as increasing of diffusion rate. We could simply realize there is a peak of the nucleation rate at a critical temperature.

Next, following the Fig. 2-16(b), the growth rate is simple comparatively. There was only factor of diffusion rate to affect the growth rate, therefore higher temperature brought higher diffusion rate, finally increase the growth rate.

Co and Fe catalyst were widely used for CNTs growing in our group's past researches, and Ni was not a good catalyst element under hydrogen pretreatment and growing CNTs in thermal CVD at any temperature.

According to the phase diagram or atomic period table, the melting temperature of Co and Fe are separately about 1700 K and 1800K, and other characters of these two elements were quite similar. Thus we made a simulation of the nucleation rate of them which was shown in Fig. 2-17. Melting temperature was the main difference between Co and Fe, so that the curve of Co nucleation rate we plotted was a shift from the curve of nucleation rate of Fe. In conclusion, we could assume surely the temperature of maximum nucleation rate of Co is low than maximum nucleation rate of Fe. By the way, focusing on the phase diagram as Fig. 2-18, we could find out the lowest temperature of α-Fe and α-Co generating which α-phase meant the first interaction occurring, about 320℃ for α-Fe and 450℃ for α-Co.

For the reason that two reasons in our assumption, we predicted the CNTs owns the superior electric characters and profiles by using Co-Ti/Al catalyst film.

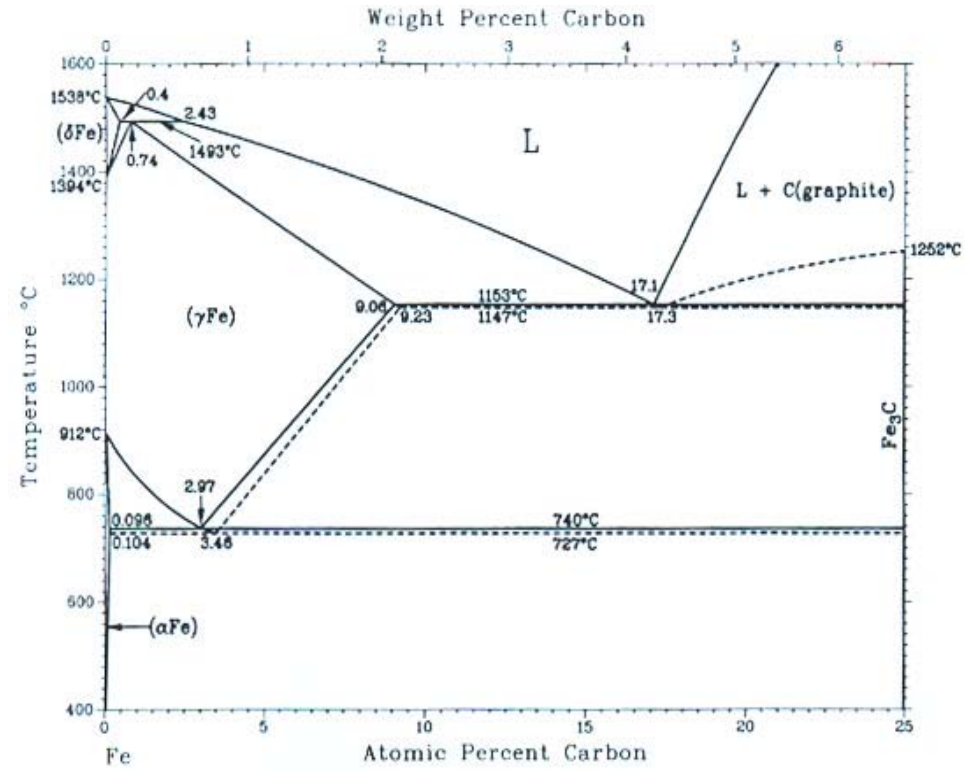

(a)

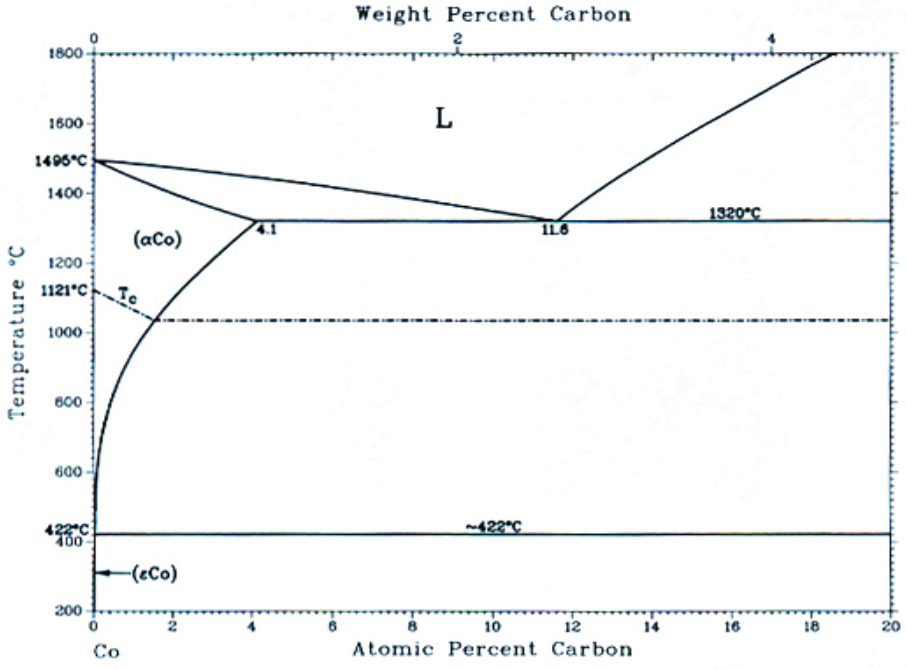

(b)

Figure 2-18 The phase diagram of (a) Fe-C, and (b) Co-C.

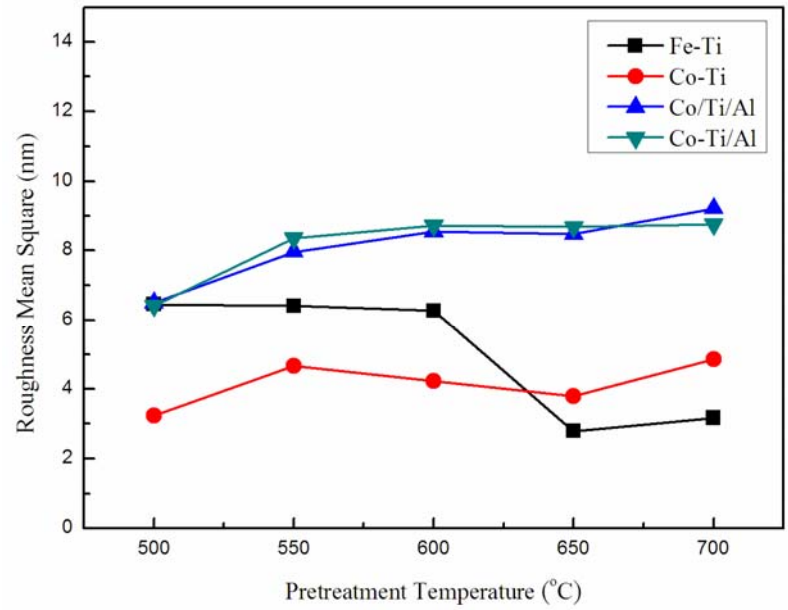

(a)

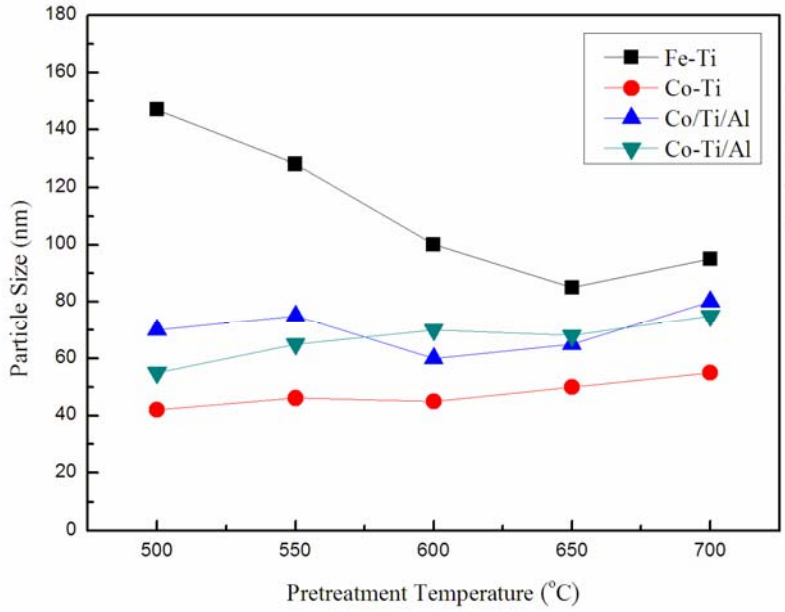

(b)

Figure 2-19 The four kinds of catalyst films at 500 to 700℃

(a) RMS (b)particle's size.

Table 2-1

The RMS of these catalyst films at different temperature

Temp. / Catalyst	500	550	600	650	700
Fe-Ti	6.452	6.396	6.258	2.788	3.163
Co-Ti	3.243	4.693	4.236	3.795	4.862
Co/Ti/Al	6.488	7.972	8.548	8.485	9.214
Co-Ti/Al	6.411	8.358	8.724	8.684	8.757

Table 2-2

The particle's size of these catalyst films at different temperature

Temp. / Catalyst	500	550	600	650	700
Fe-Ti	147	128	100	85	90
Co-Ti	42	46	45	50	55
Co/Ti/Al	70	75	60	65	80
Co-Ti/Al	55	65	70	68	75

Subsequently, we compared the experimental results [Fig.2-1, table 2-1, and table 2-2] with our past assumptions, fortunately lots of results were following our assumptions. Firstly the RMS increased by additional Al layer under catalyst. Secondly temperature of Fe-Ti nucleation rate maximum was higher than Co-Ti nucleation rate maximum, because of finest catalyst particle of Fe-Ti at about 650℃.

Comparing Co-Ti/Al with Co/Ti/Al at 500, 550, 600, 650, and 700℃, the RMS were almost the same at all temperature because of determined factor was the 10 nm Al under the

Co-Ti or Co/Ti catalyst films, and the particle size also could not be distinguished at high temperature above 600℃, the reason at our guess was that growth rate increase quickly with temperature and nucleation rate decrease with temperature at the same time, so nucleation and growth mechanism was not the domination of particle size any more. Thus the co-deposited and the tri-layer catalyst film could not be distinguished at high temperature above 600℃.

However pretreatment below 550℃, the surface energy mechanism dominated the tri-layer catalyst film (Co/Ti/Al), and co-deposited catalyst film (Co-Ti/Al) was dominated by nucleation growth rate that because of lacking of kinetic energy for diffusion freely, so two nucleated clusters could not be merged together. As the result we may observe the finest catalyst particle by co-deposited Co and Ti on Al at low temperature below 550℃.

In summary, we obviously believed Co-Ti/Al would play the best catalyst role than other three catalyst components by analysis of pretreated catalyst film.

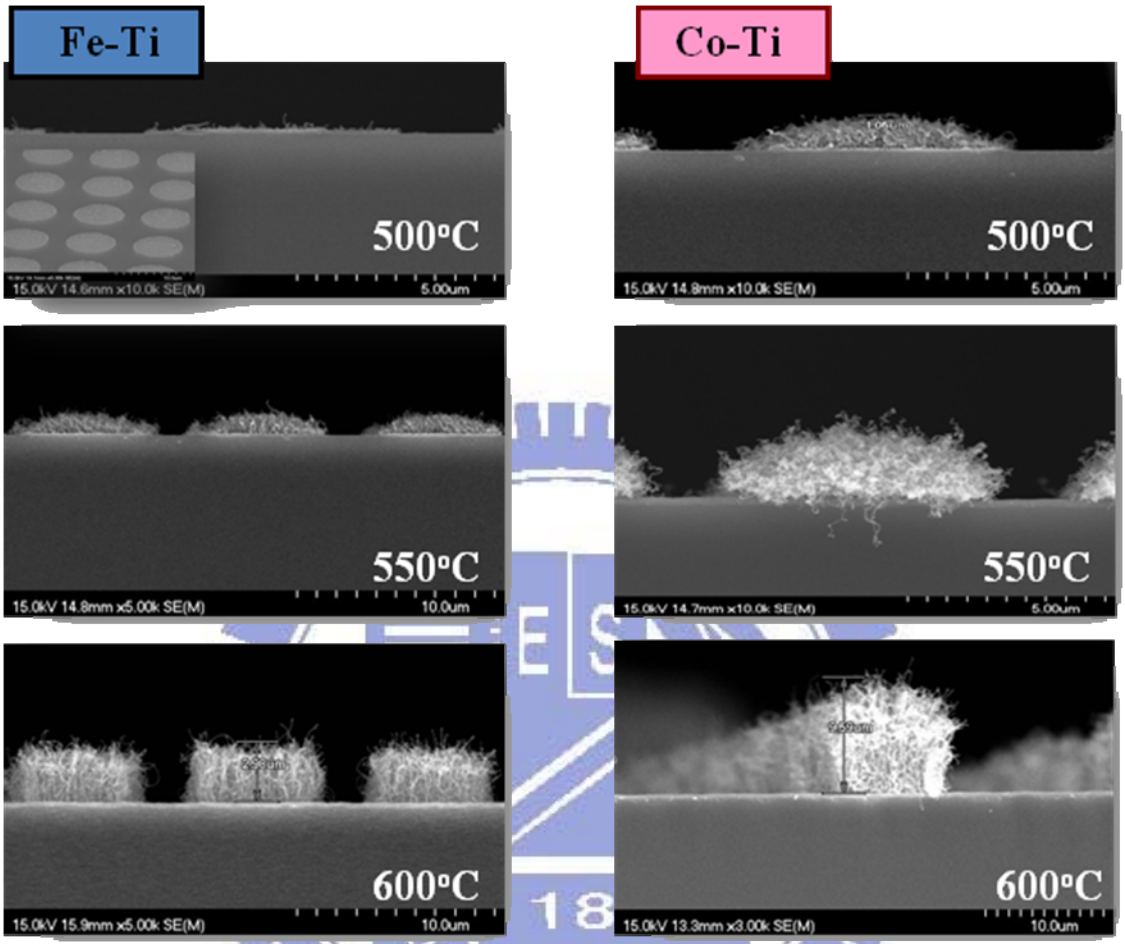

Figure 2-20 The pillar-liked CNTs profile image by SEM by (a) Fe-Ti catalyst (b) Co-Ti catalyst.

The pillar-like carbon nanotube's profiles were observed by scanning electric microscope (SEM) in our researches. The Fig. 2-20 showed comparing of pillar-like CNTs growing by Fe-Ti catalyst and by Co-Ti catalyst. At low temperature such as 500 and 550℃, CNTs by Fe-Ti catalyst nearly could not be identified with pillar shapes, just because their profiles were seem not good or high enough for field emission without clearly edges. On the other hand, Co-Ti film might be the better catalyst for growing CNTs at low temperature, but they were still not having a superior shape for field emission.

At 600℃, the difference of CNTs profiles between two catalyst was smaller than which at low temperature, that because the Fe-Ti catalyst particle was smaller with the increasing the pretreatment temperature. But in our researches, the main issue was the cost down, so we preferred growing CNTs at the low temperature below 600℃ in order to using glass substrate instead of silicon substrate. As a result, Fe-Ti was eliminated away from our following researches.

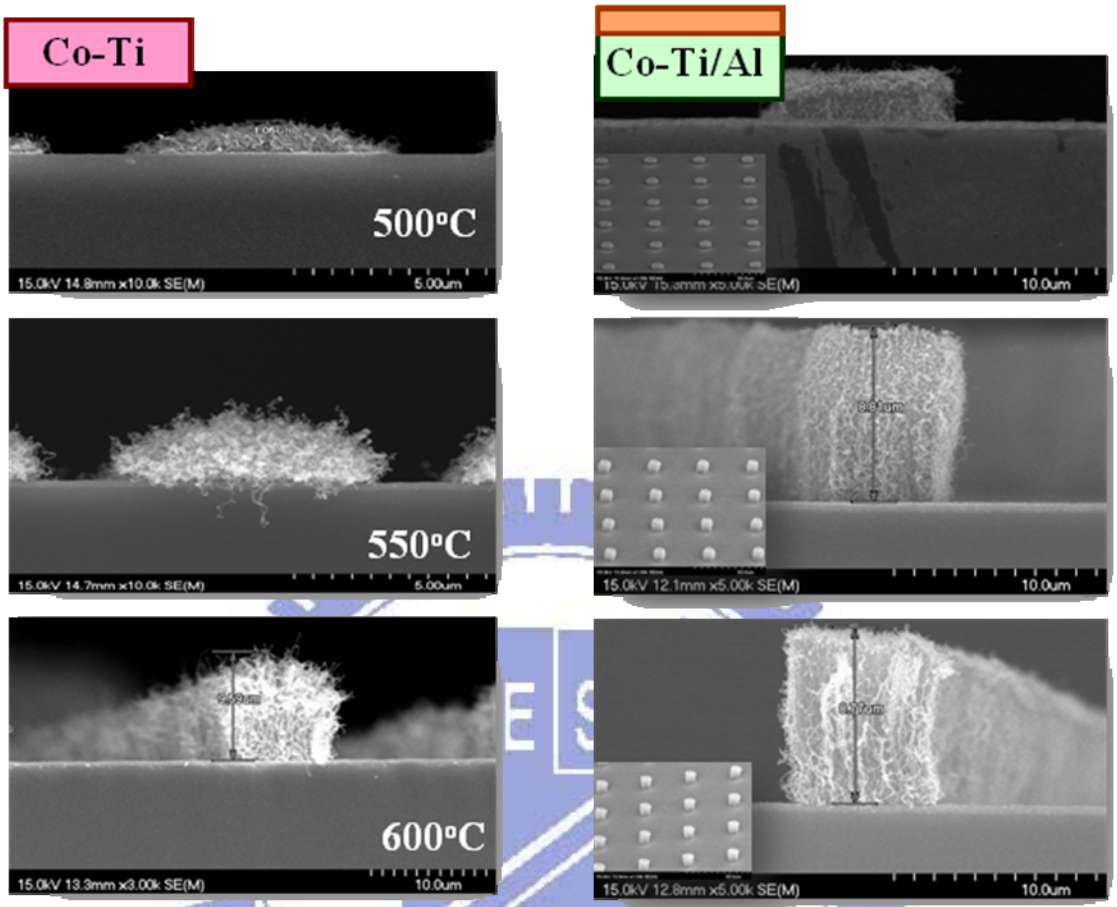

(a) **(b)**

Figure 2-21 The pillar-liked CNTs profile image by SEM by (a) Co-Ti catalyst (b) Co-Ti/Al catalyst.

Next, we compared Co-Ti and Co-Ti/Al as the assumption of catalyst, the Al plays the role of increasing RMS and increasing planar density of catalyst particle. Co-Ti/Al was assumed that was suitable or using at low temperature process. The experimental results which were shown in Fig.2-22 conformed to our assumptions, the pillar-like CNTs by Co-Ti/Al catalyst had superior profile, density, and edge.

First of the all, focusing on CNTs profile at 500℃, the pillar shape was already manifested by Co-Ti/Al catalyst film. Its density was advanced high, and its edge was quite clear, for comparison with Co-Ti. Second, at 550℃, the superior character of Co-Ti/Al was obviously attained, not only the density of CNTs but also the height and edge of a pillar were overwhelming better than Co-Ti.

This result surely proved our assumption of what role Al played again, finally we could ensure the Al additional layer was helpful for CNTs growth at low temperature.

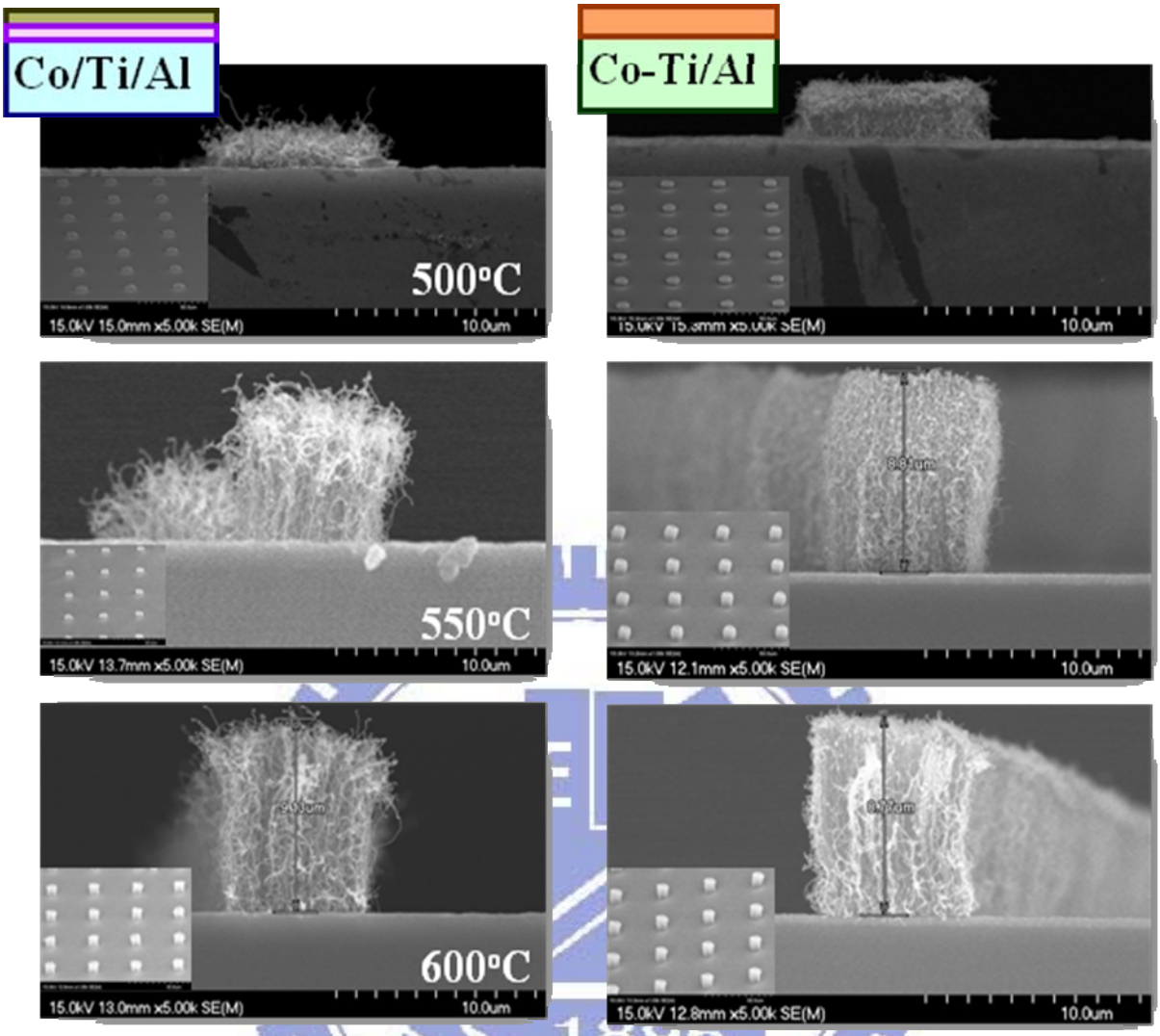

(a) **(b)**

Figure 2-22 The pillar-liked CNTs profile image by SEM by (a) Co-Ti/Al catalyst (b) Co/Ti/Al catalyst.

Lastly, the Co/Ti/Al catalyst tri-layer film in our group past researches was used as comparison with Co-Ti/Al here [as Fig.2-22]. The difference was the multi-layer or co-deposited of cobalt and titanium. At 600℃, the profiles of Co-Ti/Al and Co/Ti/Al were nearly the same, the reason was the particle size of catalysts were almost the same at higher temperature. As Fig.2-23(a), the CNT growing scheme profile was shown the CNT's density and thickness are following the catalyst particles. Furth more the atomic details of reaction on one catalyst particle was shown in Fig.2-23(b).

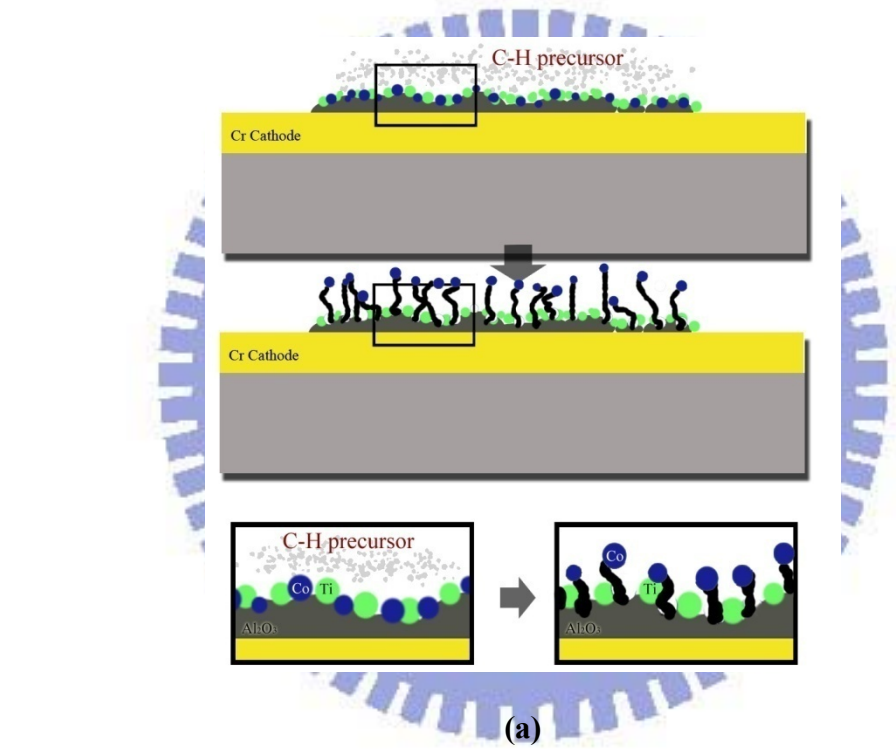

(a)

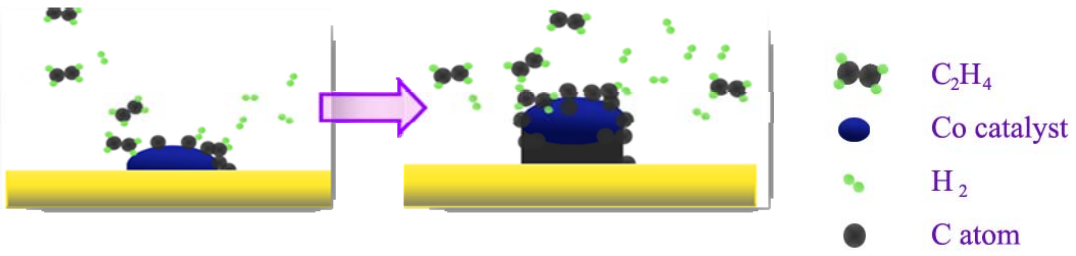

(b)

Fiugure 2-23 The CNT growing scheme profile (a) details of reaction on an pattern, (b) details of reaction on a single catalyst particle.

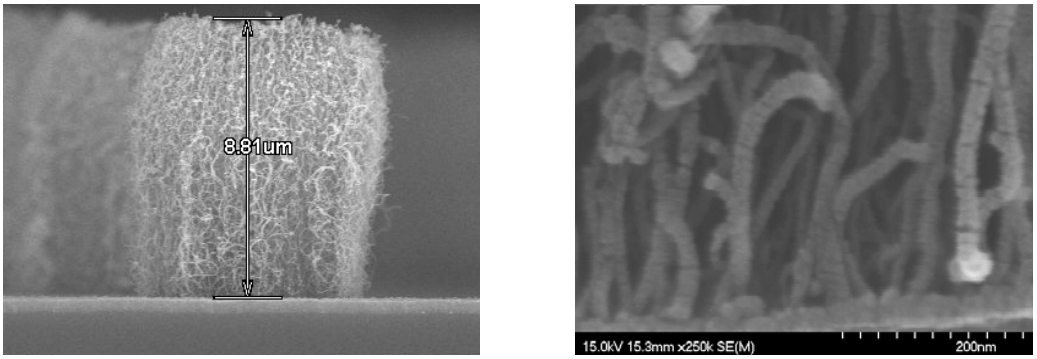

(a) (b)

Figure 2-24 The interfacial detail of CNT and substrate of Co-Ti/Al catalyst at 550℃.

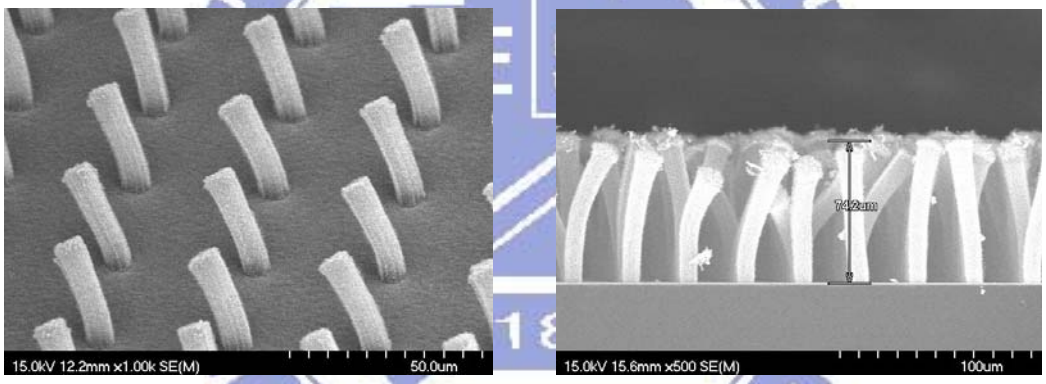

(a) (b)

Figure 2-25 The (a) top view and (b) profile of pillar-liked CNTs at high temperature on SEM. Co-Ti/Al for example.

In conclusions, the experimental results and assumptions all indicated that the best catalyst for pillar-like CNTs was Co-Ti/Al, and below glass transform temperature, we obtained the most suitable temperature for growth and pretreatment was 550℃ as Fig. 2-24. What is more, when the growing temperature was over 600℃, these four kinds of catalyst owned nearly the same external profiles, shown in Fig. 2-25.

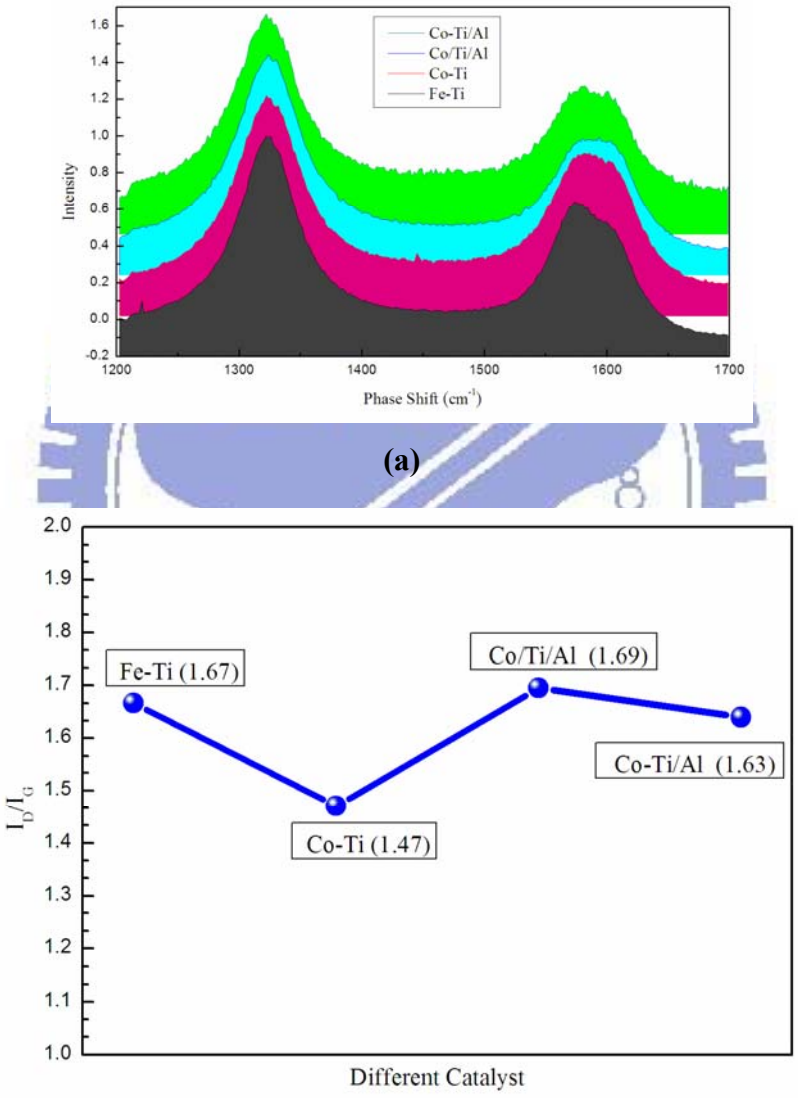

Figure 2-26 (a) Raman Spectra by difference catalysts at 550℃, (b) I_D and I_G ratios.

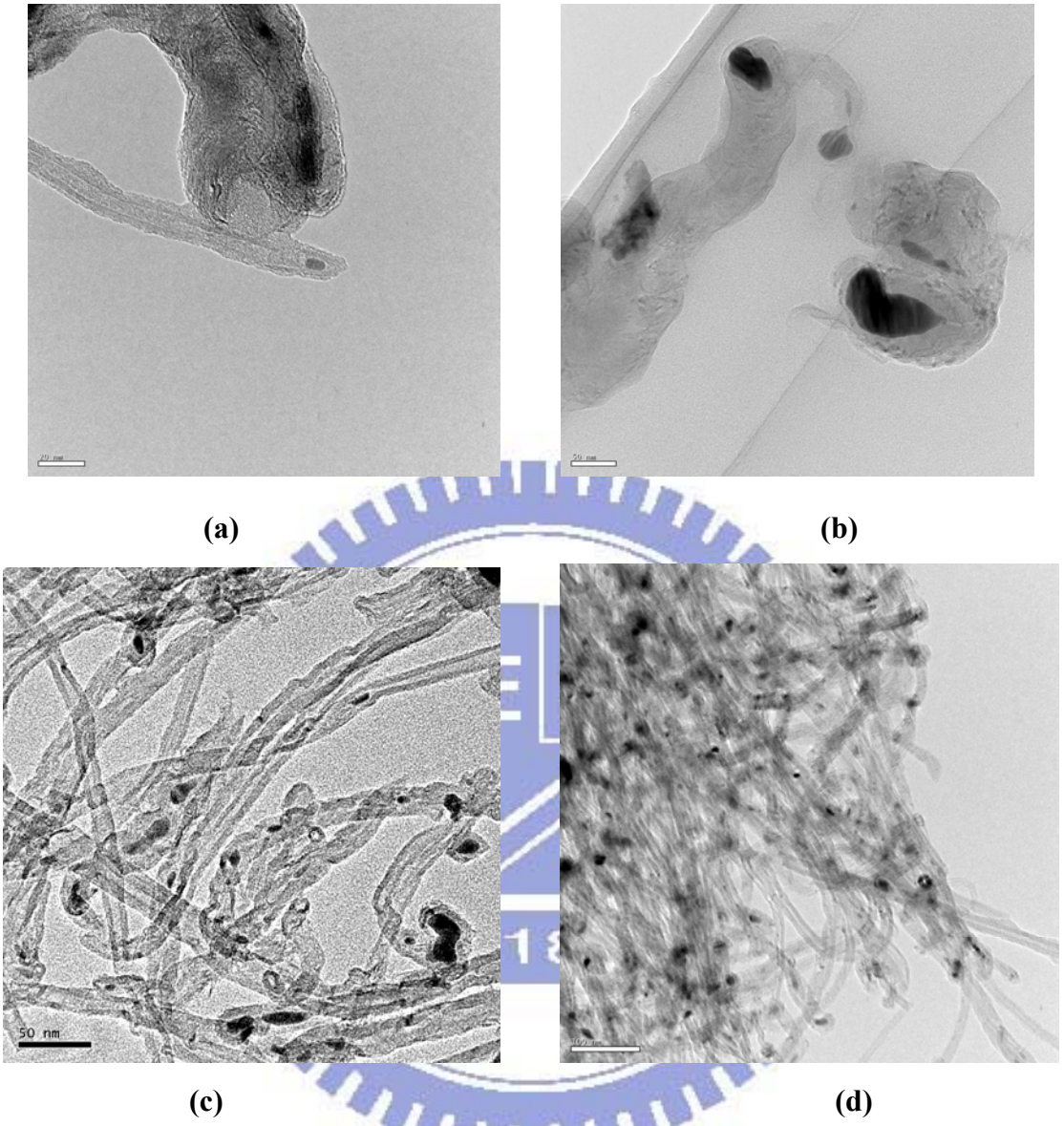

Figure 2-27 The TEM images (a)-(b) Co/Ti/Al tri-layers catalyst (c)-(d) Co-Ti/Al co-deposited catalyst.

The Raman spectra were used by detecting the kinds of bond, so we could understand how much percent of the graphite and the amorphous phase. As we known, the graphite phase was the CNTs surrounding layers and amorphous phase was the diamond like tip, defect, or rough deposited carbon. As this result, higher the graphite phase, the stronger or more stable quality and lower work function of CNTs. For another, higher the amorphous phase, more emission sites of CNTs. We tried to increase the intensity of amorphous phase if we want the higher emission current. On the other hand, we tried to increase the intensity of graphite phase in order to improve stability and reliability of CNTs. Here the stability and reliability were quite important for back light purpose, so we preferred the lower I_D (intensity of defect) / I_G (intensity of graphite) ratio to ensure the stable reliability.

The analysis of our Raman spectrum showed that the I_D / I_G ratios were not much different by four kinds of catalyst because the major factor was the growing temperature shown in our past researches. The peak of I_G (1320 cm^{-1}) was all weak than peak of I_D (1580cm^{-1}) because of the low temperature processes.

In TEM images shown as Fig. 2-27, the catalyst sizes of Co-Ti/Al [Fig. 2-27(c)-(d)] were more uniform and finer than Co/Ti/Al [Fig. 2-27(a)-(b)], then diameter of CNTs would be controlled by the catalyst.

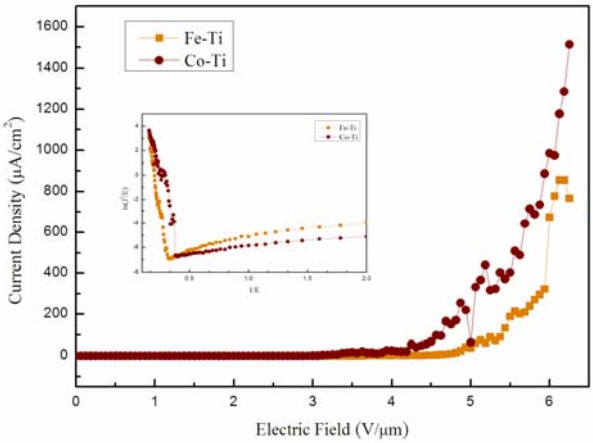

(a)

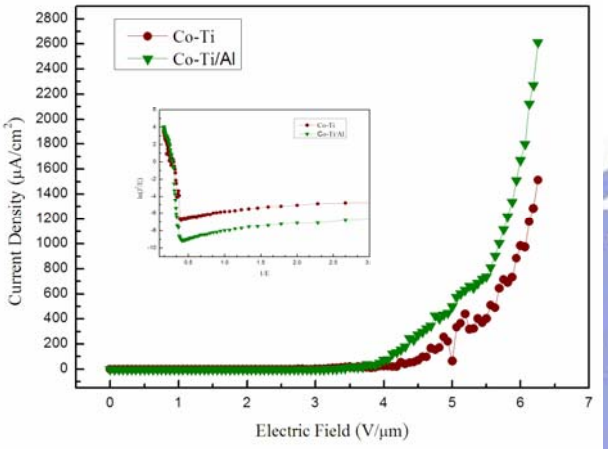

(b)

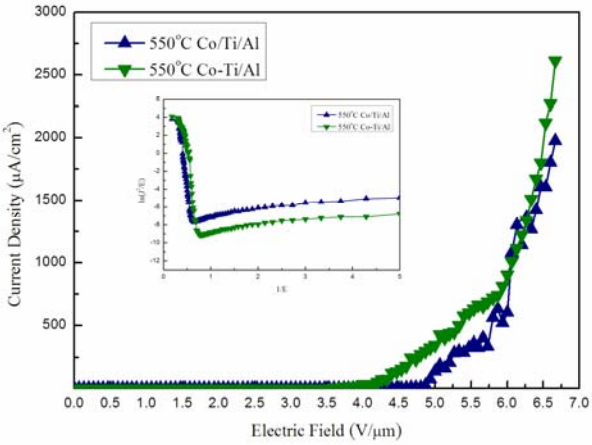

(c)

Figure 2-28 The I-V curves of comparing (a) Fe-Ti and Co-Ti, (b) Co-Ti and Co-Ti/Al, and (c) Co-Ti/Al and Co/Ti/Al.

The phenomenon of field emission occurred only under a low pressure about $5x10^{-6}$ torr, the diagrams of current versus voltage showed in Fig.2-28 by CNTs of different catalysts. Once again the experimental results proved that CNTs by Co-Ti/Al catalyst was the most applicative catalyst for low temperature CNT growth.

Next, we compared the Co-Ti/Al and Co/Ti/Al as Fig. 2-29 and Fig. 2-30 at 500℃, 550 ℃, and 600℃, because the Fig. 2-28 was not shown clearly. At 500℃, the turn-on fields were 3.5 V/μm and 4.7 V/μm by separately Co-Ti/Al and Co/Ti/Al catalyst, and current densities under 6 V/μm electric field were 13.08 $\mu A/cm^2$ and 11.58 $\mu A/cm^2$.At 550℃, the turn-on fields were 3.6 V/μm and 4.4 V/μm by separately Co-Ti/Al and Co/Ti/Al catalyst, and current densities under 6 V/μm electric field were 1272 $\mu A/cm^2$ and 1124 $\mu A/cm^2$. At 600℃, the turn-on fields were 3.8 V/μm and 3.8 V/μm by separately Co-Ti/Al and Co/Ti/Al catalyst, and current densities under 6 V/μm electric field were 1736 $\mu A/cm^2$ and 1397 $\mu A/cm^2$.

We could observed that electric properties of CNTs on Co-Ti/Al was slightly better than CNTs on Co/Ti/Al except 600℃, that results was really following our assumption over again, and CNTs growing at 500℃ was very poor because the current density was small and the turn-on field was higher than others.

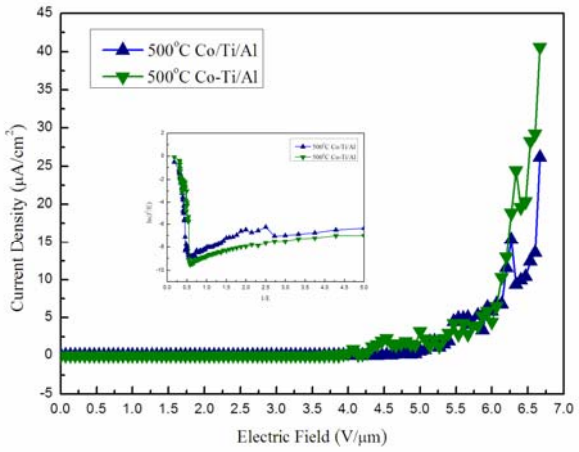

(a)

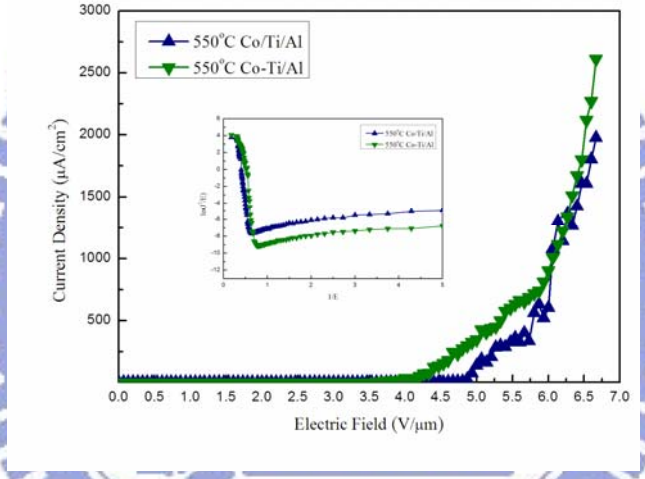

(b)

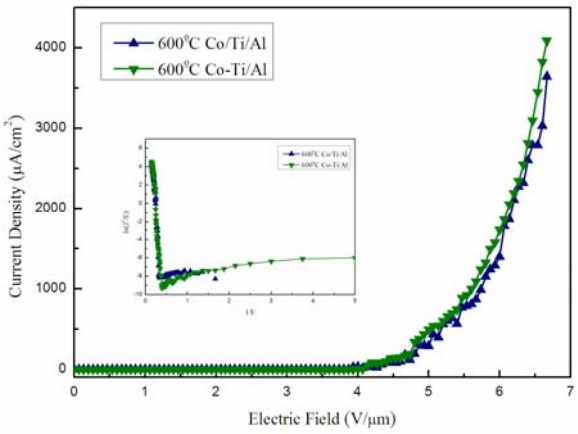

(c)

Figure 2-29 I-V curve of CNTs on Co-Ti/Al and Co/Ti/Al at (a)500℃ (b)550℃ (c)600℃.

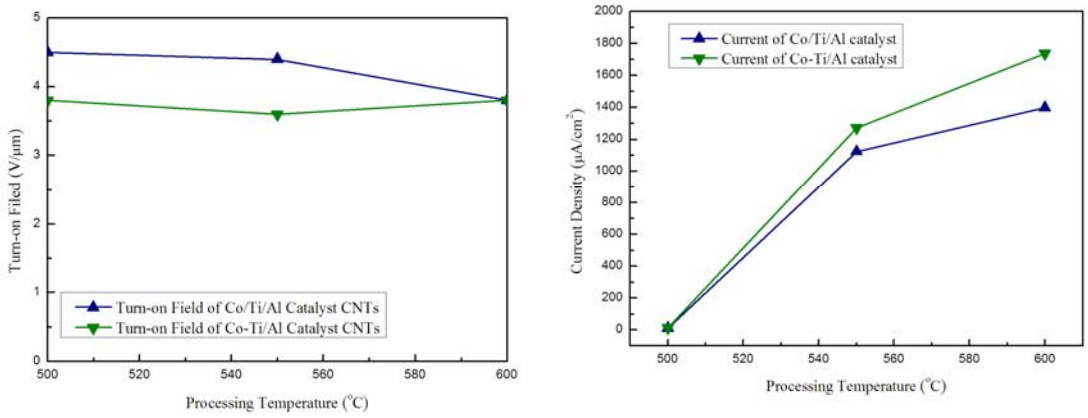

(a) **(b)**

Figure 2-30 I-V data of CNTs on Co-Ti/Al and Co/Ti/Al at different temperature (a) turn-on field (b) current density under 7 V/μm.

Table 2-3

Tables of turn-on field and current density of Fig.2-30 I-V curve

Turn-on field:

Temp. / Catalyst	500	550	600
Co/Ti/Al	4.5	4.4	3.8
Co-Ti/Al	3.7	3.6	3.8

Unit: V/μm

Current density at 6V/μm:

Temp. / Catalyst	500	550	600
Co/Ti/Al	11.58	1124	1397
Co-Ti/Al	13.08	1272	1736

Unit: μA/cm^2

Stress experimental tests were used for testing the life time of a backlight unit. In our researches, the stress test was always under the 1000V (6.78 V/μm) and keep a long time (2 hours) as Fig. 2-31 and Fig. 2-32 shown.

The advantage of co-deposited catalyst film appeared evidently, especially at 550℃, the current variation of pillar-like CNTs on Co-Ti/Al was only 7% of initial value. As a result, the co-deposited catalyst not only improved the I-V characters but also increased the reliability of pillar-like CNTs. Fig. 2-33 showed the SEM profile images before and after stress, the additional longer single CNT disappeared after stress.

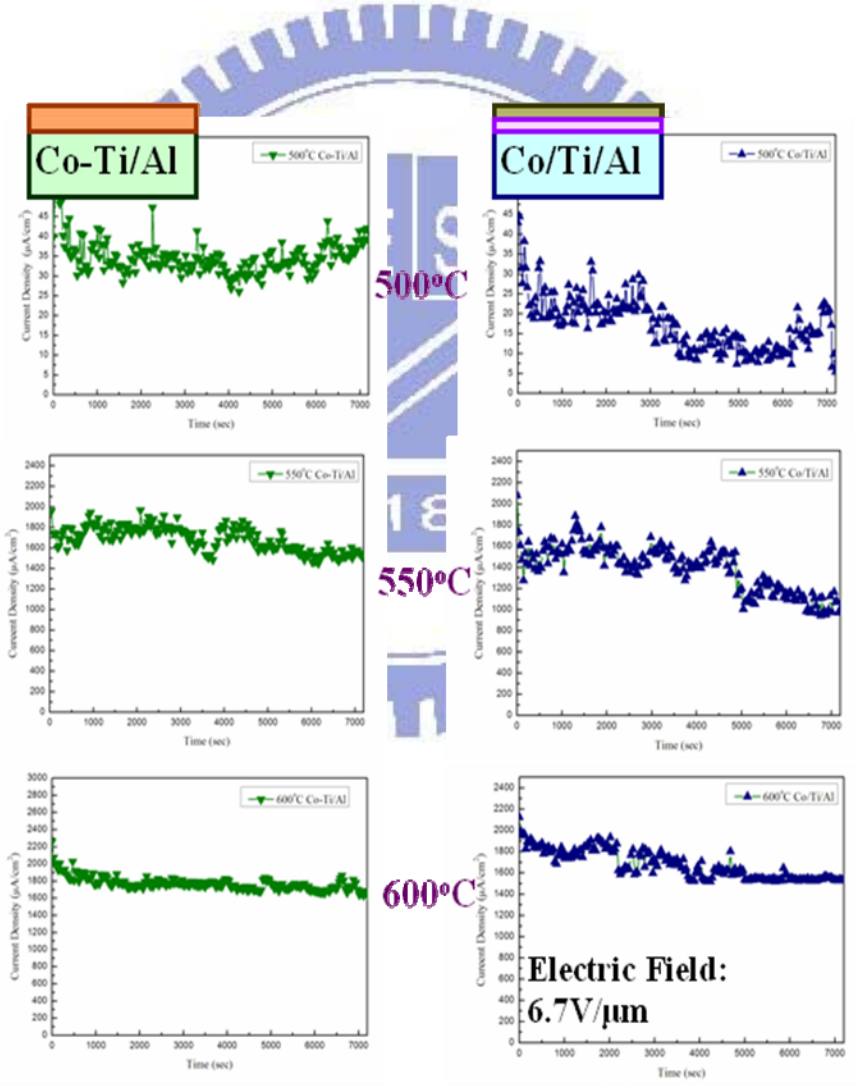

Figure 2-31 Stress testing of CNTs on Co-Ti/Al and Co/Ti/Al.

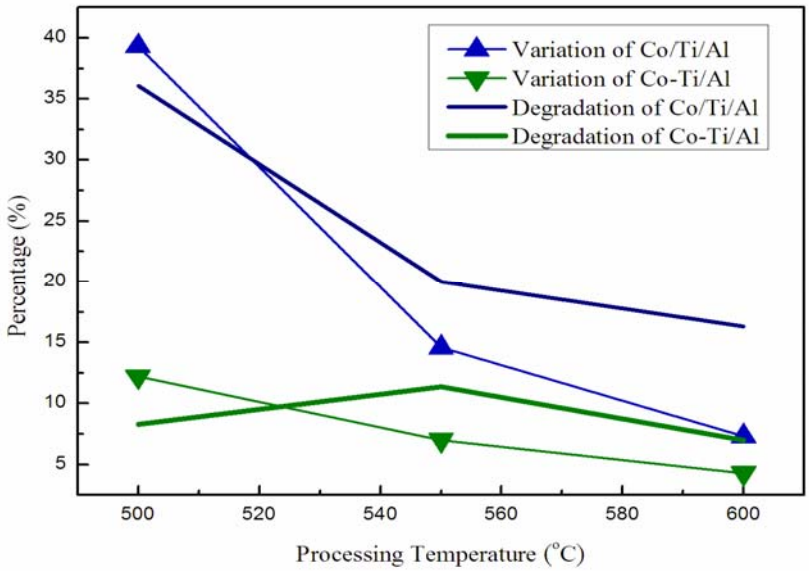

Figure 2-32 The trend of reliability of CNTs on Co-Ti/Al and Co/Ti/Al at different temperature.

Table 2-4

The data of reliability of CNTs on Fig. 2-32

Average current density:

Temp. / Catalyst	500	550	600
Co/Ti/Al	17.22	1385	1673
Co-Ti/Al	34.83	1688	1773

Unit: μA/cm^2

Variation:

Temp. / Catalyst	500	550	600
Co/Ti/Al	39.3	14.6	7.3
Co-Ti/Al	12.2	7.0	4.3

Unit: % of initial value

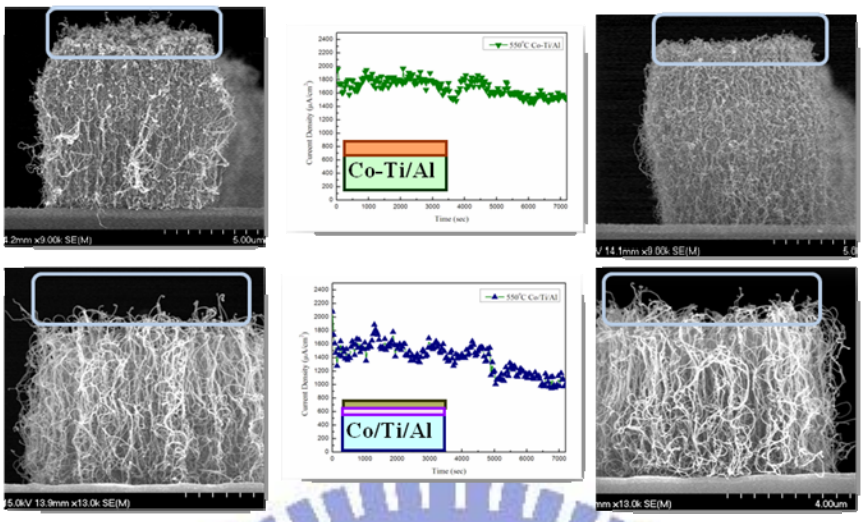

Figure 2-33 Profiles of CNTs before and after stress test.

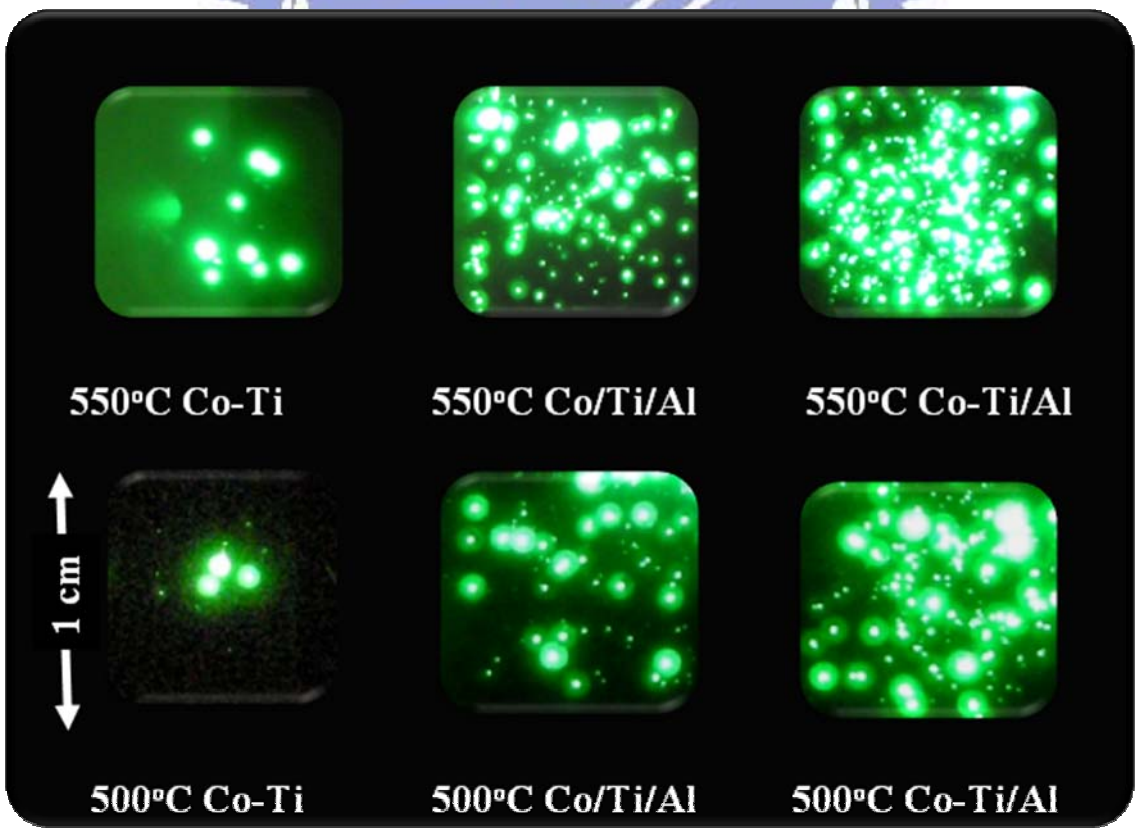

Figure 2-34 The (1cmx1cm) illuminated Images by digital camera.

Lastly, Fig. 2-34 was the demonstrations of 1x1 cm^2 pillar-like CNTs at 500℃ and 550 ℃ with 25μm pillar spacing. The illumination images of CNTs on Co-Ti catalyst were all poor at 500℃ or 550℃, so the additional Al layer was very important for low temperature CNT process. And The CNTs on Co-Ti/Al compared to CNTs on Co/Ti/Al, we could observe the CNTs on Co-Ti/Al had comparative uniformity.

In conclusions of 2.4.1, we optimized the catalyst before CNTs growing at 550℃. The best optimal recipe was Co-Ti/Al (Co 20nm, Ti 30nm, and Al 100nm), the turn-on field was 3.6 V/μm and current density was 1272 μV/cm, and owned better uniformity and reliability of 7.0% fluctuated variation.

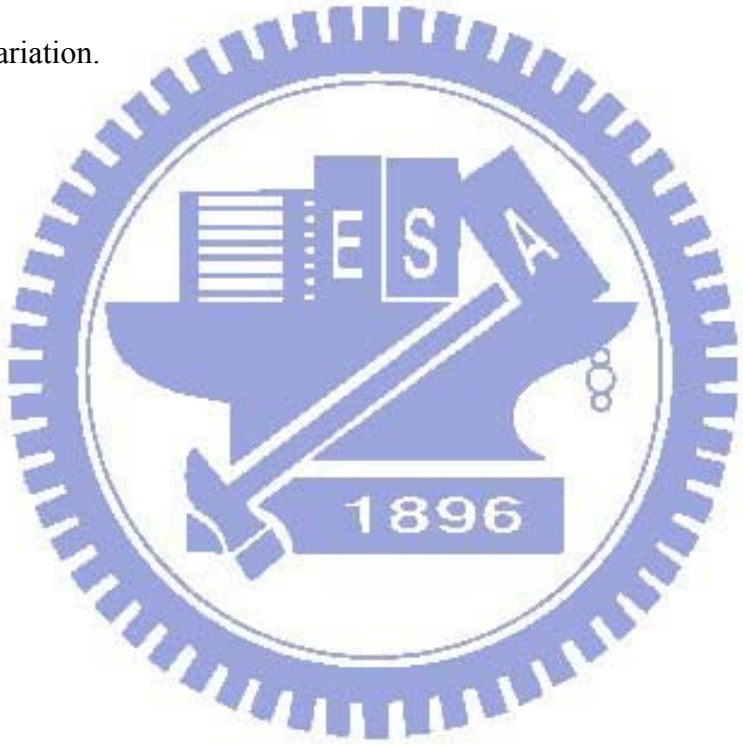

2.4.2 The Appropriate Growth Time for CNT Growing (Experiment B)

After optimizing components of catalyst at the adequate temperature, one parameter was the growing time for CNTs growth. The growing time determined the height of pillar-like CNTs for the most part, and might be bringing other effects those were what we proposed in our researches. We designed five experimental times for this research, which was 10min, 30min, 60min, 90min, and 120min in order to surely find out the optimal value. And the other terms and conditions fixed as the optimal values in 2.4.1.

Fig. 2-35 (a)-(e) showed the height of pillar-like CNTs increased with growth times, there were 1μm, 2μm, 5μm, 8μm, 8.4μm separately by 10 min to 120 min growing, and the heights increased with time without doubt by plotting as Fig. 2-36. There were two doubts about 10 min and 120 min growing which without following the slope of increasing.

Firstly, CNTs of 10 min growth as Fig. 2-36 shown was not bond each other and without direction of growing, so the increment of height was not seem to increase immediately, for the growing without any direction.

Secondly, CNTs of 120 min growth in Fig. 2-35(e), we could notice that the increment of height was not following the slope of plot after 90min. The reason would be explained by diffusion, as we knew that the CNTs formation is defined by carbon atom diffusion to the surface or interface of catalyst atom to form CNTs. But the catalyst of overgrowing CNTs owned very thick multiwall graphite phase layer outside the catalyst particle, so carbon atoms would hardly diffuse to the interface of catalyst particle to form the multiwall graphite phase.

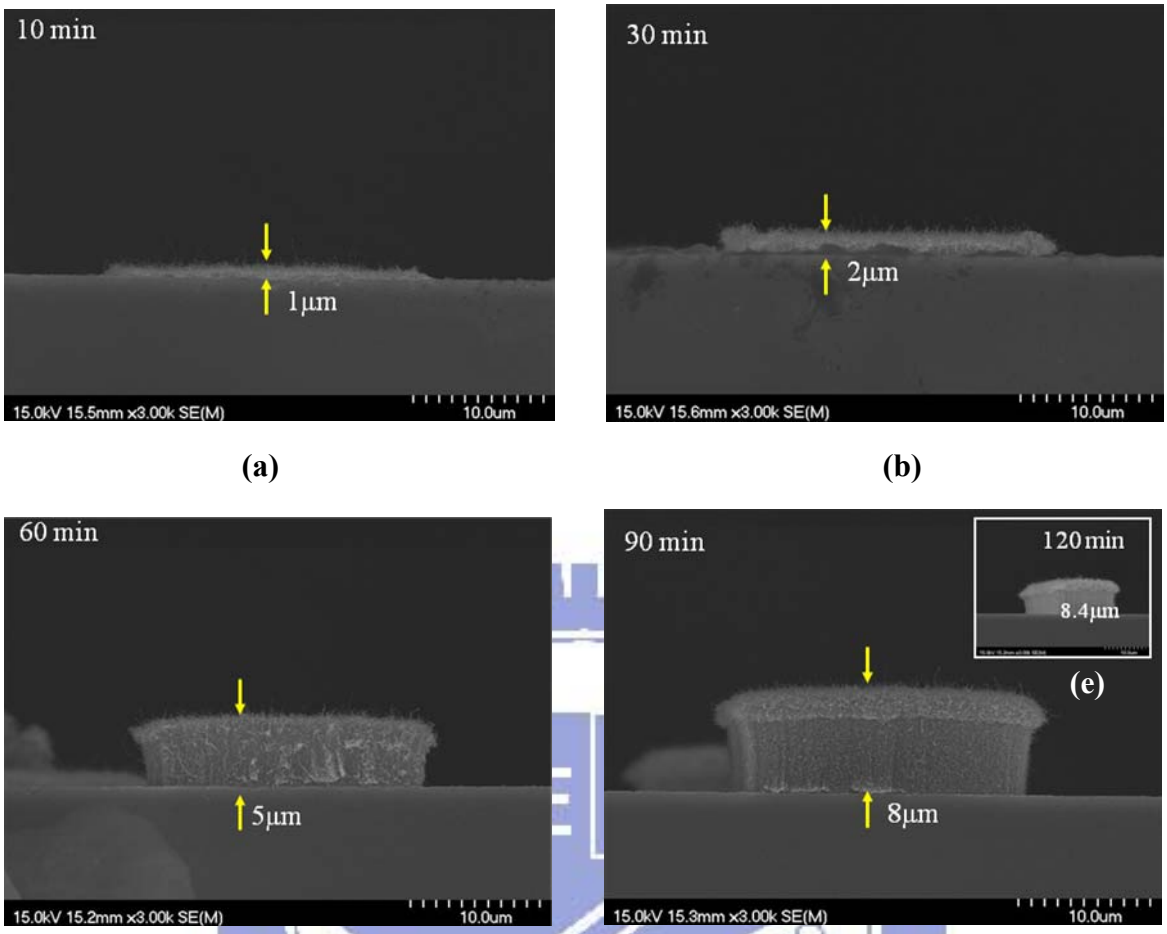

Figure 2-35　SEM micrographs of CNTs on Co-Ti/Al growing (a) 10 min (b) 30 min (c) 60 min (d) 90 min (e) 120 min at 550℃.

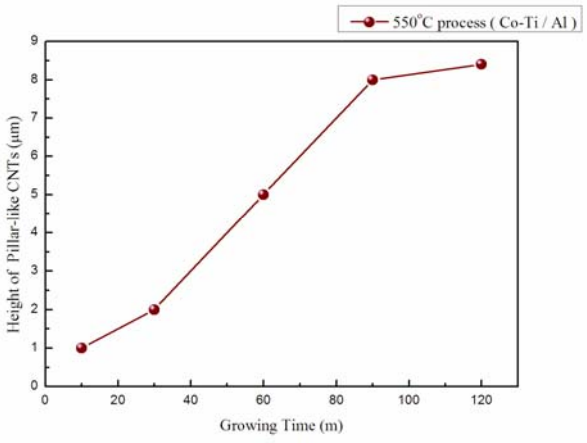

Figure 2-36　Heights of pillar-like CNTs with different growth time.

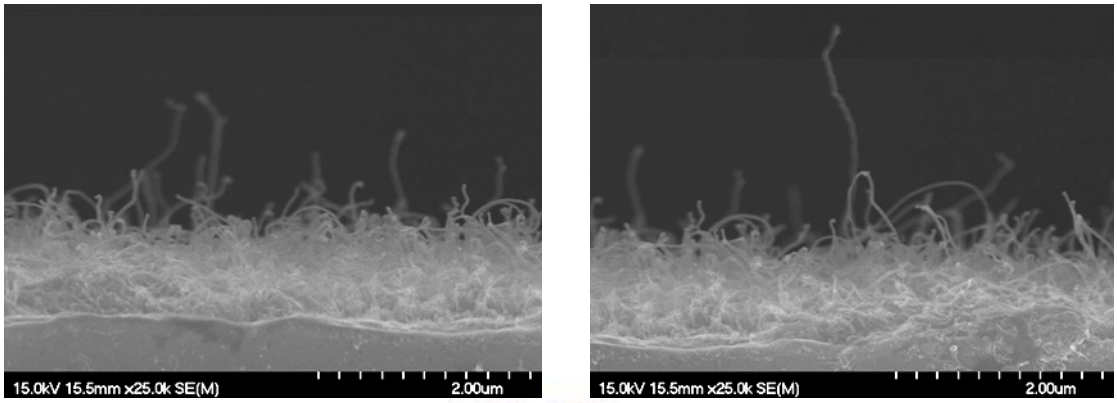

Figure 2-37 Details of a pattern pillar-like CNTs grown about 10 min.

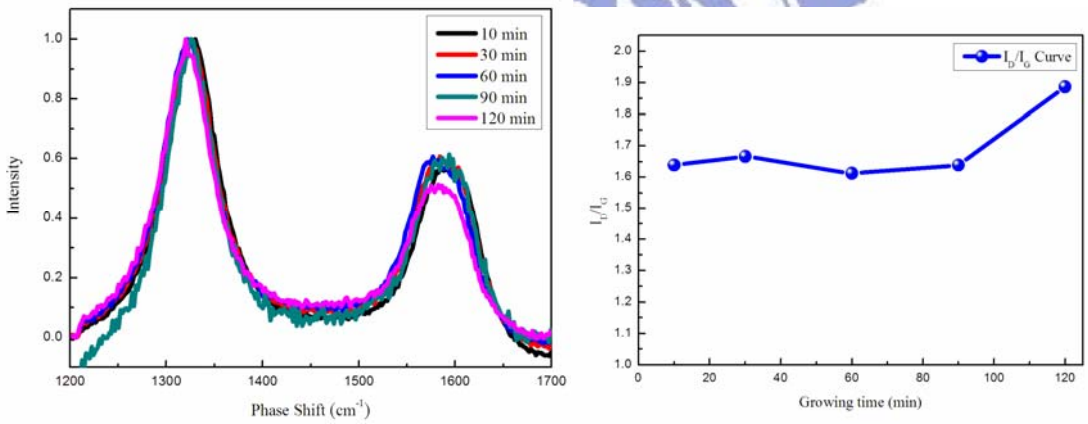

(a) **(b)**

Figure 2-38 (a) Raman analysis with the different growing times and (b) I_D/I_G ratios with different growing times.

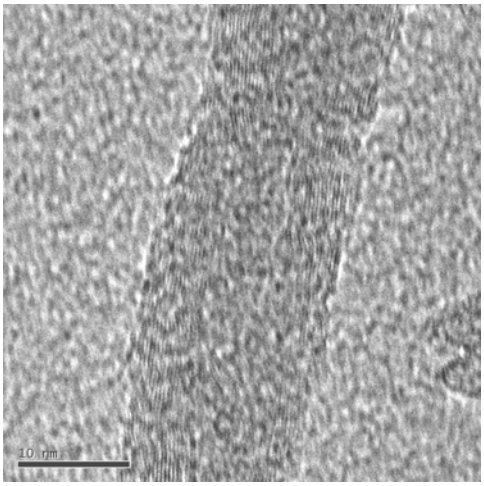

(a)

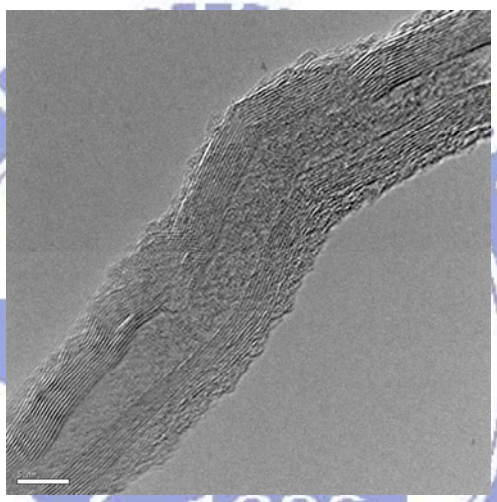

(b)

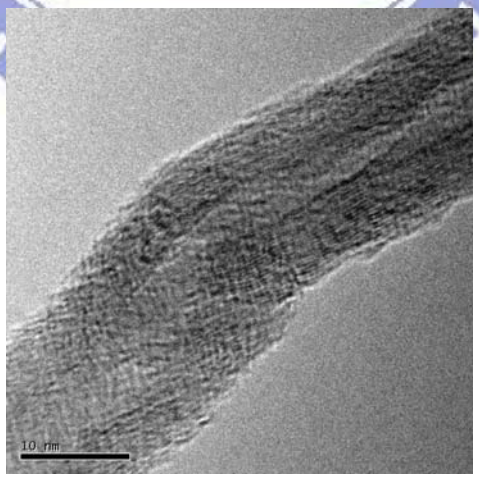

(c)

Figure 3-29 The HRTEM images of multiwall CNT with (a) 10min (b) 60min (c) 90min growth.

Raman spectrum showed the graphite or amorphous phase ratio, and we obtained the similar Raman spectrums under different growth times in Fig. 2-38(a), except 120 min. This result was quite answered our doubts and approached to our assumption. Following Fig. 2-38(b), the I_D/I_G ratios were 1.61~1.65 when growing 10 to 90 min, only 120 min growing CNTs showed higher I_D/I_G ratio (about 1.89), that indicated the defect phase (or amorphous phase) CNTs which growing 120 min was majority compared with growing 10 min to 90 min.

Under our assumptions and experimental proofs, the growth rate of height was limited when processing over 90 min, because the thickness of multiwall CNT increase with growing time, finally carbon had not enough diffusive kinetic energy for diffusion into interface of catalyst atom to form graphite CNT multiwall phase. Thus additional carbon might gather on the formative CNT, then increasing the amorphous defect phase.

In conclusions, we optimized the growing time at 550℃ on Co-Ti/Al by SEM, Raman and TEM [Fig. 3-29] analyses, and the optimal value was 90 min.

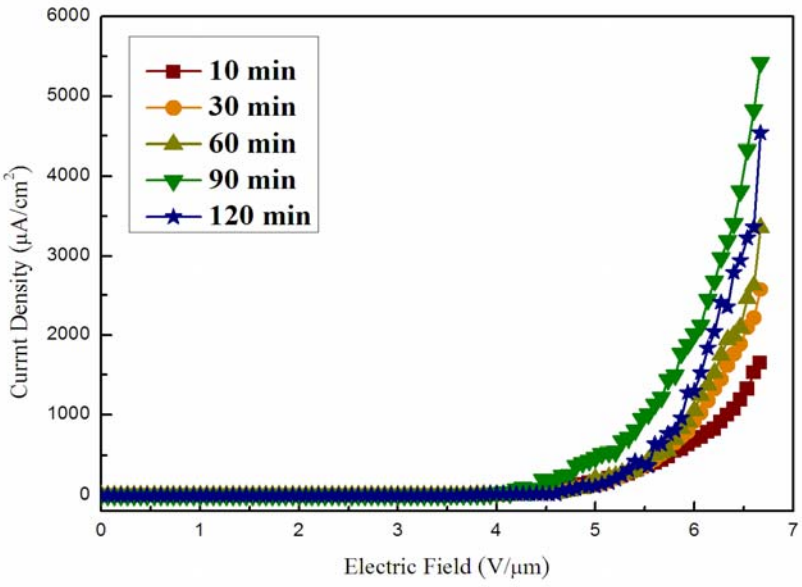

Figure 2-40 The I-V plots of pillar-like CNTs with different growing times at 550℃.

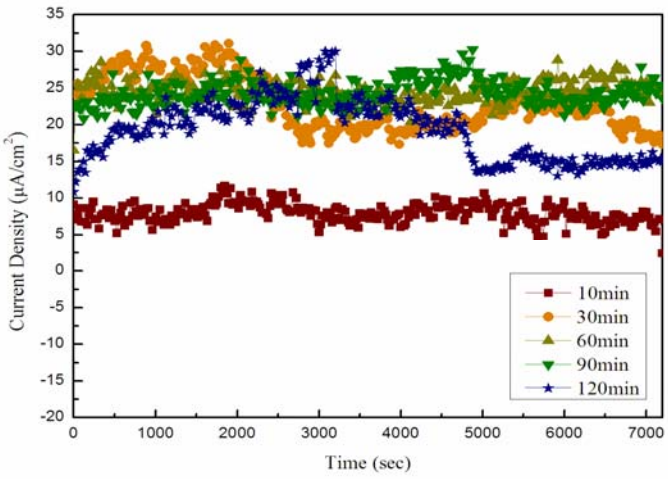

Figure 2-41　Stress testing of pillar-like CNTs with different growing times at 550℃.

Table 2-5

Overall data of pillar-like CNTs with different growing times at 500℃

Parameters \ Growing time (min)	10	30	60	90	120
Height (μm)	1.0	2.0	5.0	8.0	8.4
Turn-on (V/μm)	3.8	3.62	3.75	3.5	3.59
Degradation (%)	2.1	3.6	0.1	0.1	4.7

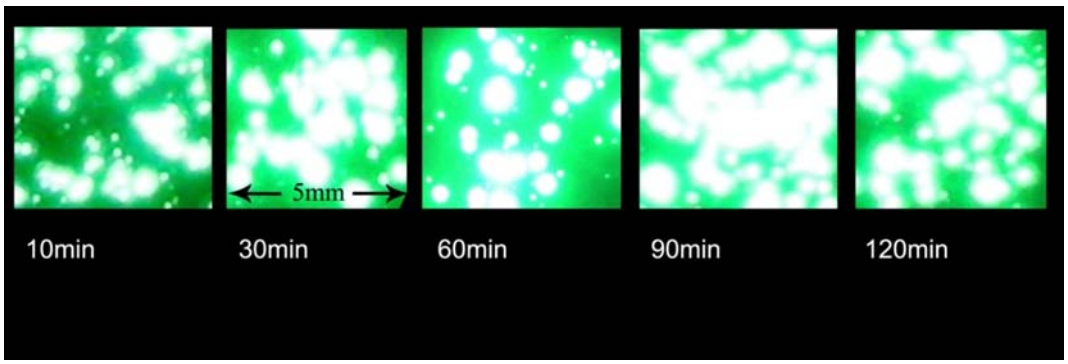

Figure 2-42　The luminescent images of pillar-like CNTs with different growing times at 550℃.

Lastly, we compared the electric characters and luminescent images with our conclusions. In Fig. 2-40, the I-V curves showed higher pillar height by longer growing time bring enhanced current density, but growing after 90 min, the current density decayed oppositely as our past assumption. The current density did not increase with height when 120 minutes growing because of too many amorphous carbon atoms deposited on CNTs, covered over some emission sites formed before, therefore decreasing current density when growing time over 90 minutes. The values were separately 3.8μV/cm, 3.62μV/cm, 3.75 μV/cm, 3.5 μV/cm, and 3.59 μV/cm when growing from 10 to 120 minutes.

The Fig. 2-41 showed the stress tests and analysis under high electric field (6.78 V/μm), and the degradation values were separately 2.1%, 3.6%, 0.1%, 0.1%, and 4.7% when growing from 10 to 120 min. We detected the phenomenon of suddenly decay of reliability when growing over 90 min, that was another proof explained for our assumption of growing times. Table 2-5 was all data of pillar-like CNTs with different growing times at 500℃.

The luminescent images of pillar-like CNTs with different growing times at 550℃ were shown on Fig. 2-42. The best macroscopic photograph presented when growing CNTs about 90 min what proved our assumption once again. So we could certainly grow CNTs about 90 min as the optimal value of growing time.

2.4.3 The Appropriate Pillar Spacing for CNT-BLUs (Experiment C)

In the experiment C, we considered the effect of spacing between two pillars, so we designed eight different patterns which pillar spacing was separately 3μm, 6μm, 9μm, 12μm, 15μm, 20μm, 25μm, and 30μm as Fig. 2-43.

The larger pillar spacing would be surely decreasing the emission area, thus the result could decrease not only the screening-effect, but also the total current and power for saving more electric power as a backlight unit. But if pillar spacing extended too long, the luminescent images might be not uniform any more. As this result, we expected the optimal pillar spacing in 2.4.3 experiment.

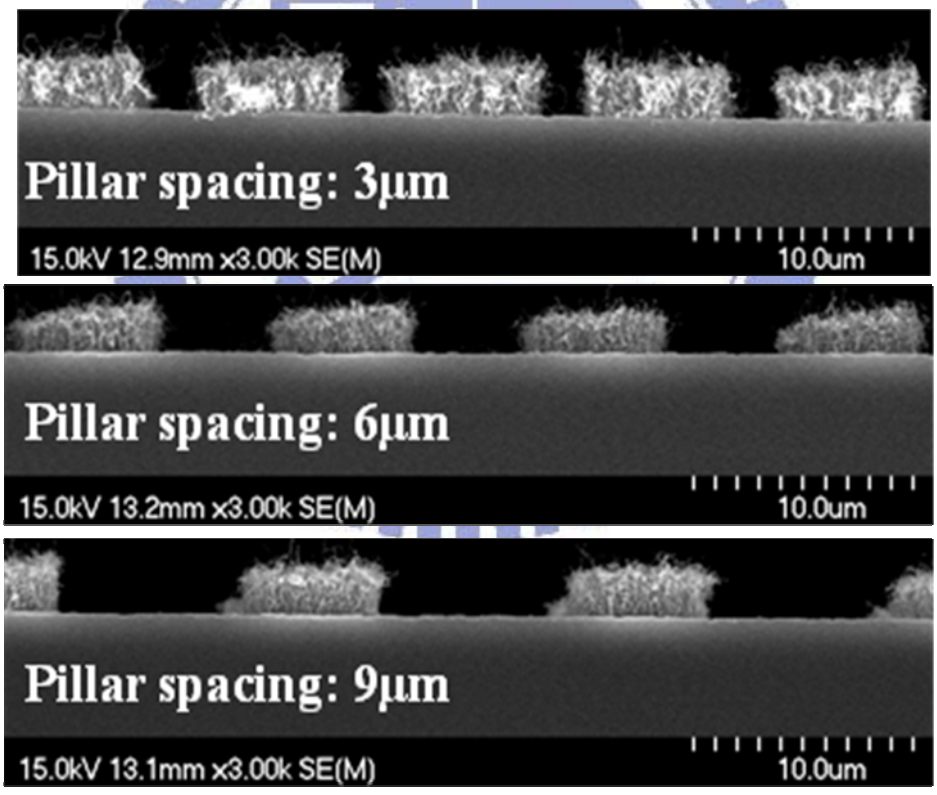

Figure 2-43 The pillar spacing as the variations in experiment C from 3μm to 30μm, 3μm, 6μm, and 9μm were shown for examples.

Depending on Fig. 2-44 I-V curves, the turn-on fields and current densities were similar except 3μm and 6μm pillar spacing, that because of screening-effect. The screening-effect height and pillar-spacing ratio were fixed by simulative electric field, and height of pillar like CNTs in the research were nearly 5μm, by our group's past study, adjusting the pillar spacing (R) and height (H) of pillar-like CNTs. The optimization of the field emission characteristics can be obtained at ratio of 2.0 [2.15].

Following the R/H ratio thesis, our optimal value will be about height of 10μm. Here we still designed this experiment again to be sure that thesis was correct. The result was no doubt certainly that we could eliminate screening-effect completely proved by the phenomenon of current density on fixed emission area.

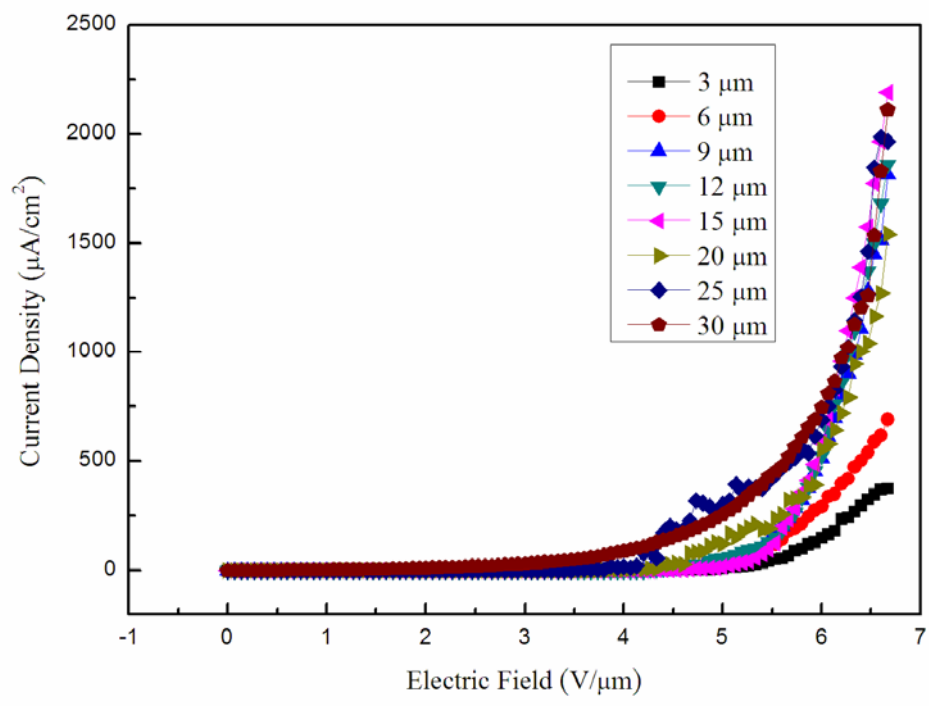

Figure 2-44 The I-V plots of pillar-like CNTs with different pillar spacing (3μm, 6μm, 9μm, 12μm, 15μm, 20μm, 25μm, and 30μm) growing at 550℃.

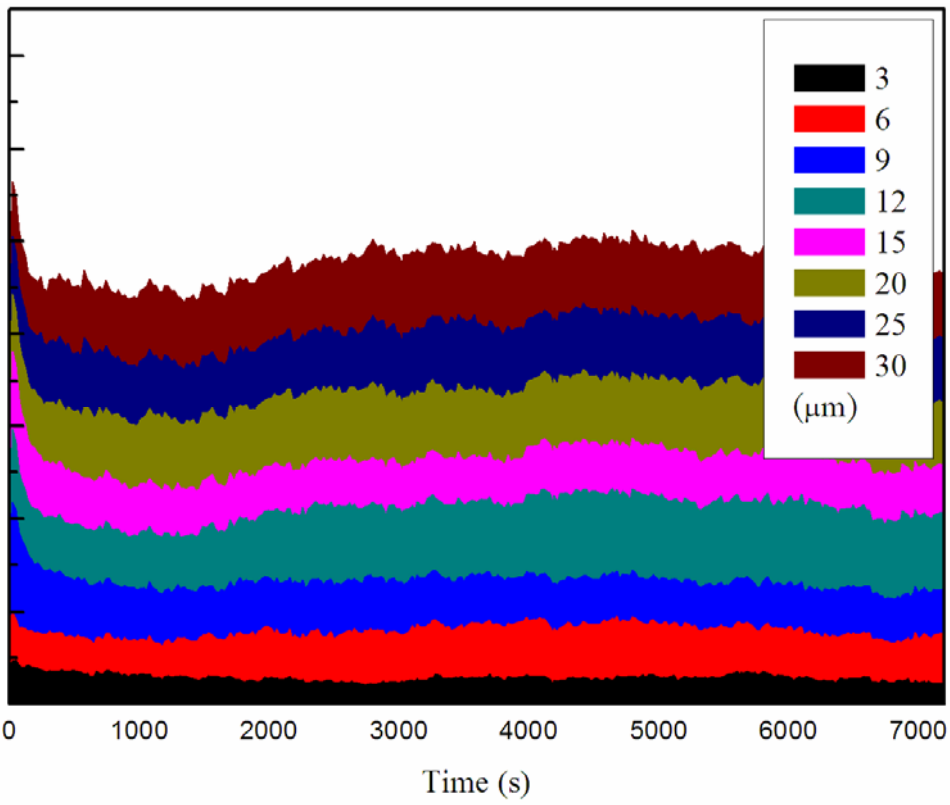

Figure 2-45 Stress testing of pillar-like CNTs with different pillar spacing (3μm, 6μm, 9μm, 12μm, 15μm, 20μm, 25μm, and 30μm) growing at 550℃.

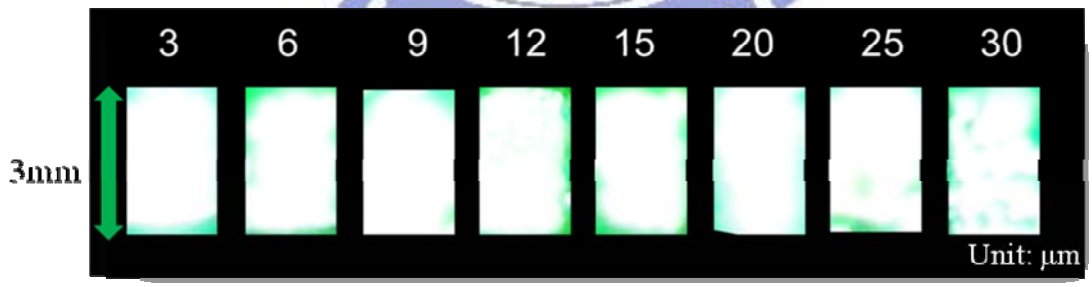

Figure 2-46 Luminescent images of pillar-like CNTs with different pillar spacing (3μm, 6μm, 9μm, 12μm, 15μm, 20μm, 25μm, and 30μm) growing at 550℃.

Following, stress testing [as Fig. 2-45] showed almost similar results trend, but we observed a phenomenon that closer pillars bring more stable reliability, the lowest variation fluctuation of current density appeared on pillar-like CNTs with 3μm, 6μm, and 9μm pillar spacing.

As a result, there were two factors determining the characters of pillar-like CNTs by enlarging or decreasing the pillar spacing: one was the screening-effect which would reduce the current density by over-decreasing of pillar spacing, and another was stability of pillar-like CNTs by over-enlarging the pillar spacing because of the electric force being dispersed on each pillar.

Finally, the luminescent images were shown in Fig. 2-46, and the uniformity of lighting decreased when pillar spacing over 20μm. On the other hand, we could not clearly distinguish the differences of 3μm to 15μm luminescent images.

2.5 Summary

The pillar-like CNTs grown from a Co-Ti/Al (2nm-3nm/10nm) catalyst at 550℃ in thermal CVD exhibited a superior characteristics of electric properties or macroscopic luminescent uniformity, comparing with other three kinds of catalyst. This novel catalyst component provided better adhesion, higher pillar height, and sharper edge.

Then, we optimized the growing time and the pillar spacing at 550℃ because we will grow this pillar like CNTs on the glass substrate in the future. The optimal growing time proved the longest height with lower I_D/I_G ratio, and the optimal pillar spacing could avoid screening-effect with the most stable reliability.

In conclusion, we obtained the optimal pillar-like CNT backlight unit which spacing of 9μm grown 90 min from a Co-Ti/Al (2nm-3nm/10nm) catalyst at 550℃ in thermal CVD. For field emission measurement, the current density of this proposed pillar-like CNTs was as high as 1688 μA/cm^2 at 6 V/μm and the turn-on field was 3.5 V/μm, and the reliability was ultra stable as lower than 1% degradation of initial current density.

Chapter 3

Enhancement of Uniformity by Utilizing a Triode Structure for CNT Field Emitters

3.1 Introduction

Nowadays, in most of field emission device panels, the phosphor materials screens are still used in CRT. These phosphors provide high efficiency of changing electric energy into light energy by bombardments of electrons at enough high voltages of the anode plate. The high-anode voltage improves the qualities of FEDs in color purity and high brightness. The high-anode voltage requires a large vacuum gap between the cathode and anode plates.

The large vacuum gap may cause a problem of high voltage requirement, and several triode structures of field emission displays had been announced to overcome this issue, such as planar-electrode type [3.1], double-gate type [3.2-3.4], and mesh-electrode type [3.5]. Triode structure could easy decrease driving voltage from 1000V to 60~80V for broadly using on many devices.

Following our group's past researches [3.6], we reduced the cross-talk noisy by using the self-gated structure for because of a problem of beam spreading. The cross-talk noisy was a drawback for FED, but it might be a advantage for the field emission backlight units (FE BLUs). Therefore, we tried to utilize the cross-talk noisy for enhancing uniformity of our field emission backlight units.

In this chapter, a lateral gated structure is fabricated with simple fabrication processes with only one step of pattering, and the results of the simulation and luminescent images show

a superior spreading in electron trajectory. This novel triode structure with simple processes is promising for backlight units because of better uniformity and lower driving voltage. We only changed some scale of the gate to get the spreading effect. It is simple, but work well.

This can make this structure scalable in extension to a large-area panel and feasible in manufacturing high-uniformity backlight devices. This lateral gated cathode structure is expected to have an excellent uniformity by ultra simple process and structure.

3.2 Simulations and Fabrication

Simulations were performed to investigate the beam spreading of emission electrons with commercial software (SIMION-3D) using the finite element method. It was found that an initial energy and divergence angles of e-beams at the moment of emission from CNTs were 5 eV and -90°~+90°, respectively [3.7].

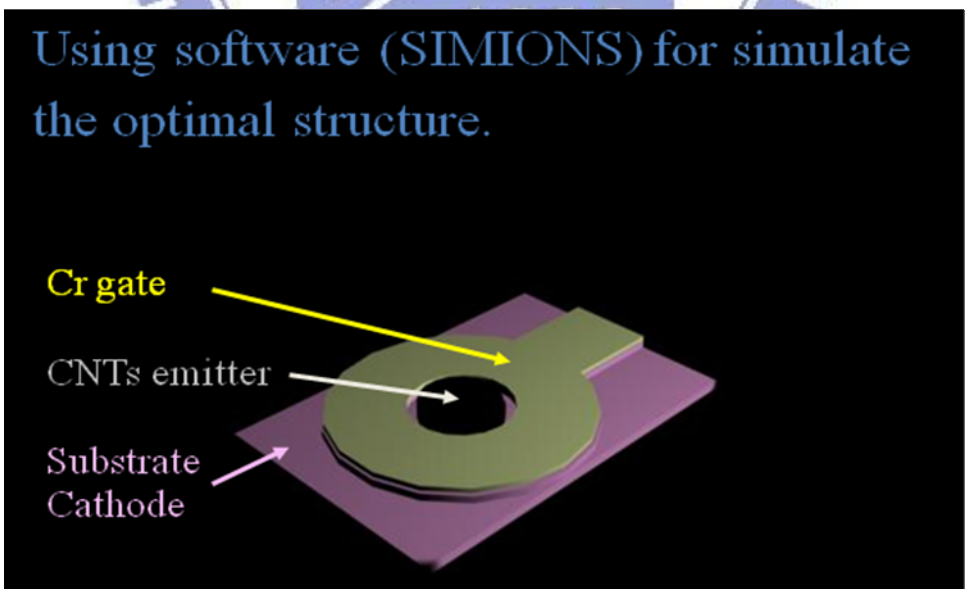

Figure 3-1 Schematic of a triode field emission pixel.

3.2.1 The Structure of the Lateral FE Triode Array

Our triode structure was design as Fig. 3-1. Central CNTs were used to be cathode electric emitter, and surrounding Cr was used to be gate of this triode structure. Basically the anode voltage was fixed as 1000V, cathode was 0V, and the gate was sweeping from 0V to 80V. Secondly, the spacing between cathode and anode was fixed as 550μm, the phosphor was deposited on anode glass plate with ITO coating.

That was the schematic figure which showed some variable parameters, such as field emission region, height of insulator, height of CNTs, gate length, and gate to emitter length. Fig. 3-2 showed some changeable parameters we could design easily. And we tried to optimize the best values of these parameters which were the gate length in 3.2.2, height of insulator and CNTs in 3.2.3, and gate to emitter length in 3.2.4. In this study, we optimized by simulations of electron trajectory.

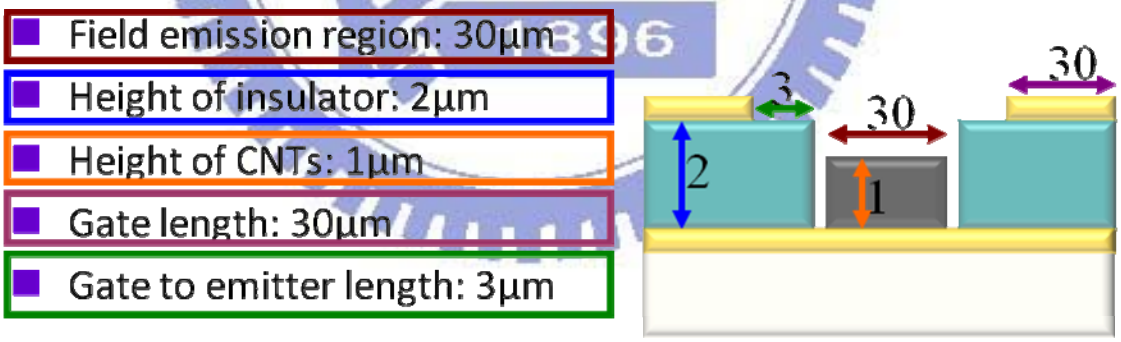

Figure 3-2 Changeable parameters of triode structure in this research.

3.2.2 The Factor of Gate Length

Firstly, the gate length was limited and decided by the spacing of two emitters. Trend of the gate length effect was simulated by using SIMIONS. In 3.2.2, we designed several values of the gate length, which were 10μm, 15μm, 20μm, 25μm, and 30μm as Fig. 3-3 shown.

Figure 3-3 The variable gate length was one of parameters.

The electron trajectory schematic figures showed in Fig. 3-4(a)-(e) by SIMIONS indicated that longer gate length induced larger area of electron spreading. After simulations, we could obtain the obvious result. The diameter of dispersion of electron from emitter was 260μm with 10μm gate length, 280μm with 15μm gate length, 295μm with 20μm gate length, 310μm with 25μm gate length, and 310μm with 30μm gate length. As a result, we could get two conclusions. One was longer gate length brought longer diameter of electron dispersion, another was saturation of dispersive diameter appeared when gate length was longer than 25μm as the Fig. 3-5 shown.

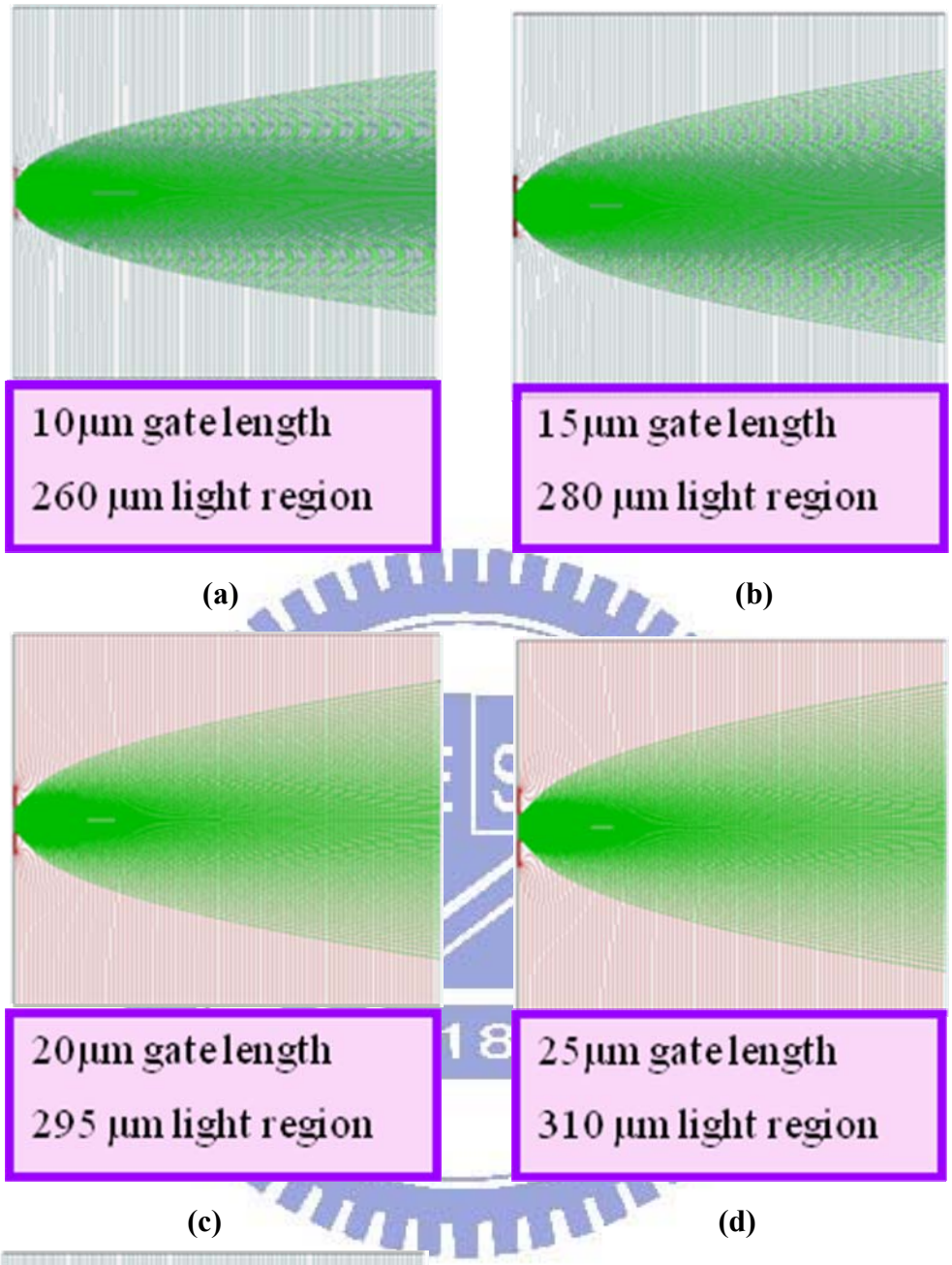

Figure 3-4 The simulations of effects by different gate length (a) 10μm (b) 15μm (c) 20μm (d) 25μm (e) 30μm.

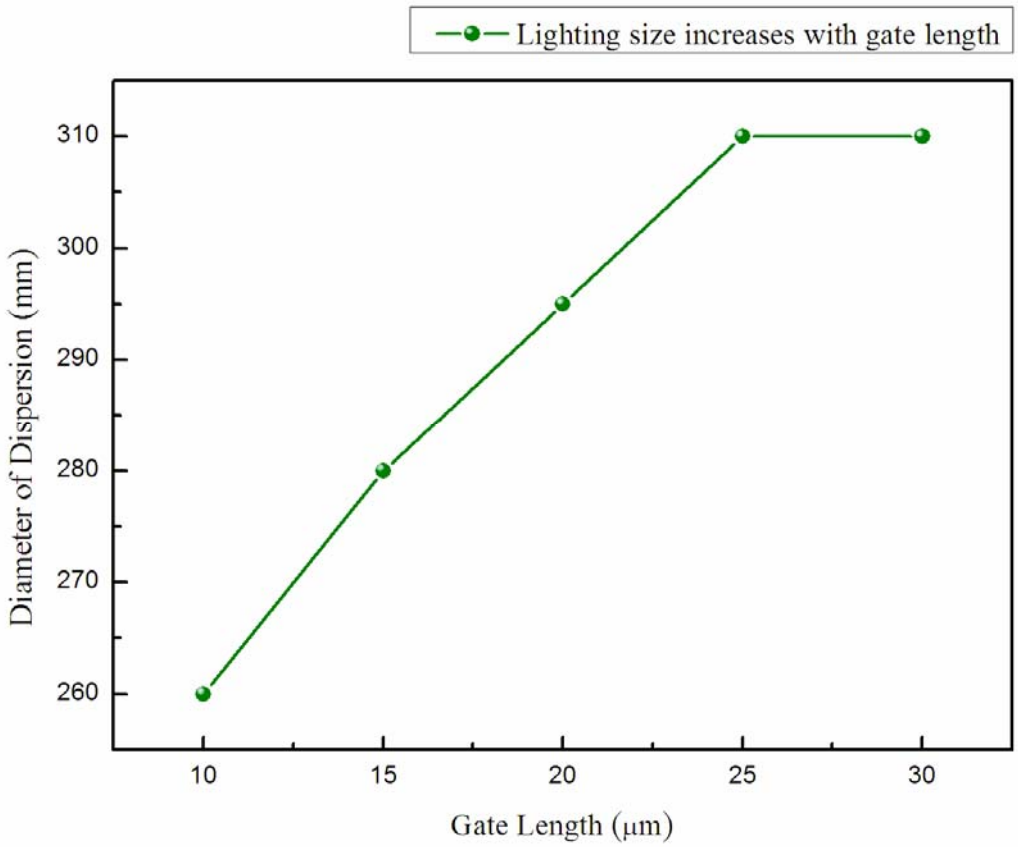

Figure 3-5 The diameter of electron dispersion (lighting size) versus gate length plot.

In conclusion, we realized the influence on diameter of electron dispersion by gate length, we could obtain the most dispersive level when the gate length was longer than 25μm. Because we wanted more degree of electron dispersion, our simulations were all fixed the gate length as more than 20μm in 3.2.3 and 3.2.4.

3.2.3 The Factor of Vertical Distance

Secondly, the vertical distance was decided by height of CNT emitter and Height of insulator (oxide), this issue also influenced the diameter of electron dispersion. There were three different values of the height of emitter and insulator, separately (a) 2μm oxide and 1μm CNTs (b) 1μm oxide and 1μm CNTs (c) 1μm oxide and 2μm CNTs as Fig. 3-6.

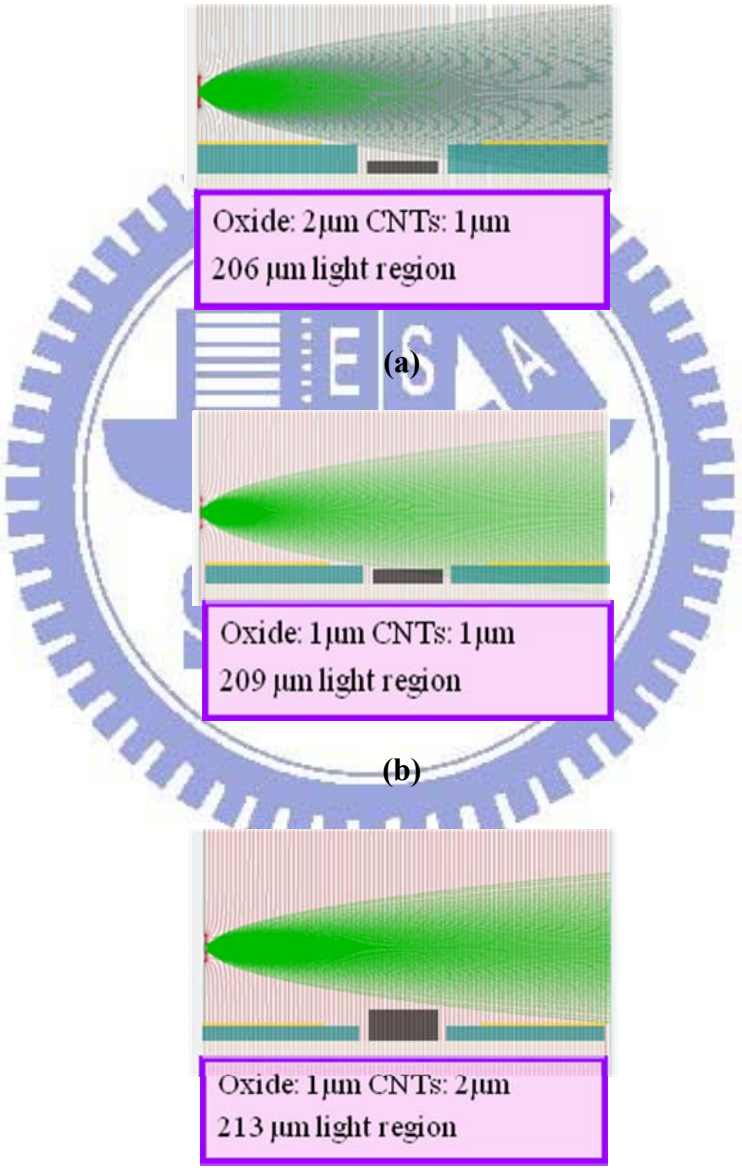

Figure 3-6 The factor of vertical distance (a) oxide was higher than CNTs, (b) oxide was as high as CNTs (c) oxide was shorter than CNTs.

As the result of Fig. 3-6, we could plot the diameter of electron dispersion versus vertical distance which was emitter height - insulator height (H_E-H_I) shown as Fig. 3-7, separately 206μm, 209μm, and 213μm.

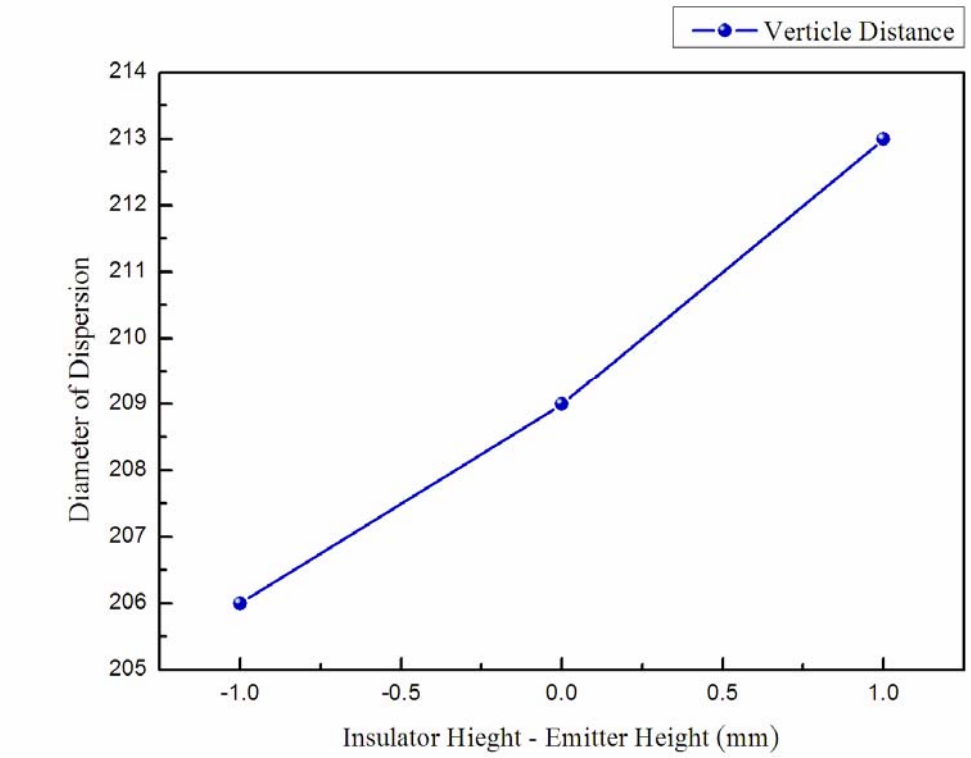

Figure 3-7 The diameter of electron dispersion versus vertical distance.

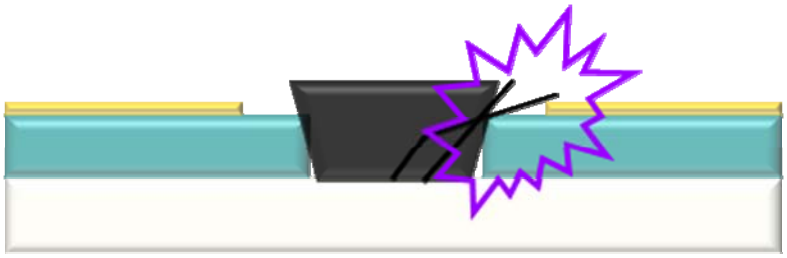

Figure 3-8 The schematic of a short situation occurred because of over height of CNTs.

Consequently, the result as Fig. 3-7 showed that the increasing H_E-H_I would positively increase the electron dispersion, that meant longer CNTs or shorter insulator could bring more dispersive and uniform lighting. But there were two situations which limited this issue:

(1) The height of CNTs was limited by growing temperature and growing time.

(2) If the height of CNTs was over enlarge and much higher than insulator, the CNTs might be absorbed by gate after gate having a positive voltage, then our device would be a short circuit [shown in Fig. 3-8]. So height of CNTs was also limited by height of insulator.

These two situations majorly focused on avoiding short occurring, so we controlled growing time to insure height of CNTs was not over the height of insulator.

On the other hand, we could realize that the risk of short circuit substantially increased by increasing of the height of CNTs, and the benefit of the higher CNTs was unobvious. As this result, we designed the structure of height of CNTs and insulator were both 1μm to prevent phenomenon of short circuit.

3.2.4 The Factor of Gate to Emitter Length

The gate to emitter length was one of the major factors to affect the diameter of electron dispersion. This issue was not only affect the electron dispersive trajectory, but also the electric field of the emitter tip. Lowering gate to emitter length would quite increase the electric field of emitter tip, then lowering the turn-on voltage of the gate or enlarging the current density at fixed gate voltage.

Because this issue was very significant, we must considered the gate to emitter length in our research and optimalize it. Firstly, we sould observed the results of simulation as Fig. 3-9 and understood the trend of this factor. Fig. 3-9(a) showed the diameter of electron dispersion was 310 μm when gate to emitter length was 1 μm, Fig. 3-9(b) showed the diameter of electron dispersion was 280 μm when gate to emitter length was 2 μm, and Fig 3-9(c) showed the diameter of electron dispersion was 240 μm when gate to emitter length was 3 μm.

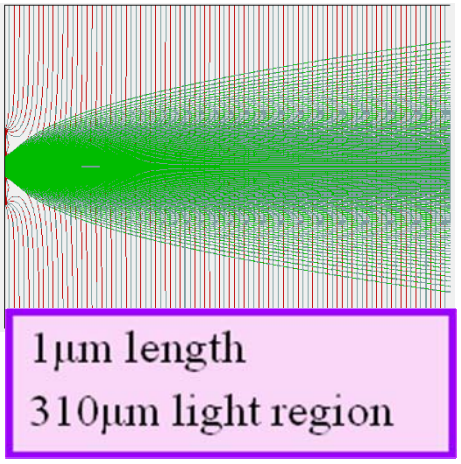

(a)

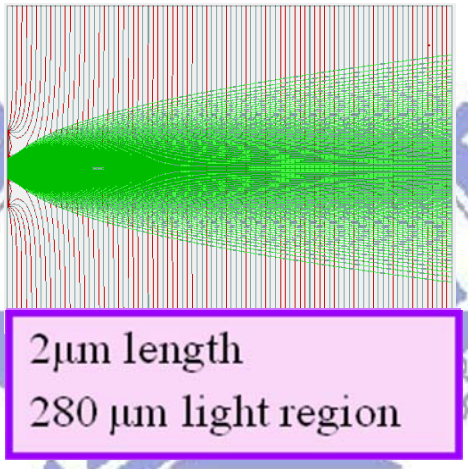

(b)

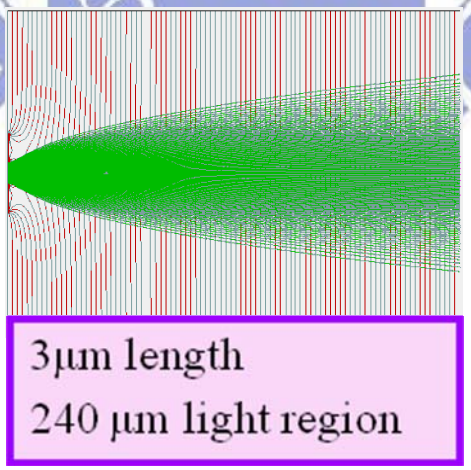

(c)

Figure 3-9 The dispersion of emission electron increased with the gate to emitter length, the lighting region was (a) 310μm by 1μm gate to emitter length (b) 280μm by 2μm gate to emitter length (c)240μm by 3μm gate to emitter length.

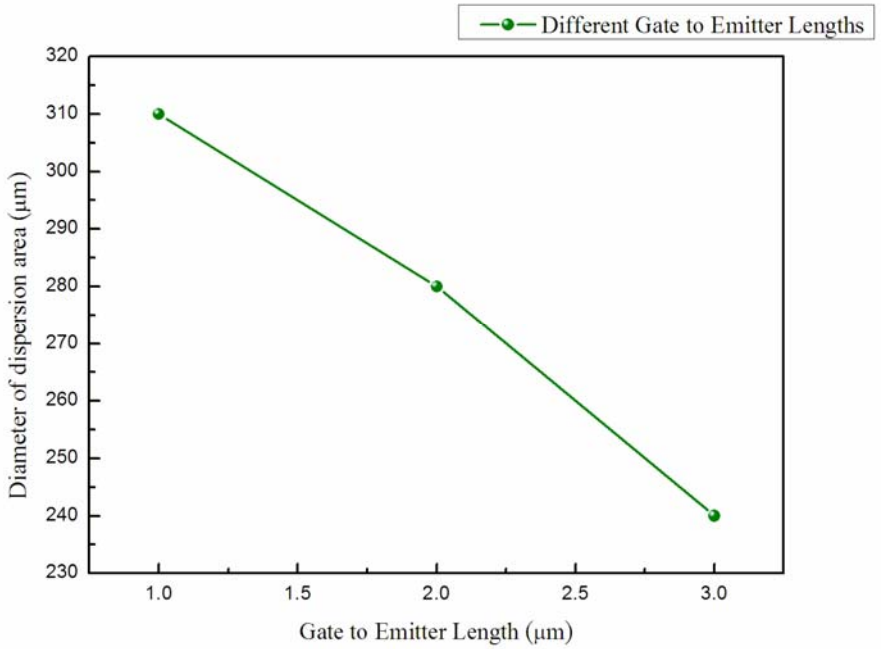

Figure 3-10 The dispersion of emission electron will increase with the gate to emitter length.

Figure 3-11 The schematic of the shorter length bring more risk of short circuit.

The trend of the gate to emitter length was shown in Fig. 3-10, lower the gate to emitter length brought larger electron dispersive region from 310μm to 240μm. But the risk of short circuit might appear with the ultra close of gate and emitter, hence we should select the most appropriate length of gate to emitter in our research in following experiments.

3.2.5 The Optimum Structure in Simulations

Instead of the diode structures of field emission were shown in Fig. 3-12(a) and Fig. 3-12(b) without gate voltage bias, the triode structures of our field emission backlight units were Fig. 3-12(c) and Fig. 3-13(d). We could obviously observe the enhancement of uniformity by triode gated structure.

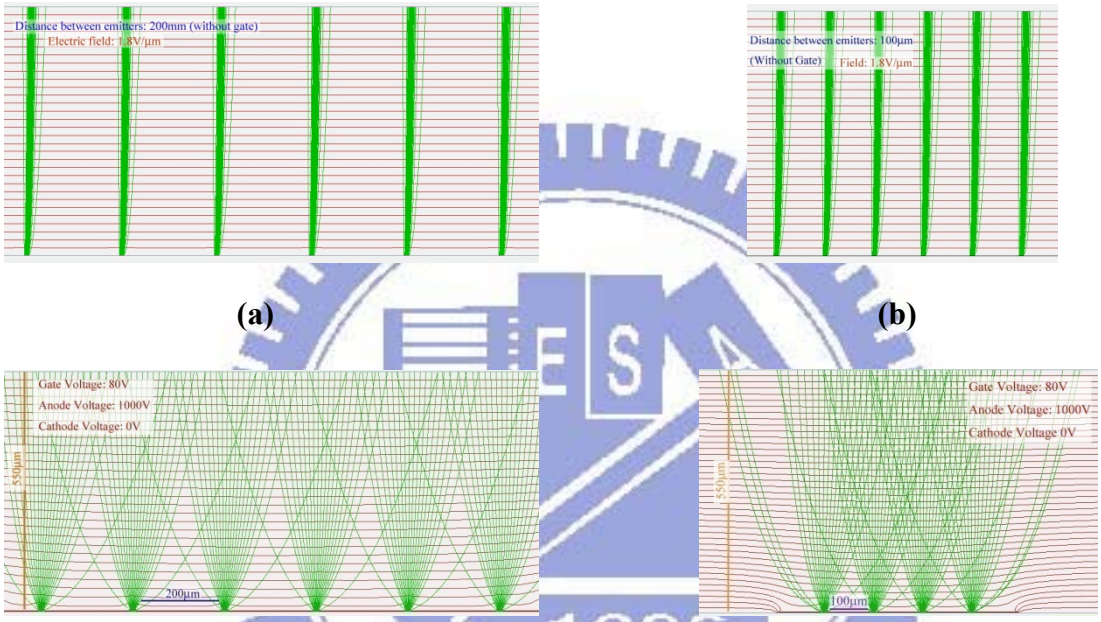

Figure 3-12 Simulations of electron dispersion of 100μm pattern spacing (a) with (c) without gate, and 200μm (b) with (d) without gate.

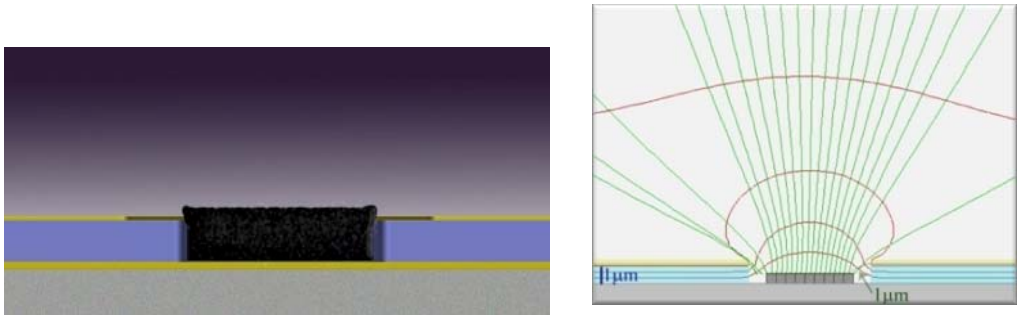

Figure 3-13 The schematic profile of triode gated structure in our research.

The schematic profile of triode grated was shown in Fig. 3-13(a), and the micro-viewpoint with contour lines of voltage was shown in Fig. 3-13(b). Following that, the electric field of our simulations was relatively high, so the turn-on field of this device by simulation only needed below 80V in our research.

After that, the schematic of electron dispersion without gate structure was shown in Fig. 3-14(a) and the central gated structure was shown in Fig. 3-14(b). These two kinds of field emission devices both owned poor uniformity comparatively, so we simulated the surrounding gate structure for improvement of uniformity.

Secondary, the issues of surrounding gate structures were structural fixed, except the gate to emitter length. That was because this was the major issue of all and the electron trajectory was sensitive to the gate to emitter length. And the gate to emitter length was controllable and variable easily by simple fabrication controlling.

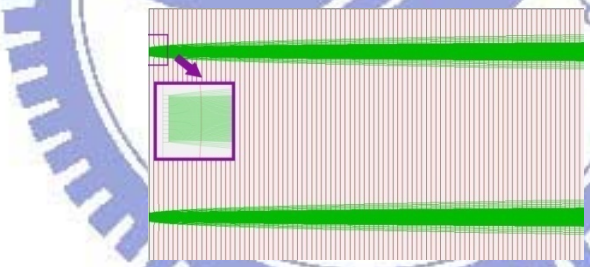

(a)

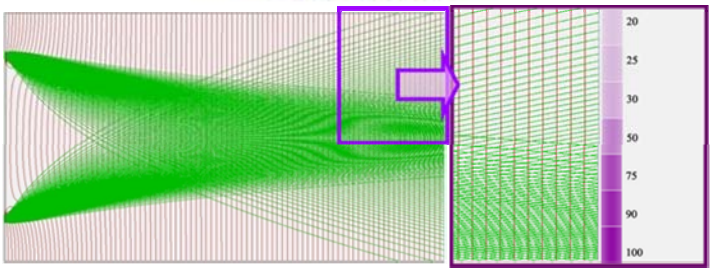

(b)

Figure 3-14 The schematic of electron trajactory (a) without gate structure and (b) with central gate structure

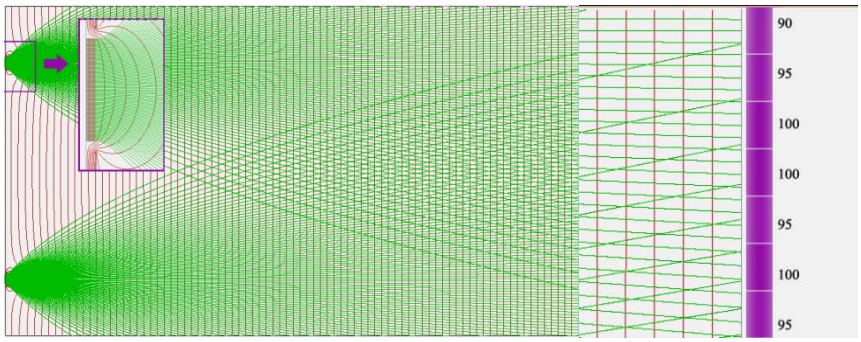

(a)

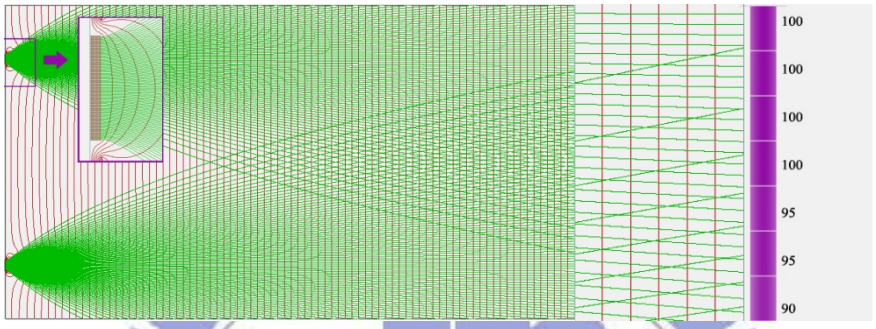

(b)

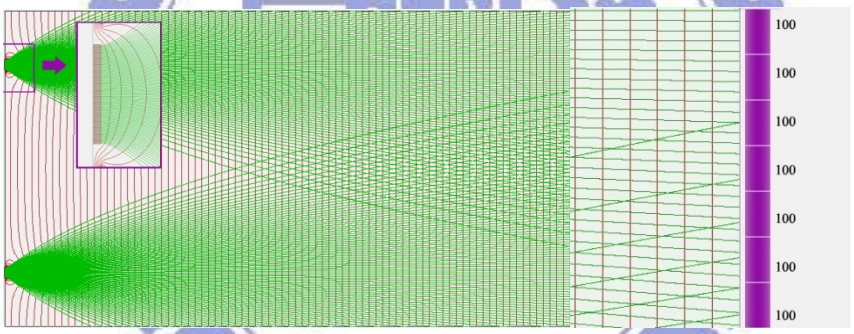

(c)

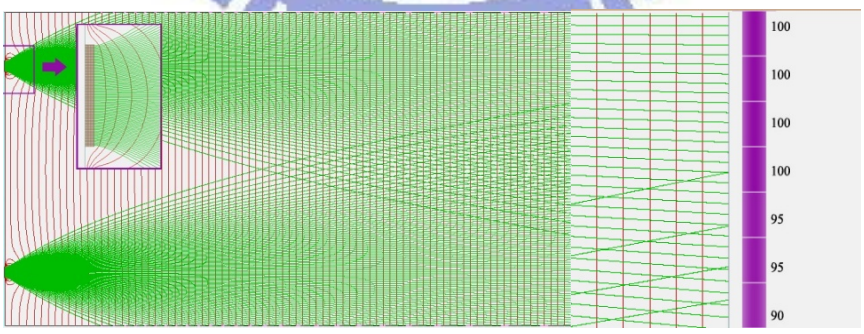

(d)

Figure 3-15 The simulations of different lengths between gate and emitter were (a) 1μm, (b) 1.5μm, (c) 2μm, and (d) 2.5μm

As this result, Fig. 3-15(a)-(b) showed the pattern of 200μm pillar spacing with different length between gate and emitter. Because we could easily control this issue by fabrication step of gate lateral etching, we could simulate any value we wanted. We controlled the gate to emitter length from 1μm to 2.5μm, and then observed the conditions of the electron dispersion. Finally, the optimal gate to emitter length was 2μm, not enough electron dispersion if length more than 2μm, over dispersion if length less than 2μm.

On the other hand, considering the emitting electron density by F-N theory as the Eq. (3-1):

$$J = \frac{aE^2}{\phi t^2(y)} \exp\left[-\frac{b\phi^{\frac{3}{2}} v(y)}{E}\right] \quad (3\text{-}1)$$

where J is the current density (A/cm^2). E is the applied electric field (V/cm), ϕ is the work function (in eV), $a = 1.56\times10^{-6}$, $b = -6.831\times10^{-7}$, $y = 3.79x10^{-4}\times10^{-4}E^{1/2}/\phi$, $t^2(y)\sim1.1$ and v(y) can be approximated as [1.10]. And the Eq. (3-2) eliminated the other parameters except electric field.

$$J = E^2 \exp\left(\frac{-1}{E}\right) \quad (3\text{-}2)$$

Therefore, we could simulate more correctly on current density, table 3-1 and Fig. 3-16 were the calculated current density of one emitter patter in our research.

Table 3-1

The calculated current density of one emitter patter

Parameters / Position	E	E^2	exp(-1/E)	ratio of J
Edge	**25**	**625**	**0.96**	**6.67**
Middle	**15**	**225**	**0.94**	**2.35**
Center	**10**	**100**	**0.90**	**1.00**

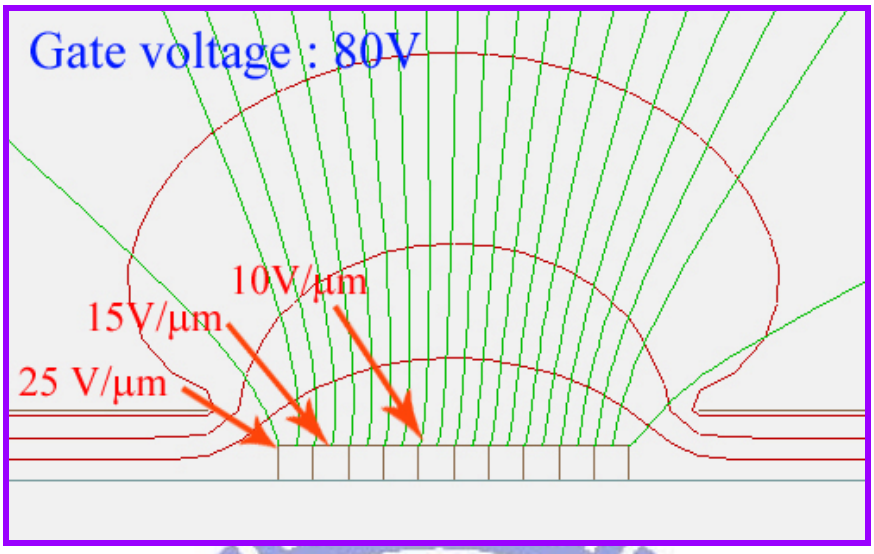

Figure 3-16 The calculated current density of one emitter patter.

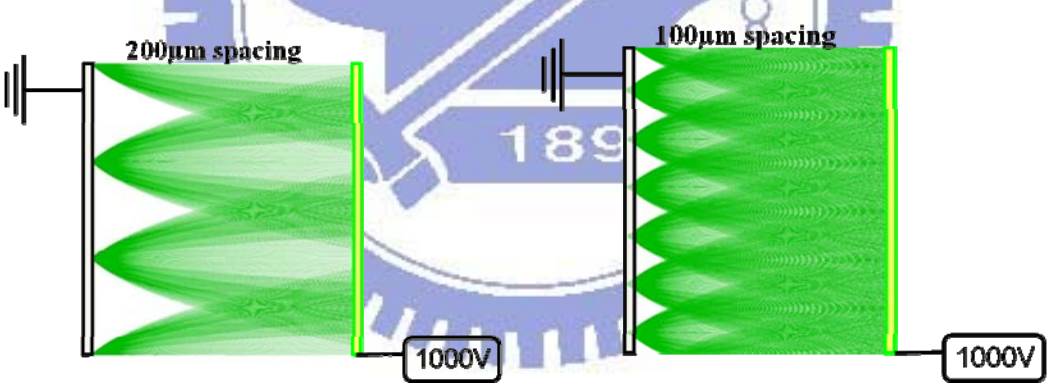

(a) **(b)**

Figure 3-17 The schematic figure with (a) 200μm pattern spacing and 80V gate voltage by our simulation with F-N theory, (b) 100μm pattern spacing.

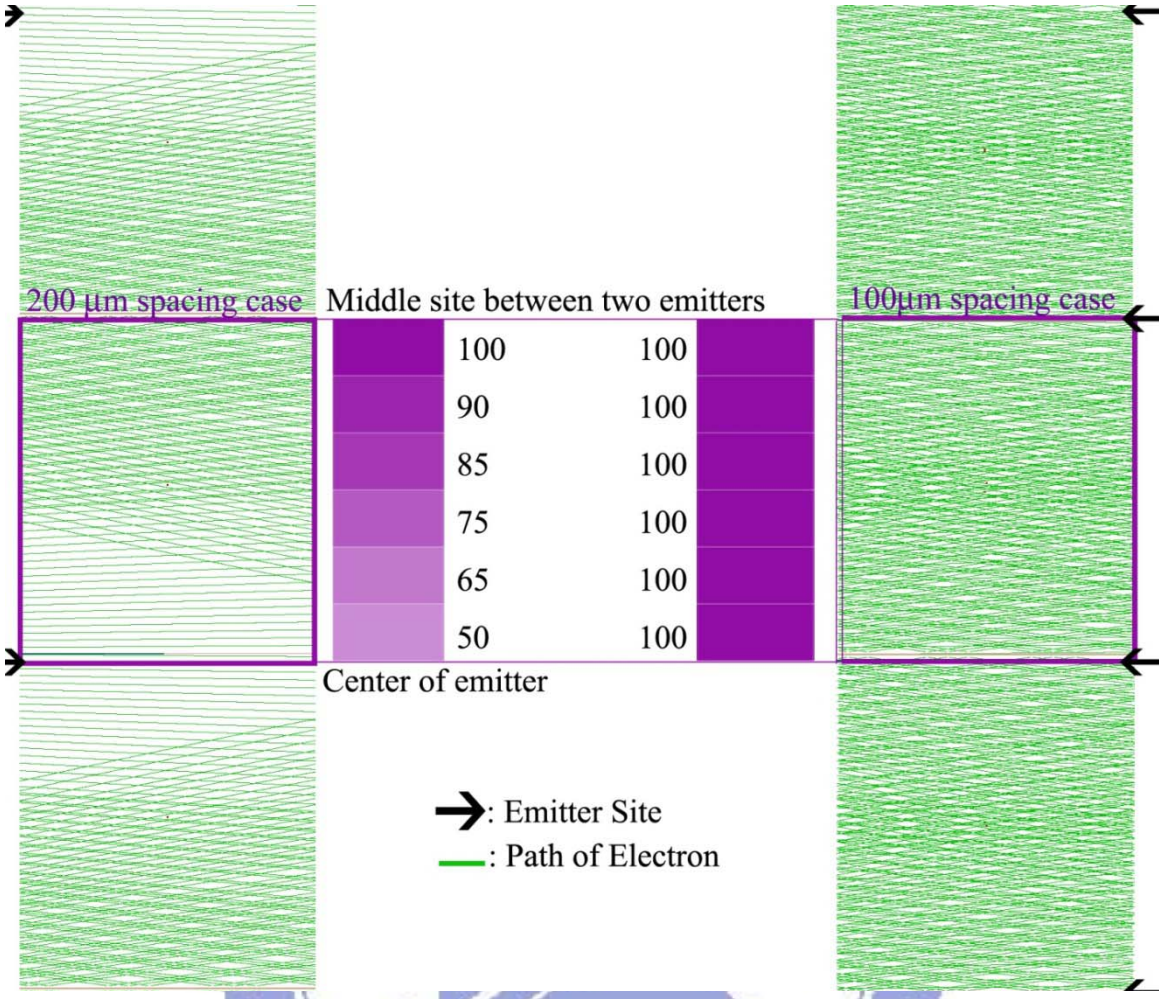

Figure 3-18 the F-N theory dominated this experiment, the 100μm would show the superior uniform dispersion than 200μm.

Fig. 3-17(a) was the schematic figure with 200μm pattern spacing and 80V gate voltage by our simulation with F-N theory, and Fig. 3-17(b) was the schematic figure with 100μm pattern spacing.

As a result, if the F-N theory was not the dominative issue in this experiment, the 200μm gate to emitter length was the optimum pattern spacing. And if the F-N theory dominated this experiment, the 100μm would show the superior uniform dispersion as Fig. 3-18.

3.3 Experimental Procedures

Following the simulation of parameters we adjusted, the optimal device was shown as Fig. 3-19. The emitter area was a circle with 10μm diameter, the height of oxide and CNTs were both fixed as 1μm, and gate to emitter length was 2μm.

This triode structure was comparatively simple than other novel triode field emission devices, and only one mask step for patterning. Fig. 3-20 was the processing flow of our experiment, Fig. 3-20(a) showed first of all we prepared a Si (100) substrate after RCA clean. In Fig. 3-20(b), 100nm Cr cathode electrode was coated by dual E-gun. In Fig. 3-20(c), 1000nm oxide was deposited by plasma enhance chemical vapor deposition (PE-CVD), Fig. 3-20(d) showed 100nm Cr gate electrode was coated by dual E-gun. In Fig. 3-20(e)-(g) showed the patterning of emitter circle and etch Cr gate and oxide insulator layer by wet etch. Finally, the CNTs growing was showed in Fig. 3-20(h).

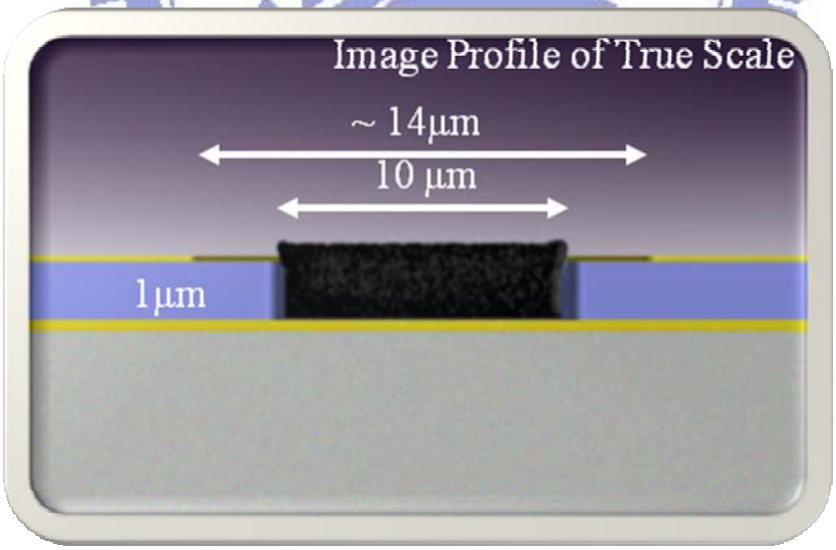

Figure 3-19 The schematic profile and scales of each parameter.

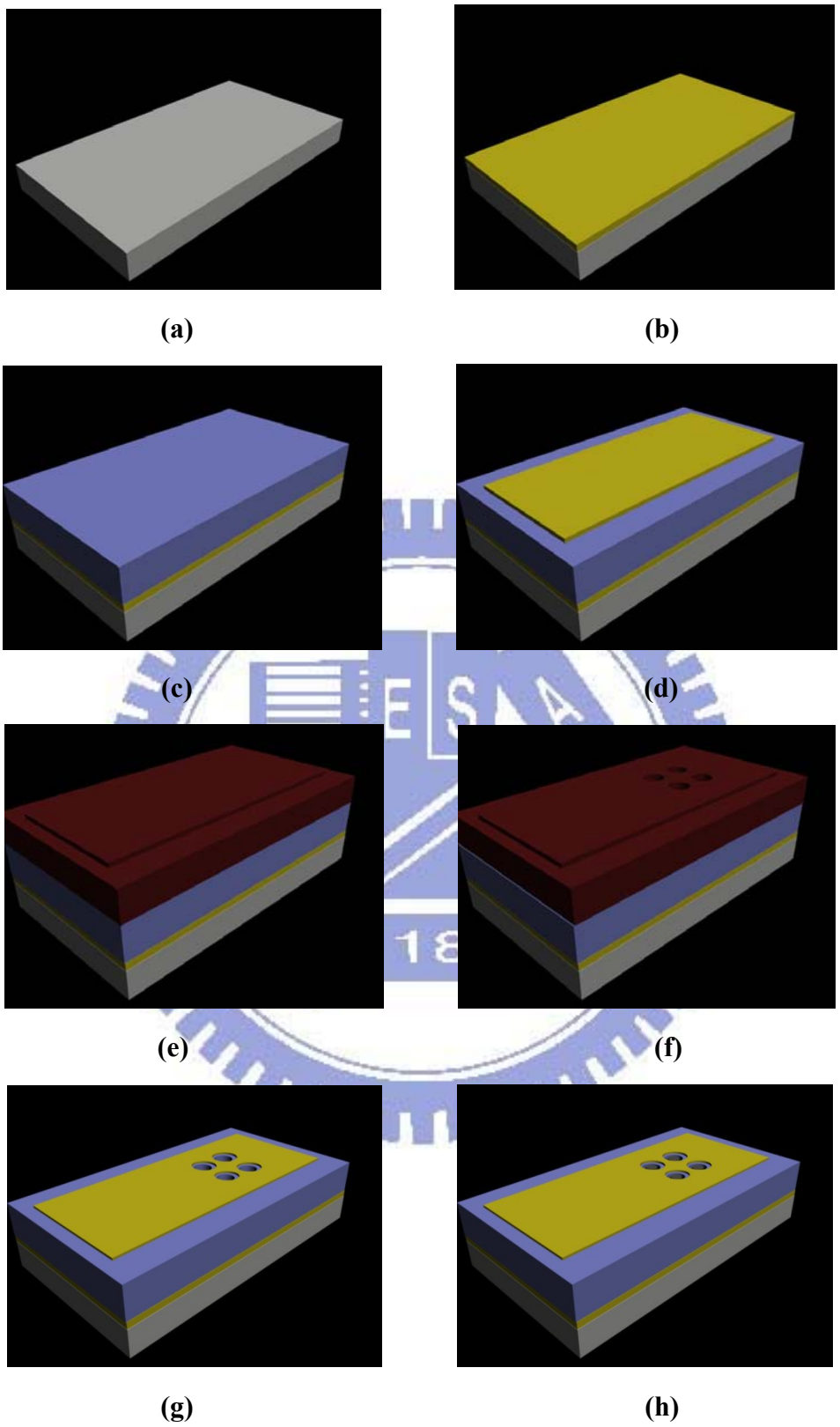

Figure 3-20 The process of fabrication of triode field emission structure (a) preparing Si (100) substrate, (b) 100nm Cr electrode, (c) 1000nm SiO_2, (d) Cr gate 100nm, (e) photo-resistance (PR) coating, (f) developing, (g) clear out the PR, and (h) CNTs growth.

3.4 Results and Discussion

The top views of these devices in our research were showed in Fig. 3-21(a)-(b) by optical microscope, separately 100μm spacing array and 200μm spacing array. Firstly, we analyzed the profiles of one device by scanning electric microscope (SEM). In Fig. 3-22(a), the emitter was CNTs which have been grown 10min by recipes of Co-Ti/Al catalyst at 550℃ in chapter 2. And in Fig. 3-22(b), it was CNTs which have been grown 30min by recipes of Co-Ti/Al catalyst at 550℃.

We could observe the CNTs grown on Co-Ti/Al catalyst in our triode structure were high density and well aligned on the interface of the substrate no matter the growing time was 10min or 30min. Let focus on Fig. 3-22(b) after 30min growth, the height of CNTs was about 2.5μm and the gate to emission length was 2μm, the risk of short circuit arose obviously, as this result, even through how well the electric properties it was, we should give a priority to avoid short circuit, so following experiments were all growth CNTs only 10 min for controlling the length of the CNTs.

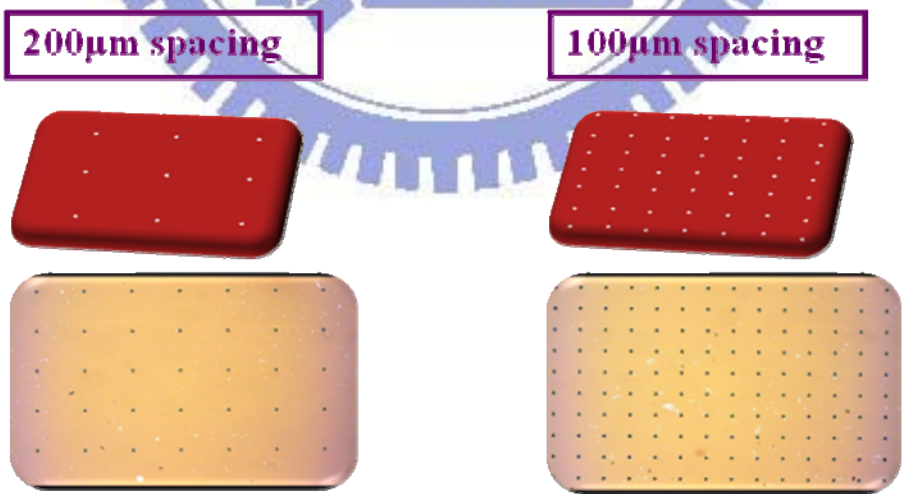

(a) **(b)**

Figure 3-21 The mask and top view of optical microscope (a) 200μm, (b)100μm.

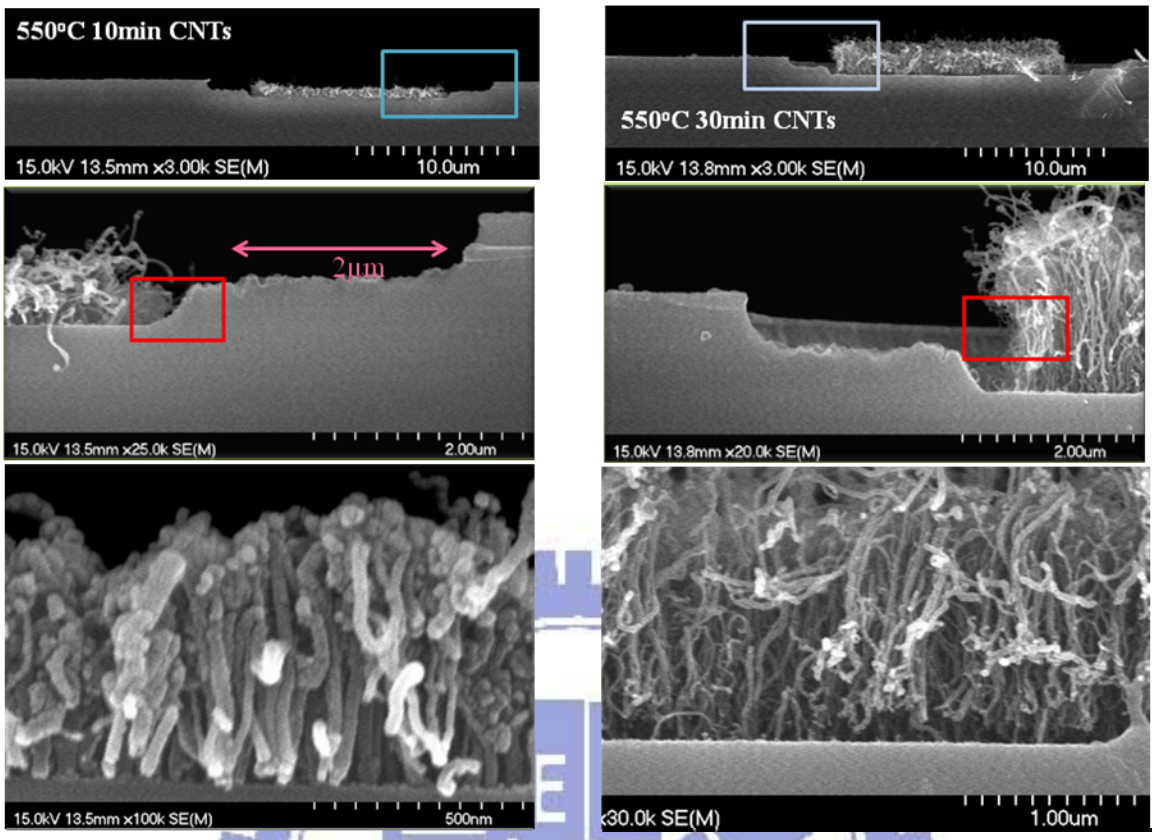

(a) (b)

Figure 3-22 The cross section images of our triode structure by SEM which CNTs growing time was (a) 10min and (b) 30min.

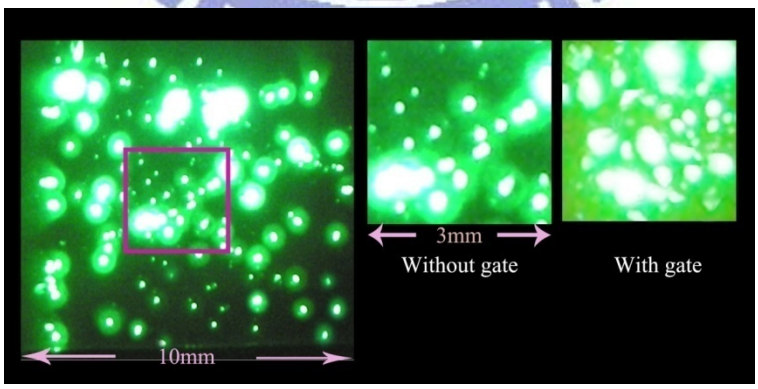

Figure 3-23 Comparing of diode pillar and this simple triode structure.

Secondly, the luminescent image was shown as Fig. 3-23, which compared with the diode field emission backlight unit in our research in chapter 2. We could detect the luminescent image by triode field emission structure was more uniform than diode one by naked eyes, and need less current density without sacrificing the brightness. So we could obtain a conclusion which the triode field emission structure would improve the uniformity by large angle of electron dispersion.

Lastly, we made an experiment on electric field emission testing to accurately get the turn-on voltage and current density as Fig. 3-24(a), and the turn-on voltage defined by logarithm I-V plot as Fig. 3-24(b). In Fig. 3-24(a)-(b) shown, the current densities of 100μm and 200μm spacing were owned the same value about 800μA/cm^2 and the turn-on voltages were 43V to 44V [table 3-2], this result showed the screening-effect was totally avoided.

Table 3-2

The turn-on voltage and of the triode gate structure

Pattern spacing / Parameters	100μm Spacing	200μm Spacing
Turn-on voltage	43V	44V
Current density	803μA/cm^2	791μA/cm^2

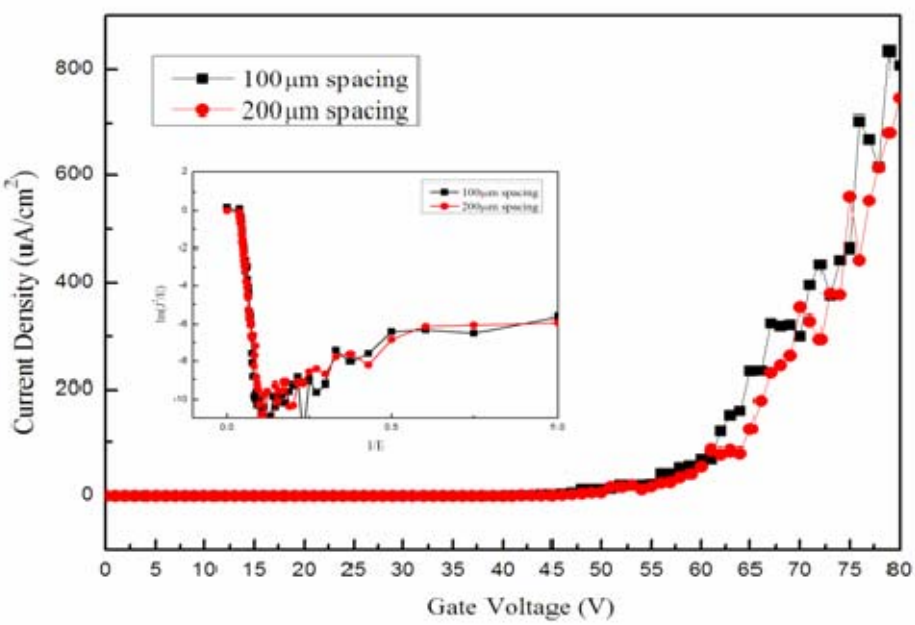

(a)

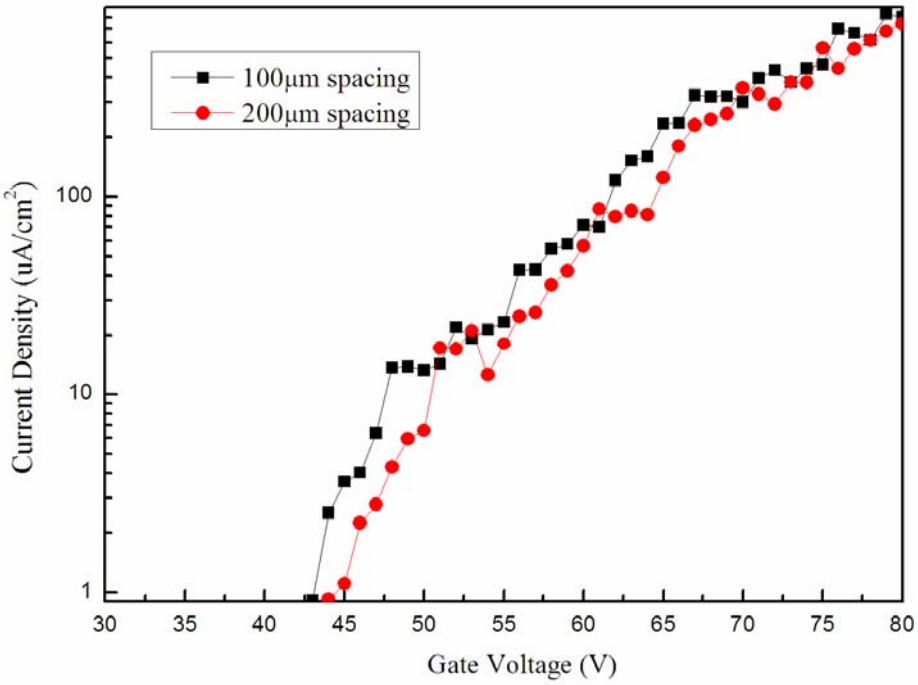

(b)

Figure 3-24 (a) The I-V plots of our triode structure with F-N plot inside (b) the logarithm I-V plot for detecting the turn-on voltage.

3.4 Summary

We successfully manufactured an ultra simple triode gate structure with CNT emitters, which showed a superior uniformity in luminescent image compared with those with conventional diode structure. The results of simulations and luminescent images clearly indicated that this gate structure employed surrounding gate electrodes close to the emitters could cause larger angle of electron dispersion, and the emitted electrons traveling through the spacing between cathode and anode plates would give rise to a lighting region on the anode plate.

Because of the dispersion of electron beams, the luminescent images could be more uniform as compared with conventional diode or pillar-like CNT emitter structure which has a serious issue of beam dispersion, and the experimental luminescent images also showed to insure this issue.

In conclusion, the current density was about 800μA/cm^2 and the turn-on gate voltage was 43V to 44V without screening-effect. The simple triode structure which only one step mask patterning could be applied to all kind of emitter materials, such as ZnO nano-rods or nano-particles instead of CNT emitters, therefore, the triode gate structure with a simple manufacturing process is potential for the application to enhance the uniformity on field emission backlight units.

Chapter 4

Summary and Conclusions

4.1 Summary and Conclusions

The pillar-like CNTs grown with Co-Ti/Al (2nm-3nm/10nm) catalyst at 550℃ in thermal CVD exhibited superior characteristics of electric properties and macroscopic luminescent uniformity, as compared with other kinds of catalysts. This novel catalyst component provided better adhesion between CNTs and substrates, higher pillar height, and sharper pillar edge. And, we optimized the growth time and the pillar spacing at 550℃ in order to enhance uniformity and reliability. The optimum growth time improved the morphologies of CNT pillars with lower I_D/I_G ratio, and the optimum pillar spacing could avoid screening-effect with the best stability. Consequently, the optimal pillar-like CNT backlight unit of pillar spacing of 9 μm grown 90 minutes showed a good field emission characteristics and photo-luminescent images. The current density of this proposed pillar-like CNTs was as high as 1688 $\mu A/cm^2$ at the electric field of 6 V/μm and the turn-on field was 3.5 V/μm; meanwhile, and the reliability was ultra stable since the degradation of initial current density was lower than 1%.

We successfully manufactured a simple triode gate structure with CNT emitters, which showed a superior uniformity in luminescent image compared with conventional diode structure and decreased the driving voltage. The results of the simulations and luminescent images clearly indicated that this gate structure with surrounding gate electrodes close to the emitters could cause larger divergence angle of electrons and the emitted electrons traveling

through the spacing between cathode and anode plates would give rise to a more uniform lighting region on the anode plate. As compared of conventional diode or pillar-like CNT emitter structure, it is attributed to the spreading of electron beams. Finally, the optimum parameters of the triode field emission device were obtained according to the simulations, the gate-to-emitter length was 2 μm, and the vertical distance between gate and CNTs was 1 μm, and the current density was about 800 $\mu A/cm^2$ and the turn-on gate voltage was 43 V to 44 V. Additionally, the simple triode structure which employed only one step of mask patterning could be applied to all kinds of emitter materials, such as ZnO nano-rods or nano-particles; therefore, the triode gate structure with a simple manufacturing process is potential in the applications of field emission backlight units with high uniformity.

In conclusions, the main concern in our research was uniformity and reliability of CNT emitters synthesized by thermal CVD at low temperatures. The reliability of CNT BLUs were improved by pillar-like CNTs, and the uniformity of CNT BLUs were improved by triode-typed structure. As a result, the CNT field emission arrays had an potential in backlight industry.

Even though the uniformity and reliability were quite improved in our researches, there were still some issues and parameters to be controlled or optimized by experiments. Following are some further research we proposed for pillar-like CNT field emitter arrays with low temperature processes. One is designing a new pixel pattern with pillar-like CNT arrays in the diode configuration. Another is Growing the optimum pillar-like CNTs on the glass substrate actually at 550℃ and comparing with that on the silicon substrate. The other is trying to further improve the uniformity of height between each pillar-like CNT emitters. And Finally, we will try to package the field emission device with CNT emitters in vacuum environment, and testing the sealed devices.

References

Chapter 1:

[1.1] J. Bardeen and W. H. Brattain, "*The Transistor, A Semi-Conductor Triode*," Phys. Rev., vol.74, pp.230-231, 1948.

[1.2] C. A. Spindt, I. Brodie, L. Humpnrey, and E. R. Westerberg, "*Electrical Properties of Thin-film Field Emission Cathodes with Molybdenum Cones,*" J. Appl. Phys., vol. 47, pp. 5248-5251, 1976.

[1.3] S. M. Sze, "*Physics of Semiconductor Devices*," 2nd ed., John-Wiley & Sons pulisher, New York, pp. 648-651, 1981.

[1.4] R. H. Fowler and L. W. Nordheim, "*Electron Emission in Intense Field*," Proc. R. SOC. A229, pp. 173-181, 1928.

[1.5] S. Itoh, T. Watanabe, T. Yamaura, and K. Yano, "*A Challenge to Field Emission Displays*," in Proc. Asia Display, pp. 617-620, Oct. 1995.

[1.6] R. Meyer, "*Recent Development on Microtips Display at LETI,*" IVMC'91 Technical Digest, pp. 6-9, 1991.

[1.7] N. E. McGruer and K. Warner, "*Oxidation-sharpened Gated Field Emitter Array Process*," IEEE Trans. Electron Devices, vol. 38, no. 10, pp. 2389-2391, 1991.

[1.8] S. E. Huq and L. Chen, "*Fabrication of sub-10 nm Silicon Tips: A New Approach*," J. Vac. Sci. & Technol. B, vol. 13, no. 6, pp. 2718-2721, Nov. 1995.

[1.9] D. W. Branston and D. Stephani, "*Field Emission from Metal-coated Silicon Tips*," IEEE Trans. Electron Devices, vol. 38, no. 10, pp. 2329-2333, Oct. 1991.

[1.10] V. V. Zhirnov and E. I. Givargizov, "*Field Emission from Silicon Spikes with Diamond Coating*," J. Vac. Sci. & Technol. B, vol. 13, no. 2, pp. 418-421, 1995.

[1.11] R. B. Marcus, T. S. Ravi, T. Gmitter, H. H. Busta, J. T. Niccum, K. K. Chin, and D. Liu, "*Atomically sharp silicon and metal field emitters*," IEEE Trans. Electron Devices, Vol. 38, pp. 2289-2291, 1991.

[1.12] P. Vaudaine and R. Meyer, "*Microtips fluorescent display,*" IEEE IEDM'91, pp.197-201, 1991.

[1.13] C. Curtin, "*The field emission display*," International Display Research Conference pp. 12-15, 1991.

[1.14] C. A. Spindt, C. E. Holland, I. Brodie, J. B. Mooney, and E. R. Westerberg, "*Field-emitter array applied to vacuum fluorescent displays*," IEEE Trans. Electron Devices, Vol. 36, No. 1, pp. 225-228, 1989.

[1.15] David A. Cathey, "*Field emission displays*," Information Display, p. 16, Oct., 1995.

[1.16] "*Pixtech to produce color FEDs from November*," News reported in Nikkei Electronics ASIA, p. 42, Nov., 1995.

[1.17] H. G. Kosmahl, "*A wide-bandwidth high-gain small size distributed amplifier with field-emission triodes (FETRODE's) for the 10 to 300 GHz frequency range*," IEEE Trans. Electron Devices, Vol. 36, No.11, pp. 2728-2737, 1989.

[1.18] P. M. Larry, E. A. Netteshiem, Y. Goren, C. A. Spindt, and A. Rosengreen, "*10 GHz turned amplifier based on the SRI thin film field emission cathode,*" IEEE IEDM'88, pp. 522-525, 1988.

[1.19] C. A. Spindt, C. E. Hollard, A. Rosengreen, and I. Brodie, "*Field emitter array development for high frequency operation*," J. Vac. Sci. & Technol. B, Vol. 11, pp. 486-473, 1993.

[1.20] C. A. Spindt, "*Microfabricated field emission and field ionization sources*," Surface Science, Vol. 266, pp. 145-154, 1992.

[1.21] T. H. P. Chang, D. P. Kern, "*A scanning tunneling microscope controlled field emission microprobe system*," J. Vac. Sci. & Technol. B, Vol. 9, p. 438-443, 1991.

[1.22] H. H. Busta, J. E. Pogemiller, and B. J. Zimmerman, "*The field emission triode as a displacement/process sensor,*" J. Micromech. Microeng., Vol. 3, pp. 45-56, 1993.

[1.23] H. C. Lee and R. S. Huang, "*A novel field emission array pressure sensor*," IEEE Transducers- International Solid-State Sensors and Actuators, pp. 241-244, 1991.

[1.24] Wikipedia "http://en.wikipedia.org/wiki/Image:Cathode_ray_Tube.PNG" 2005

[1.25] C. A. Spindt, "*A Thin Film Emission Cathode,*" J. Appl. Phys., vol. 39, pp. 3504-3505, 1968.

[1.26] R. Meyer, A. Ghis, P. Rambaud, and F. Muller, "*Microtips Fluores-cent Display,*" in Proc. Japan Display, pp. 512-514, Sept./Oct. 1986.

[1.27] S. Itoh AND M. Tanaka, "*Current Status of Field-Emission Displays*", Proceedings of the IEEE, vol. 90, no. 4, pp. 514-520, April. 2002.

[1.28] M. Ding, H. Kim, and A. I. Akinwande "*Highly Uniform and Low Turn-On Voltage Si Field Emitter Arrays Fabricated Using Chemical Mechanical Polishing*", IEEE Electron Device Letters, vol. 21, no. 2, pp. 66-69, Feb. 2000.

[1.29] J Itoh, Y Tohma, K Morigawa, S. Kanemaru and K. Shimizu "*Fabrication of Double Gate Si Field Emitter Arrays for Focused Electron Beam Generation*" J. Vac. Sci. & Technol. B., vol. 13, no. 5, pp. 1968-1972, 1995.

[1.30] K. Yamamoto, I. Nomura, K. Yamazaki, S. Uzawa and K. Hatanaka, "F*abrication and Characterization of Surface Conduction Electron Emitters*," SID Digest, pp. 1933-1935, 2005.

[1.31] T. Oguchi, E. Yamaguchi, K. Sasaki, K. Suzuki, S. Uzawa and K. Hatanake, "*A 36-inch Surface Conduction Electron Emitter Display (SED)* ," SID Digest, pp. 1929-1931, 2005.

[1.32] Iijima S.," *Helical microtubules of graphitic carbon* ," Nature Vol. 354 (6348), pp.56–58, 1991.

[1.33] Baughman, Ray H., Zakhidov, Anvar A., de Heer, and Walt A. ," *Carbon*

Nanotubes—The Route Toward Application ," Science, Vol.297 pp.787-790, 2002.

[1.34] Gamaly EG and Ebbesen TW," *Mechanism of carbon nanotube formation in the arc discharge* ," Phys Rev B, 1995,52(3), pp.2083–2089.

[1.35] Guo T, Nikolaev P, Thess A, Colbert DT, and Smalley RE.," *Catalytic growth of single-walled nanotubes by laser vaporization* ," Chem Phys Lett, Vol. 243, pp.49–54, 1995.

[1.36] M. P. Siegal, D. L. Overmyer, and F. H. Kaatz ," *Controlling the site density of multiwall carbon nanotubes via growth conditions,*"App. Phys. Lett., Vol. 84, No. 25, pp. 5156-5158, 2004

[1.37] Yih-Ming Shyu and Franklin Chau-Nan Hong," *The effects of pre-treatment and catalyst composition on growth of carbon nanofibers at low temperature* ,"Diamond and Related Materials Vol.10, pp. 1241-1245, 2001.

[1.38] Nolan, Peter E., Schabel, Michael J., Lynch, David C," *Hydrogen control of carbon deposit morphology* ,"Carbon , Vol. 33 , No. 1 , pp. 79-85 , 1995

[1.39] Mi Chen, Chieng-Ming Chen, and Chia-Fu Chen," *Growth of carbon nanotubes by microwave plasma chemical vapor deposition using CH_4 and CO_2 gas mixture* ,"Thin Solid Films, Vol. 420/421, pp. 230-234. 2002

[1.40] Mi Chen, Chieng-Ming Chen, Shin-Chen Shi and Chia-Fu Chen," *Low-Temperature Synthesis Multiwalled Carbon Nanotubes by Microwave Plasma Chemical Vapor Deposition Using CH_4-CO_2 Gas Mixture* ,"Jpn. J. Appl. Phys. Vol. 42, pp. 614–619, 2003.

[1.41] M. S. Dresselhaus, G. Dresselhaus, K. Sugihara, L. I. Spain, and H. A. Goldberg, "*Graphite fibers and filaments*," Springer-Verlag, New York, pp. 185-186, 1998.

[1.42] P. M. Ajayan, "*Nanotubes from carbon*," Chem. Rev., Vol. 99, pp. 1787-1790, 1999.

[1.43] S. Iijima and T. Ichihashi, "*Single-shell carbon nanotubes of 1-nm diameter,*" Nature, Vol. 363, pp. 603-605, 1993.

[1.44] D. S. Bethune, C. H. Kiang, M. S. de Vries, G. Gorman, R. Savoy, J. Vazquez, and R. Beyers, "*Cobalt-catalyzed growth of carbon nanotubes with single-atomic-layer walls*," Nature, Vol. 363, pp. 605-607, 1993

[1.45] "http://en.wikipedia.org/wiki/Image:CNTnames.png" 2006

[1.46] "http://online.itp.ucsb.edu/online/qhall_c98/dekker/" 2006

[1.47] Y. K. Kwon, T. H. Lee, S. G. Kim, P. Jund, D. Tomanek, and R. E. Smalley. "*Morphology and Stability of Growing Multiwall Carbon Nanotubes"* Phys Rev. Lett., Vol. 79, pp. 2065-2068, 1997

[1.48] Y. Saito, "*Carbon Nanotubes: Preparation and Physical Properties*," Asia Display/IDW'01, pp. 11-14, 2001

[1.49] Min-Feng Yu et al., "*Strength and Breaking Mechanism of Multiwalled Carbon Nanotubes Under Tensile Load*," Science, Vol. 287, pp. 637-640, 2000.

[1.50] Philip G. Collins and Phaedon Avouris, "*Nanotubes for Electronics- Scientific American December*", Vol. 69, 8 pages., 2000

[1.51] Jing Kong, Nathan R. Franklin, Chongwu Zhou, Michael G. Chapline, Shu Peng, Kyeongjae Cho, Hongjie Dai**,"** *Nanotube Molecular Wires as Chemical Sensors* **,"** Science 28, Vol. 287. no. 5453, pp. 622 – 625, 2000

[1.52] Cheng H-M, Yang Q-H, and Liu C.," *Hydrogen storage in carbon nanotubes* ," Carbon, Vol. 39, pp.1447–1457, 2001

[1.53] Derycke, V., Martel, R.; Appenzeller, J. and Avouris, Ph.," *Carbon Nanotube Inter- and Intramolecular Logic Gates,*"Nano Letters Vol. 9, pp. 453-456. 2001

[1.54] W. B. Choi, D. S. Chung, J. H. Kang, H. Y. Kim, Y. W. Jin, I. T. Han, Y. H. Lee, J. E. Jung, N. S. Lee, G. S. Park, and J. M. Kim, "*Fully Sealed, High-brightness Carbon-nanotube Field-emission Display*," Appl. Phys. Lett., vol. 75, no. 20, pp. 3129-3131, 1999

[1.55] Mitsubishi Rayon Co. Ltd. May 24, 2007

[1.56] Waxin mage Inc. “http://www.wanix.com.tw” 2004-2005

[1.57] Stefanie “Large-Sized TFT-LCD Industry Report” 2006

[1.58] L. Nilsson, O. Groening, C. Emmenegger, O. Kuettel, E. Schaller, and L. Schlapbach “ *Scanning field emission from patterned carbon nanotube films* ”, Appl. Phys. Lett., Vol. 76, pp.2071-2074, 2000

[1.59] *Choi G.S.; Son K.H.; Kim D.J ”* Fabrication of high performance carbon nanotube field emitters ”**,** Microelectronic Engineering Vol. 66, pp. 206–212, 2003

[1.60] Chaogang Lou; Xiaobing Zhang; Wei Lei; Qilong Wang; Hui Mu; Zhuoya Zhu; Mei Xiao; Yong Cao “*Influence of Catalyat Film Thickness on Carbon Nanotubes*”**,** Applied Surface Science, Vol. 251 pp. 254–257, 2005

[1.61] Jae-Hee Han, Su Hong Lee, A.S. Berdinsky, Yong Weon Kim, Ji-Beom Yoo, Chong-Yun Park, Jin Ju Choi, Taewon Jung, In Taek Han, Jong Min Kim, “*Effects of various post-treatments on carbon nanotube films for reliable field emission*”, Diamond & Related Materials, Vol. 14, pp. 1891 – 1896, 2005

[1.62] Huang-Chung Cheng, Rui-Ling Lai, Yao-Ren Chang, Kao-Chao Lin, Chuan-Ping Juan, Pei-Chi Chang, Chien-Ying Lee, and Jiun-Kai Shiu, “*Improvement of Luminescent Uniformity via Synthesizing the Carbon Nanotubes on an Fe–Ti Co-deposited Catalytic Layer*,” Japanese Journal of Applied Physics, Vol. 46, No. 2, pp. 863-866, 2007.

[1.63] Jin Seung Lee and Jung Sang Suh “ *Uniform field emission from aligned carbon nanotubes prepared by CO disproportionation* “ J. Appl. Phys. Vol.92 No.12, pp. 7519-7522, 2002

[1.64] Ke Yu, Ziqiang Zhu, Min Xu, Qiong Li, Wei Lu, and Qun Chen “ *Soluble carbon nanotube films treated using a hydrogen plasma for uniform electron field emission*” Surface and Coating Tech. Vol.179 pp. 63-69, 2004

[1.65] H. J. Lee, Y. D. Lee, W. S. Cho, B. K. Ju, Yun-Hi Lee, J. H. Han, and J. K. Kim ”

Field-emission enhancement from change of printed carbon nanotube morphology by an elastomer" Appl. Phys. Lett. 88 pp.093115, 2006

[1.66] H. J. Lee, S. I. Moon, J. K. Kim, Y. D. Lee, S. Nahm, J. E. Yoo, H. Han, Y. H. Lee, S. W. Hwang, and B. K. Ju, " *Improvement of field emission from printed carbon nanotubes by a critical bias field* " J. Appl. Phys. 98, pp. 016107-016107-3, 2005

[1.67] Changkun Dong and Mool C. Gupta," *Influences of the surface reactions on the field emission from multiwall carbon nanotubes* ,"Appl. Phys. Lett., Vol.83, id 159 No.1, 2003

[1.68] Lee, Cheol Jin; Park, Jeunghee; Han, Seungwu; and Ihm, Jisoon," *Growth and field emission of carbon nanotubes on sodalime glass at 550°C using thermal chemical vapor deposition,*"Chemical Physics Letters Vol. 337, pp. 398-402, 2001

[1.69] N.F. Mott, Proc. R. Soc." *Proceedings of the Royal Society of London. Series A, Containing Papers of a Mathematical and Physical Character*" Vol. 146, pp. 465-472, 1934

[1.70] Q. Jiang, N. Aya, and F.G. Shi, " *Nanotube size-dependent melting of single crystals in carbon nanotubes*, "Appl. Phys. Vol. 64, pp.627-629. 1997

[1.71] C.-M. Tang, T. A. Swyden, and A. C. Ting, "*Planar lenses for field-emitter arrays*," J. Vac. Sci. Technol. Vol. 13, pp. 571-575,1995

[1.72] Kozaburo SHIBAYAMA, Masaaki HIRAKI, Yuusaku SAITOU and Akihiko HOSONO," *Improvement of Lighting Uniformity in Field Emission Display with Carbon Nano-Tube Cathode*s," Jpn. J. Appl. Phys. Vol. 42, pp. 3698–3701, 2003

Chapter 2:

[2.1] Y. K. Kwon, T. H. Lee, S. G. Kim, P. Jund, D. Tomanek, and R. E. Smalley. "*Morphology and Stability of Growing Multiwall Carbon Nanotubes*," Phys Rev. Lett., vol. 79, pp. 2065-2068, 1997.

[2.2] Y. Saito, "*Carbon Nanotubes: Preparation and Physical Properties*," Asia Display/IDW'01, pp. 11-14, 2001.

[2.3] M. Okai, T. Fujieda, K. Hidaka, T. Muneyyoshi, and T. Yaguchi, "*In Situ Transmission Electron Microscope Observation of Carbon Nanotubes in Electric Fields* ," Jpn. J. of Appl. Phys. vol. 44, no. 4A, pp. 2051-2055, 2005.

[2.4] Jean-Marc Bonard and Christian Klinke, "*Degradation and Failure of Carbon Nanotube Field Emitter*s," Phys. Rev. B, vol. 67, no. 11, pp. 115406-115406-10, 2003.

[2.5] Jae-Hee Han, Su Hong Lee, A.S. Berdinsky, "*Effects of Various Post-treatments on Carbon Nanotube Films for Reliable Field Emission*," Diamond & Related Materials, vol. 14, pp. 1891-1896, 2005.

[2.6] Chaogang Lou, Xiaobing Zhang, Wei Lei, and Chen Qi, "*New Method to Fabricate Field-emission Cathode of Carbon Nanotubes,*" Applied Surface Science, vo. 251, pp. 254–257, 2005.

[2.7] Ke Yu, Ziqiang Zhu, Min Xu, Qiong Li, Wei Lu, Qun Chen "*Soluble carbon nanotube films treated using a hydrogen plasma for uniform electron field emission"* Surface and Coating Tech. Vol. 179 pp. 63-69, 2004

[2.8] Jin Seung Lee and Jung Sang Suh "*Uniform field emission from aligned carbon nanotubes prepared by CO disproportionation*" J. Appl. Phys. Vol. 92, pp. 7519-7522, No. 12, 2002

[2.9] Q. Jiang, N. Aya, and F. G. Shi, "*Nanotube Sized-dependent Melting of Single Crystals in Carbon Nanotubes*," Appl. Phys. A 64, pp. 627-629, 1997.

[2.10] W. H. Oi, "*Size Effect on Melting Temperature of Nanosolid*," Physica B, vol. 368, pp. 46-50, 2005.

[2.11] Huang-Chung Cheng, Rui-Ling Lai, Yao-Ren Chang, Kao-Chao Lin, Chuan-Ping Juan, Pei-Chi Chang, Chein-Ying Lee, and Jiun-Kai Shiu, "*Improvement of*

Luminescent Uniformity via Synthesizing the Carbon Nanotubes on an Fe–Ti Co-deposited Catalytic Layer," Japanese Journal of Applied Physics, vol. 46, No. 2, pp. 863-866, 2007.

[2.12] "http://www.wanxin.com.tw" Wanxin mage Inc. 2004-2005

[2.13] Hsia-Wei Chen "*Study on the Carbon-Nanotube Field Emission Devices with the Co/Ti/Al Catalyst and Novel Self-Focusing Gate Structure*" 2007

[2.14] Michael J. Bronikowski, "*CVD Growth of Carbon Nanotube Bundle Arrays*" CarBon, Vol.44, pp. 1822-2832, 2006

[2.15] Jun-Hun Lin "*Study on the Field Emission Characteristics of Carbon- Nanotubes Pillar Arrays Using Co/Ti Bi-Layered Catalyst*" 2007

Chapter 3:

[3.1] C.-M. Tang, T. A. Swyden, and A. C. Ting, "*Planar lenses for field-emitter arrays*," J. Vac. Sci. Technol. Vol. 13, pp. 571-575, 1995.

[3.2] L. Dvorson and A. I. Akinwande, "*Novel cmp-based process for fabricating arrays of Double-gated silicon field emitters*," J. Vac. Sci. Technol. Vol. 20, pp. 139-140, 2002

[3.3] Jun Hee Choi, Andrei R. Zoulkarneev, Young-Jun Park and Deuk Seok Chung, "*Optimization of Electron Beam Focusing for Gated Carbon Nanotube Field Emitter Arrays*," IEEE TRANSACTIONS ON ELECTRON DEVICES, VOL. 52, NO. 12, pp. 2584-2590, Dec 2005

[3.4] Leonard Dvorson and Akintunde I. Akinwande, "*Double-gated Spindt emitters with stacked focusing electrode*," J. Vac. Sci. Technol. Vol. B 20(1), pp. 53-59, Jan/Feb 2002

[3.5] Kozaburo SHIBAYAMA, Masaaki HIRAKI, Yuusaku SAITOU and Akihiko

HOSONO,“ *Improvement of Lighting Uniformity in Field Emission Display with Carbon Nano-Tube Cathodes*,” Jpn. J. Appl. Phys. Vol. 42, pp. 3698–3701, 2003

[3.6] Hsia-Wei Chen “*Study on the Carbon Nanotubes Field Emission Devices with the Co/Ti/Al Catalyst and Novel Self-Focusing Gate Structure*” 2007

[3.7] J. H. Choi, A. R. Zoulkarneev, Y. W. Jin, Y. J. Park, D. S. Chung, B. K. Song, I. T. Han, H. W. Lee, S. H. Park, H. S. Kang, H. J. Kim, J. E. Jung, and J. M. Kim, “*Carbon nanotube field emitter arrays having an electron beam focusing structure*,” Appl. Phys. Lett., vol. 84, no. 6, pp.1022–1024, Feb. 2004.

簡　歷

姓　名: 李建穎

性　別: 男

生　日: 民國七十三年六月十日

籍　貫: 台北市

地　址: 台北縣中和市忠孝街 58 巷 16 弄 21 號 5 樓

學　歷: 國立交大學材料科學與工程學系

(91 年 9 月～95 年 7 月)

國立交通大學電機學院電子工程研究所碩士班

(95 年 9 月～97 年 7 月)

論文題目:

低溫製程之奈米碳管場發射背光模組和利用三極結構增進均勻性之研究

Study on the Carbon Nanotube Field Emission Backlight Units with Low Temperature Processes and Enhancement of Uniformity by Utilizing a Triode Structure

97

碩士論文

低溫製程之奈米碳管場發射背光模組和利用三極結構增進均勻性之研究

交通大學　電機學院
電子工程學系電子研究所

李　建　穎
Lee Chein-Ying